University of Florence

International Doctorate in Structural Biology

Cycle XXI (2006-2008)

Copper proteins and their mutations related to diseases

Ph. D. thesis of

Mirela Boca

Tutor

Prof. Lucia Banci

Coordinator

Prof. Claudio Luchinat

S.S.D. Chim/03

This thesis has been approved by the University of Florence,
the University of Frankfurt and the Utrecht University

…this thesis is dedicated to my parents

Table of Contents

Acknowledgments

I am deeply grateful to:

Professor Ivano Bertini for giving me the chance of carrying out my PhD in Structural Biology at CERM,

Professor Lucia Banci, who always stimulated me to constantly improve my research approach,

Dr. Stefania Girotto for her guidance throughout this nice project, for all the support and constant help she gave me every time I needed it,

Dr. Manuele Martinelli, who actually introduced me to the world of DNA and proteins.

I also want to bring special thanks to:

My parents (mami si tati) for all their love and constant support, Cosminel (Tudor-Cosmin) who always believed in me, my cousin Vio, Zoli, Paul, Adi, Flori, Soso si Dea, my neighbours and friends from Romania,

My dear colleagues: Doros (Doraki mu), Jerome, Niko (Nikolaki mu), Miguela, Kwon Joo, Iliana, Ele (Eleonoritos), Roberta, Tania (Taniuska mia), Maciek (Macieko), Petros (Petraki mu), Chiara, some of which became also very good friends of mine,

All the guys who passed by or are still living in Val di Rose, the house which was my home during all these 3 years: Jerome, Malte, Vlad and Ala, Anna, Petros, Maciek, Fiore, mio caro Maxime, Marco, Michele, Vaishali, Deepa, Andris, Marcin. Some of them became really good friends of mine.

1

Introduction

1.1 Neurodegenerative diseases and protein aggregation

Neurodegenerative diseases such as Alzheimer's disease (AD), Parkinson's disease (PD), Huntington's disease (HD), prion diseases and amyotrophic lateral sclerosis (ALS) appear to have common cellular and molecular mechanisms, including protein aggregation and inclusion bodies formation, features, which seem to be directly related to neurotoxicity (Table1).

Table 1. Human diseases associated with formation of extracellular amyloid deposits or intracellular inclusions with amyloid-like characteristics. (Reprinted from Chiti F., Dobson C.M. (2006) Protein misfolding, functional amyloid and human disease *Annu. Rev. Biochem.* **75**, 333–366)

Disease	Aggregating protein or peptide	Number of residues[a]	Native structure of protein or peptide[b]
Neurodegenerative diseases			
Alzheimer's disease[c]	Amyloid β peptide	40 or 42[f]	Natively unfolded
Spongiform encephalopathies[c,e]	Prion protein or fragments thereof	253	Natively unfolded (residues 1–120) and α-helical (residues 121–230)
Parkinson's disease[c]	α-Synuclein	140	Natively unfolded
Dementia with Lewy bodies[c]	α-Synuclein	140	Natively unfolded
Frontotemporal dementia with Parkinsonism[c]	Tau	352–441[f]	Natively unfolded
Amyotrophic lateral sclerosis[c]	Superoxide dismutase 1	153	All-β, Ig like
Huntington's disease[d]	Huntingtin with polyQ expansion	3144[g]	Largely natively unfolded
Spinocerebellar ataxias[d]	Ataxins with polyQ expansion	816[g,h]	All-β, AXH domain (residues 562–694); the rest are unknown
Spinocerebellar ataxia 17[d]	TATA box-binding protein with polyQ expansion	339[g]	α+β, TBP like (residues 159–339); unknown (residues 1–158)
Spinal and bulbar muscular atrophy[d]	Androgen receptor with polyQ expansion	919[g]	All-α, nuclear receptor ligand-binding domain (residues 669–919); the rest are unknown
Hereditary dentatorubral-pallidoluysian atrophy[d]	Atrophin-1 with polyQ expansion	1185[g]	Unknown
Familial British dementia[d]	ABri	23	Natively unfolded
Familial Danish dementia[d]	ADan	23	Natively unfolded

[a]Data refer to the number of residues of the processed polypeptide chains that deposit into aggregates, not of the precursor proteins.

[b]According to Structural Classification Of Proteins (SCOP), these are the structural class and fold of the native states of the processed peptides or proteins that deposit into aggregates prior to aggregation.

[c]Predominantly sporadic, although in some cases hereditary forms associated with specific mutations are well documented.

[d]Predominantly hereditary, although in some cases sporadic forms are documented.

[e]Five percent of the cases are transmitted (e.g., iatrogenic).

[f]Fragments of various lengths are generated and have been reported to be present in ex vivo fibrils.

[g]Lengths shown refer to the normal sequences with nonpathogenic traits of polyQ.

[h]Length shown is for ataxin-1

The aggregates usually consist of fibers containing misfolded proteins arranged in a β-sheet conformation, termed amyloid. There is partial, but not perfect, overlap among the cells in which abnormal proteins are deposited and the cells that degenerate. The most likely explanation is that inclusions and other visible protein aggregates represent an end stage of a molecular cascade of several steps, and that earlier steps in the cascade may be more directly tied to pathogenesis than the inclusions themselves (1).

Correct folding requires proteins to assume one particular structure from a constellation of possible but incorrect conformations, the failure of polypeptides to adopt their proper structure is a major threat to cell function and viability and neurons are particularly vulnerable to the toxic effects of mutant or misfolded proteins (2).

The common characteristics of all these neurodegenerative disorders suggest parallel approaches to treatment, based on an understanding of the factors preventing the correct protein folding and the normal cellular mechanisms for disposing of not correctly functioning and potentially noxious proteins.

1.1.1 Protein folding and misfolding related to neurodegenerative diseases

In a cell, proteins are synthesized on ribosomes from the genetic information encoded in the cellular DNA. Folding *in vivo* is, in some cases, co-translational, which means that it is initiated before the completion of protein synthesis, whereas the nascent chain is still attached to the ribosome (3). Other proteins, however, undergo the major part of their folding in the cytoplasm after release from the ribosome, whereas yet others fold in specific compartments, such as mitochondria or the endoplasmic reticulum (ER), after trafficking and translocation through membranes (4, 5). Many details of the folding process depend on the particular environment in which folding takes place, although the fundamental principles of folding, discussed above, are undoubtedly universal.

Following biosynthesis, a polypeptide chain, which is initially unfolded, can populate a wide distribution of conformations, each of which contains little persistent structure, as in the case of natively unfolded proteins, or fold to a unique compact structure, often through one or more partly folded intermediates (6) (Fig.1).

Even during the latter intermediate steps incompletely folded proteins must inevitably expose to the solvent, at least some regions of structure that are buried in the native state, so, they are prone to inappropriate interaction with other molecules within the crowded environment of a cell (7). Living systems have therefore evolved a range of strategies to prevent such behaviour (4–7). All of the different conformational states assumed by the

proteins and their interconversions are carefully regulated in the biological environment, much as enzymes regulate all the chemistry in cells, by using machinery such as molecular chaperones, degradatory systems, and quality control processes (6). Of particular importance are the many molecular chaperones that are present in all types of cells and cellular compartments. Some chaperones interact with nascent chains as they emerge from the ribosome, whereas others are involved in guiding later stages of the folding process (4, 5). Molecular chaperones often work in tandem to ensure that the various stages in the folding of such systems are all completed efficiently.

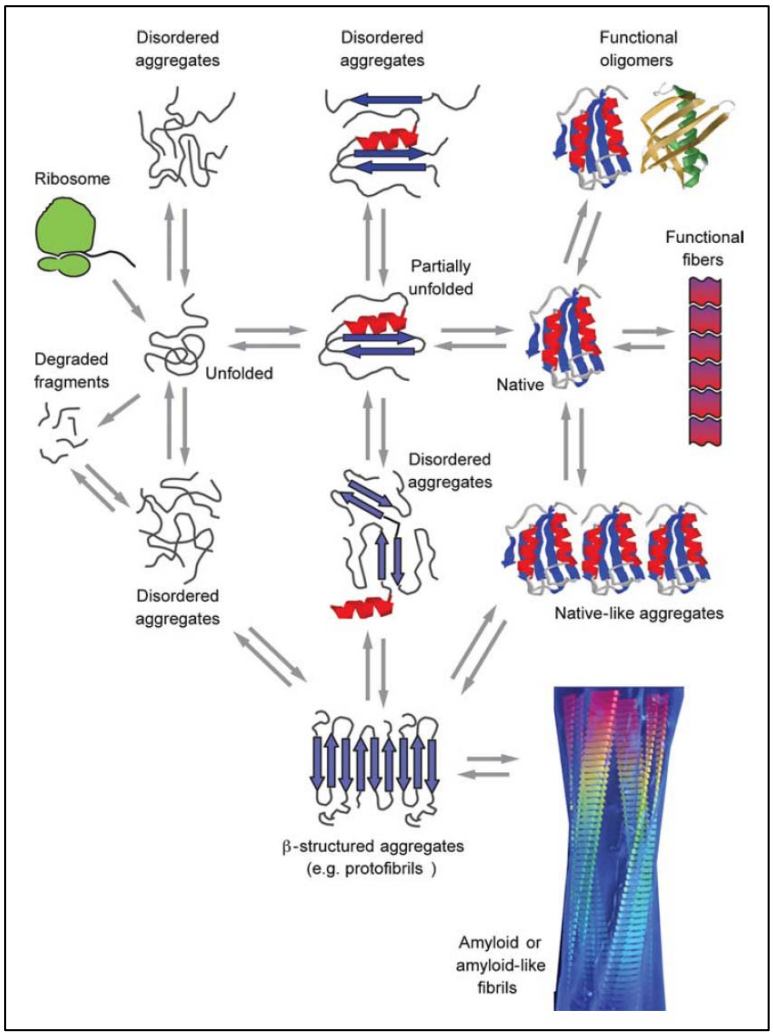

Fig. 1 A schematic representation of some of the many conformational states that can be adopted by polypeptide chains and of the means by which they can be interconverted. (Reprinted from Chiti F., Dobson C.M. (2006) Protein misfolding, functional amyloid and human disease *Annu. Rev. Biochem.* **75,** 333–366)

A large fraction of newly translated proteins nonetheless fails to fold correctly, generating a substantial burden of defective polypeptide (8). These proteins are degraded

primarily by the ubiquitin-proteasome system (UPS) (Fig. 2), a multicomponent system that identifies and degrades unwanted proteins (9, 10). In addition to its role in clearing defective proteins, the UPS carries out selective degradation of many short-lived normal proteins, under very carefully controlled conditions and as a part of normal biochemical processes, thereby contributing to the regulation of numerous cellular processes. Failure to detect and eliminate misfolded proteins may contribute to the pathogenesis of neurodegenerative diseases. Conversely, it has been suggested that the UPS itself may be a target for toxic proteins (11). Under some circumstances, misfolded proteins may evade the quality control systems designed to promote correct folding and eliminate faulty proteins. When they accumulate in sufficient quantity, misfolded proteins are prone to aggregation. Insoluble aggregates of disease-related proteins may be deposited in microscopically visible inclusions or plaques, the characteristics of which are often disease specific (2).

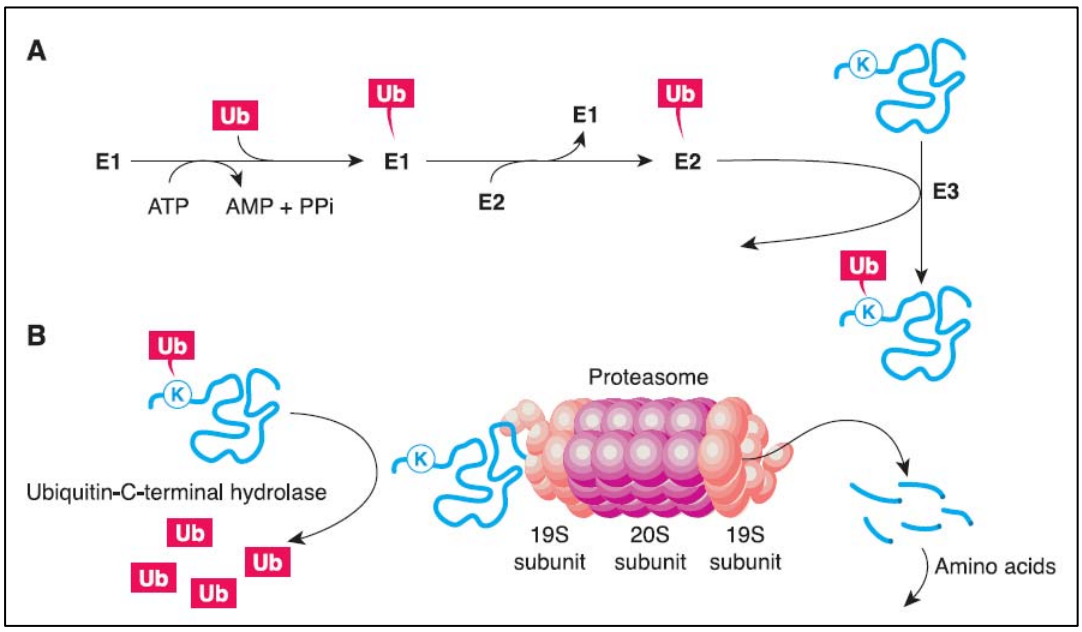

Fig. 2 The ubiquitin-proteasome system. (A) Proteins targeted for degradation are identified by covalent linkage to ubiquitin. Selective ubiquitination is accomplished by a series of enzymes (E1, E2, and E3) that constitute the ubiquitin ligase system. **(B)** Ubiquitinated substrates are recognized, unfolded, and degraded in an energy-dependent manner by the proteasome. (Reprinted from Taylor J.P., Hardy J., Fischbeck, K.H. (2002) Toxic proteins in neurodegenerative disease *Science* **296**, 1991−1995)

1.1.2 Amyloid fibrils formation related to neurodegenerative diseases

Each amyloid disease involves predominantly the aggregation of a specific protein, although a range of other components including additional proteins and carbohydrates are incorporated into the deposits when they form *in vivo* (12). In neurodegenerative diseases, the

quantities of aggregates involved can sometimes be so small as to be almost undetectable, whereas in some systemic diseases literally kilograms of protein can be found in one or more organs (13). The fibrillar structures typical of many of the aggregates have very similar morphologies (long, unbranched and often twisted structures a few nanometres in diameter) and a characteristic 'cross-β' X-ray fibre diffraction pattern. The latter reveals that the organized core structure is composed of β-sheets whose strands run perpendicular to the fibril axis (14). The ability of polypeptide chains to form amyloid structures is not restricted to the relatively small number of proteins associated with recognized clinical disorders, and it now seems to be a generic feature of polypeptide chains (15, 16). The core structure of the fibrils seems to be stabilized primarily by interactions, particularly hydrogen bonds, involving the polypeptide main chain. Because the main chain is common to all polypeptides, this observation explains why fibrils formed from polypeptides of very different sequence seem to be so similar (14, 16). The generic amyloid structure contrasts strongly with the highly individualistic globular structures of most natural proteins (12). In these latter structures the interactions associated with the very specific packing of the side chains seem to override the main-chain preferences (16, 17). The state of a protein that is adopted under specific conditions depends on the relative thermodynamic stabilities of the various accessible conformations and on the kinetics of their interconversion (Fig. 1) (15, 18). Amyloid fibrils are just one of the types of aggregate that can be formed by proteins, although a significant feature of this particular species is that its highly organized hydrogen-bonded structure is likely to give it unique kinetic stability. Thus, once formed, such aggregates can persist for long periods, allowing a progressive build-up of deposits in tissue, and indeed enabling seeding of the subsequent conversion of additional quantities of the same protein into amyloid fibrils (12). It is therefore not surprising that biological systems have almost universally avoided the deliberate formation of such material. Nevertheless, there is increasing evidence that the unique properties of amyloid structures have been exploited by some species, including bacteria, fungi and even mammals, for specific, and carefully regulated, purposes (19–21). One particularly well-studied example of functional amyloid is that of the proteinaceous fibrils formed from the curlin protein, which are used by *Escherichia coli* to colonize inert surfaces and mediate binding to host proteins (6).

The fibrils have the ability to bind specific dyes such as thioflavin T (ThT) and Congo red (CR) (22), although the specificity of binding of CR to amyloid fibrils and the resulting green birefringence under cross-polarized light has recently been questioned (23).

For many years the only structural information about amyloid fibrils came from imaging techniques such as transmission electron microscopy (TEM), and more recently atomic force microscopy (AFM), and from X-ray fiber diffraction (24–27). Despite the structural insights given by these techniques, as outlined above, until few years ago one of the most common statements found in the introductory sections of articles related to this field was reporting that amyloid fibrils could not be characterized in detail at the molecular level because they were not crystalline and too large to be studied by solution NMR spectroscopy. The situation has recently changed dramatically as a result of major progress in the application of solid-state NMR (SSNMR) spectroscopy to preparations of amyloid fibrils (28–30) and of successes in growing nano- or microcrystals of small peptide fragments that have characteristics of amyloid fibrils yet are amenable to single crystal X-ray diffraction analysis (31, 32).

1.2 Amyotrophic Lateral Sclerosis

The most common motor neuron disease in human adults is amyotrophic lateral sclerosis (ALS). Initially described (33) in 1869 by the famous French neurobiologist and physician Jean-Martin Charcot, ALS first became known as Charcot's sclerosis. ALS is now familiarly known in the United States as Lou Gehrig's disease, in honor of the great baseball player who developed the disease in the 1930s.

Generally fatal within 1–5 years from onset, ALS has a yearly incidence (new cases in the population) of about 2 to 3 per 100 000 people with a prevalence of 5–7/100 000. The lifetime risk of developing the disease is approximately 1 in 2000. The typical age of onset is between 50 and 60. Before 65 years of age, male incidence is twice that of females. However, after 65 years, the incidence becomes equal (34).

The primary hallmark of ALS is the selective dysfunction and death of motor neurons in the brain and spinal cord which leads to spasticity, hyperreflexia, generalized weakness, muscle atrophy and paralysis. Denervation of the respiratory muscles and diaphragm is generally the fatal event.

"Amyotrophic" refers to the muscle atrophy, weakness, and fasciculation that signify disease of the lower motor neurons (LMN). "Lateral sclerosis" refers to the hardness to palpation of the lateral columns of the spinal cord in autopsy specimens, where gliosis follows degeneration of the corticospinal tracts. The clinical results are upper motor neuron (UMN) signs as spasticity and hyperreflexia (35) (Fig. 3).

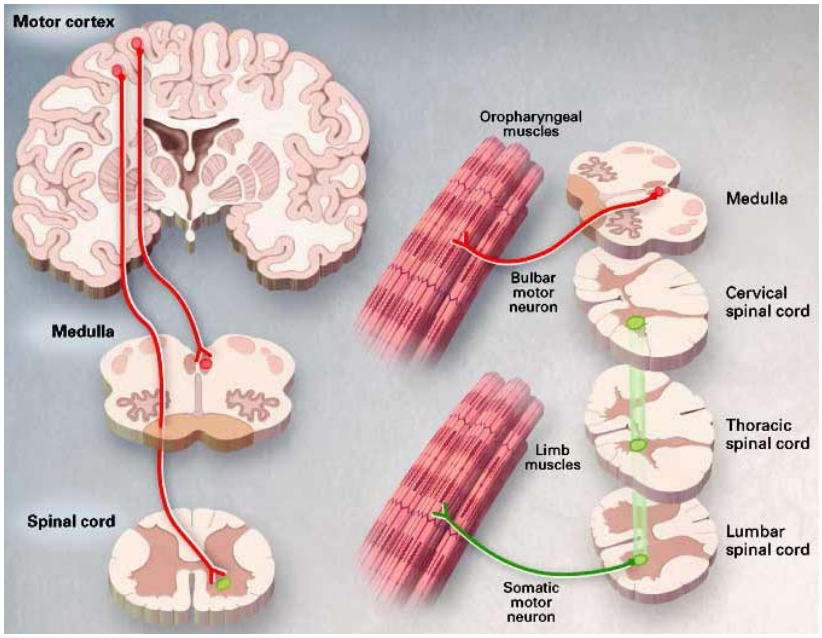

Fig. 3 Motor Neurons Selectively Affected in ALS. Degeneration of motor neurons in the motor cortex leads to clinically apparent signs of UMN abnormalities: spasticity and hyperreflexia (left). Degeneration of motor neurons in the brain stem and spinal cord (LMN) causes muscle atrophy, weakness, and fasciculation (right) (Reprinted from Rowland LP, Shneider NA. (2001) Amyotrophic lateral sclerosis *N. Engl. J. Med.* **344,** 1688–1700)

The causes of almost all occurrences of the disease remain unknown and the clinical course is highly variable, suggesting that multiple factors underlie the disease mechanism. In 90–95% of instances, there is no apparent genetic linkage, a form of the disease referred to as sporadic ALS (sALS), but in the remaining 5–10% of cases, the disease is inherited in a predominantly dominant manner, a form referred to as familial ALS (fALS) (36). Of these familial cases, ~25% are caused by mutations in the gene encoding copper-zinc superoxide dismutase (37).

.

1.3 Structural aspects and physiological roles of copper-zinc superoxide dismutase

The antioxidant enzyme, copper-zinc superoxide dismutase (SOD1), is one of the cellular defense systems for oxidative stress. Its functional role is that of catalyzing the dismutation of two superoxide anions to dioxygen and hydrogen peroxide according to the following reactions (38):

$Cu^{2+}, Zn^{2+} - SOD1 + O_2^- \leftrightarrow Cu^{1+}, Zn^{2+} - SOD1 + O_2$

$Cu^{1+}, Zn^{2+} - SOD1 + O_2^- + 2H^+ \leftrightarrow Cu^{2+}, Zn^{2+} - SOD1 + H_2O_2$

Eukaryotic SOD1 is a 32 kDa homodimeric metalloenzyme, found predominantly in the cytosol, but it is also found in other cellular compartments, including nucleus (39, 40), lysosomes, peroxisomes (40, 41**)**, endoplasmic reticulum (42), and mitochondria. In the latter, SOD1 is concentrated in the intermembrane space (IMS) (43–46), but it can also be detected in the matrix (47) and on the outer membrane (OM) (48–50).

Each of the two subunits of human SOD1 has 153 amino acids arranged in a Greek key β-barrel structure composed of eight antiparallel β-strands connected by loops of various lengths. Each subunit of the dimer contains an intramolecular disulfide bond, between Cys57 and Cys146, which is localized near the active site that binds a catalytic copper ion (binding residues: His46, His48, His63 and His120) and a structural zinc ion (binding residues: His63, His71, His80 and Asp83) (51–55) (Fig. 4).

Primary sequence as well as three-dimensional structure of SOD1 is highly conserved from prokaryotes to eukaryotes (56). Several structural variations have been found in bacterial SOD1 proteins: a monomeric form in *Escherichia coli* (57), a heme binding site in *Haemophilus ducreyi* (58), no Zn binding site in *Mycobacterium tuberculosis* (59).

Wild-type (WT) human SOD1 actually contains four cysteine residues per monomer. Besides the two cysteines involved in the formation of the intra-subunit disulfide bond, two reduced cysteines, Cys6 and Cys111, are located on β strand 1 and loop VI, respectively. The internal disulfide bond between Cys57 and Cys146 which contributes to the high stability of the SOD1 protein, is highly conserved in SOD1s from various organisms, including yeast, plants, flies, fishes and mammals (51, 60). In contrast, the other two free cysteines, Cys6 and Cys111, are not conserved. Actually, yeast, fungi and spinach (plants) have no free cysteines, and residue 6 is an alanine (Ala) while residue 111 is a serine (Ser) in these organisms (61). More evolved organisms, such as flies, fishes and mammals, including the Japanase monkey, have only one free cysteine, Cys6. Only humans and great apes (chimpanzee and orangutan)

have two free cysteines, Cys6 and Cys111 (62). Notably, the amino acid sequence of chimpanzee SOD1 is identical to that of human SOD1. Although the evolutionary process may differ from humans and great apes, chicken SOD1 has three free cysteines including Cys6 and Cys111. The third free Cys residue is located at the C-terminus, Cys154 (63). Because free cysteines generally are reactive and WTSOD1 is less thermo-stable than Ser111-SOD1 or Ala6-SOD1 (64), the Ala6Cys and Ser111Cys mutations during evolution are puzzling. In particular, Cys111 is located at the surface of the SOD1 molecule and is thought to be highly reactive (65).

Among the loops connecting the eight β strands, which characterize SOD1 structure, two have structural and functional role. The electrostatic loop (loop VII, residues 121–144) contains positive charged residues (Lys136 and Arg143) that contribute to guide the negatively charged superoxide substrate (O_2^-) towards the catalytic copper site. The long zinc loop (loop IV, residues 49–84) contains all the zinc binding residues including His63, which acts as a ligand to both metals (53) (Fig. 4).

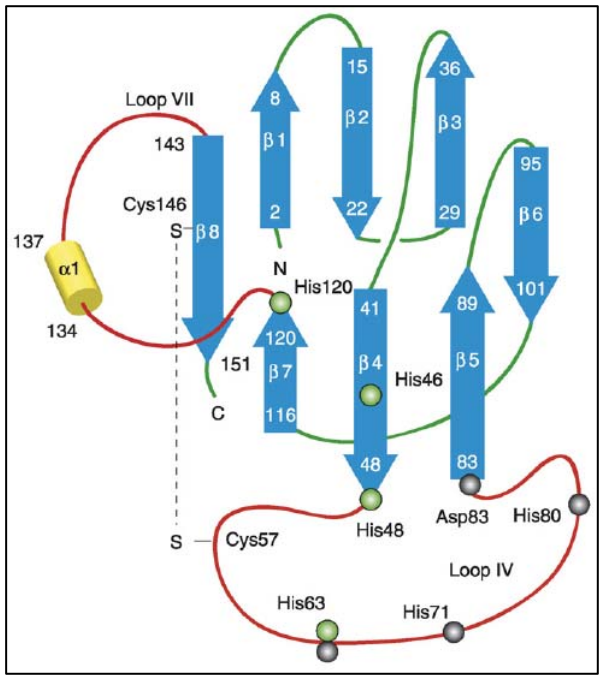

Fig. 4 Secondary structural elements of human SOD1. The β-strands and β-strand residues are numbered; the short α-helix (α1) that forms on Cu and Zn binding is shown as a cylinder. The Zn-coordinating residues, His63, His71, His80 and Asp83, are shown as gray spheres; the Cu-coordinating residues, His46, His48, His63 and His120, are shown as green spheres (the Cu–Zn bridging ligand, His63, is shown as two adjacent spheres). The disulfide bond between Cys57 and Cys146 is indicated with a broken line. The two large loops in SOD1 (loops IV and VII) are colored in red. (Reprinted from Shaw B. F., and Valentine J. S. (2007) How do ALS-associated mutations in superoxide dismutase 1 promote aggregation of the protein? *Trends Biochem. Sci.* **32,** 78–85)

1.4 Post-translational modifications and stability aspects of SOD1

The mature, correctly folded and enzymatically active form of SOD1 is obtained, *in vivo*, through several post-translational modifications such as the acquisition of zinc and copper ions, disulfide bond formation, and dimerization (66–70) (Fig. 5). While the mechanism by which SOD1 acquires Zn(II) is not fully understood, several aspects of copper insertion by the copper chaperone for SOD1 (CCS) are well established (71–76). Furukawa et al. (77) have shown that the intra-subunit disulfide bond is correctly introduced in yeast SOD1 by the copper-bound form of yeast CCS.

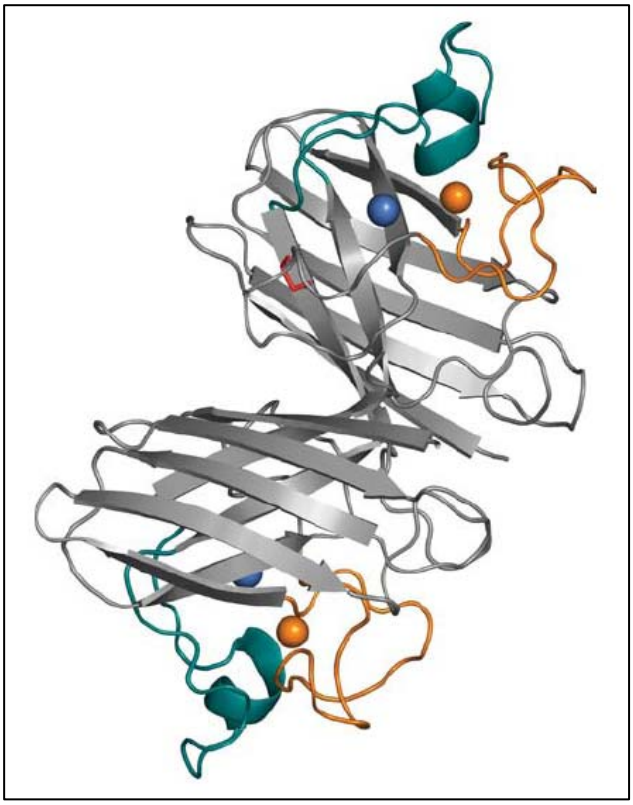

Fig. 5 The structure of metal bound dimeric human SOD1. Copper and zinc ions are shown as blue and orange spheres, respectively. The zinc loop is depicted in orange and the electrostatic loop in teal. The intrasubunit disulfide bond is shown in red. (Reprinted from Valentine J. S., Doucette P. A., Potter S. Z. (2005) Copper-zinc superoxide dismutase and amyotrophic lateral sclerosis *Annu. Rev. Biochem*. **74**, 563–593)

However, given that the cytosol is a strongly reducing environment, due to the high ratio of reduced glutathione to the disulfide form (GSH/GSSG) which ranges from 100:1 to 1000:1 (78), the disulfide formation is an unfavourable process. These aspects suggest that the immature disulfide-reduced human SOD1s are more important species in the cytosolic environment than previously thought. Field et al. (79) have shown that uptake of the SOD1

molecule into the mitochondrial IMS is dependent on the status of the disulfide bond. The reduced form of SOD1 is imported through the mitochondrial OM, but the disulfide-bonded metal-free (apo) SOD1, the Zn(II)-loaded SOD1, and the holo-form of fully mature form of SOD1 are not readily transferred from the cytosol into the mitochondrial IMS.

The tight dimer formed by SOD1, having a dissociation constant of ~1.0×10^{-10} M^{-1} (80), provides it with the characteristics of a very robust protein with respect to physical and chemical denaturation; the holo protein remains folded at temperatures near the boiling point of water (81, 82). In addition, it retains a dimeric quaternary structure in 1% SDS (83) and enzymatic activity can be observed in the presence of 10 *M* urea or after 1 h in 4% SDS and at 80°C (84). Furthermore, active fragments of SOD1 have been isolated from an Egyptian mummy dating to 1200 BC (85). Unlike the fully metallated protein (Cu_2Zn_2 $SOD1^{S\text{-}S}$), which has a melting temperature (T_m) of ~95°C (81, 82), the metal-free, disulfide-reduced SOD1 polypeptide (apo-$SOD1^{2SH}$) is relatively unstable and has a T_m value of 42°C at pH 7.4 (86). The metal-free, disulfide-intact protein (apo-$SOD1^{S\text{-}S}$) has a T_m value of ~52°C (86).

As far as the enzymatic activity of this protein is concern, while nonenzymatic dismutation of O_2^- to O_2 and H_2O_2 occurs with a rate constant of 2×10^5 $M^{-1}s^{-1}$, at pH 7.4, SOD1-catalyzed dismutation is significantly accelerated to an extent that it is diffusion-controlled (2×10^9 $M^{-1}s^{-1}$) (87). Interestingly, this enzymatic rate of disproportionation is very similar to that of copper salts; however, given that intracellular free copper concentrations are quite low under normal aerobic growth (70), there has been a strong selection for organisms to elaborate a more efficient defense. The intracellular concentration of SOD1 is high (ranging from 10 to 100 μ*M*) (88, 89), and apparently sufficient to consume physiological levels of superoxide radical. While superoxide is produced in the cytosol by several enzymes such as xanthine oxidase (90), the respiration process in mitochondria is a major source of O_2^- generation (91).

WTSOD1 localized into the mitochondrial IMS is providing protection from superoxide produced by the respiratory chain on the outer side of the inner membrane (IM), which is inaccessible to the matrix-residing Mn-superoxide dismutase (SOD2) present there in high levels (ca. 1×10^{-5} *M*) (92).

At a tissue level, SOD1 is widely expressed in liver and kidney (93). It is also abundant in motor neurons (94). This correlates with high expression of xanthine oxidase in liver and with high susceptibility of neuronal cells to oxidative stress. Knockout studies indicate that elimination of the SOD1 gene in these cells results in widespread oxidative damage (41).

1.5 SOD1 and SOD1 mutations related to ALS

At a first glance, SOD1, which is a highly thermo-stable enzyme (41, 95), seems an unlikely candidate for participation in any process involving protein instability, alterations or misfolding. Nonetheless, a link between SOD1 and ALS was first establish in 1993, by Rosen et al. (37) which described several point mutations in the gene encoding SOD1, localized on chromosome 21q22.1, accounting for 20–25% of fALS cases. The remaining 75–80% of fALS cases are caused by mutations in other genes (96).

More than 100 different mutations have been identified, spanning all five exons of *sod1* gene. Most of these mutations result in the substitution of a single amino acid throughout the 153-residue SOD1 polypeptide, although some mutations result in amino acid insertions and deletions and in truncations of the C terminus. An updated list of the mutations can be found at the online database for ALS genetics, http://www.alsod.org. The vast majority of the mutations are genetically dominant. The only one known exception, D90A, is an oddity since in certain families it is recessive (97), whereas in others it is dominant (98).

Biophysical studies of fALS mutant SOD1 proteins suggest their partition into two groups with distinctly different biophysical characteristics with respect to metal content, SOD activity, and spectroscopy. These two groups have been termed metal-binding region (MBR) and wild-type like (WTL) fALS mutant SOD1 proteins (Fig. 6) on the basis of their SOD activities and metal-binding properties (69). The MBR subset of SOD1 proteins have mutations that are localized in and around the metal-binding sites, including the electrostatic and zinc loops, and were found to have significantly altered biophysical properties relative to WTSOD1. By contrast, the WTL subset of SOD1 protein was found to be remarkably similar to WTSOD1 in most of their properties.

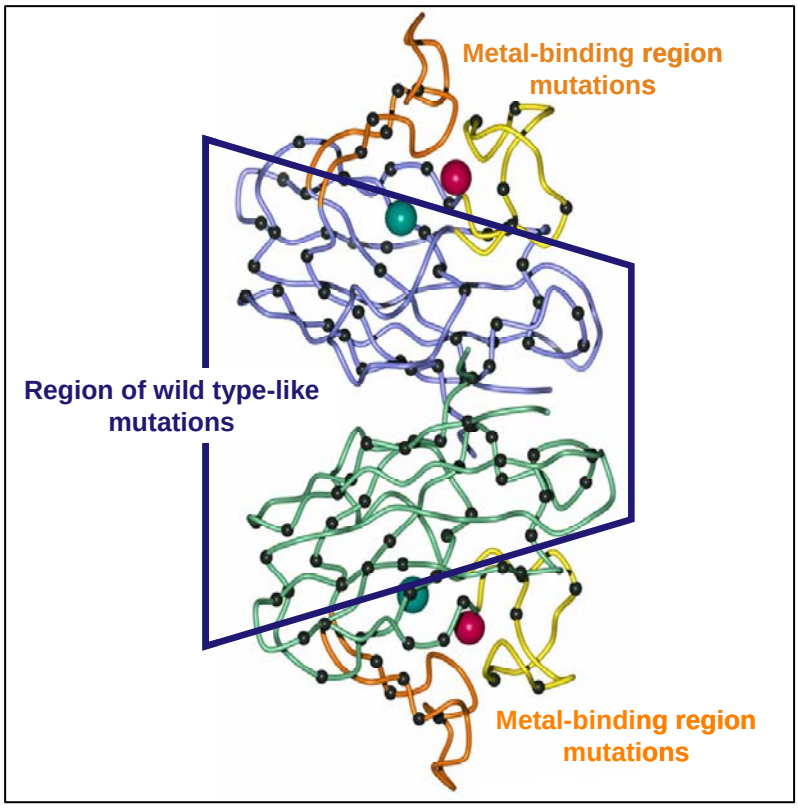

Fig. 6 The two classes of fALS mutant SOD1 proteins: WTL and MBR. Biophysical, biochemical and bioinorganic investigations have shown that ALS-associated variant SOD1 proteins have extremely diverse characters.

Thorough investigations of a broad range of ALS-associated SOD1 variants describe the effects induced by the mutations as one or more of the following perturbations (95):

(a) destabilization of the apo-SOD1$^{S\text{-}S}$ native state (decreased Tm), wherein instability remains even after metallation (relative to the WT protein with an equivalent metallation state);

(b) decrease in the affinity for binding Cu or Zn;

(c) decrease in overall net charge.

On the other hand, there are also few mutations, which can increase the stability of apo-SOD1 (e.g. D124V) or increase the net charge of the protein (e.g. V7E). Examples of perturbations induced by specific single point mutations are reported in Table 2.

Table 2. Biophysical effects induced by some ALS-associated amino acid substitutions in SOD1. (Reprinted from Shaw B. F., Valentine J. S. (2007) How do ALS-associated mutations in superoxide dismutase 1 promote aggregation of the protein? *Trends Biochem. Sci*. **32,** 78–85)

SOD1 variant	Melting temperature (T_m)	Cu,Zn binding affinity	Net charge (pH 7.4)
G85R	↓	↓	↓
G37R	↓	–	↓
G93R	↓	–	↓
H48Q	↓	↓	–
D125H	–	↓	↓
D124V	↑	↓	↓
H46R	↑	↓	↓
G93A	↓	–	–
A4V	↓	–	–
L38V	↓	–	–
L84V	↓	–	–
I113T	↓	–	–
L144F	↓	–	–
V7E	↓	–	↑
E100G	↓	–	↓
S134N	–	↓	–
D90A	–	–	↓
E100K	–	–	↓
D101N	–	–	↓
N139K	–	–	↓

'–' indicates no perturbation of these parameters

1.5.1 Toxic gain of function of SOD1 mutant proteins

Beside a huge effort of data acquisition and speculative debates, how mutated SOD1 leads to motor neuron degeneration remains actually unclear. However, it is well established that SOD1-mediated toxicity in ALS is not due to loss of function but instead to a gain of one or more toxic properties that are independent of the levels of SOD1 activity. The main arguments against the importance of loss of dismutase function are that:

(*a*) SOD1 null mice do not develop motor neuron disease and

(*b*) removal of the normal SOD1 genes in mice that develop motor neuron disease from expressing a dismutase inactive mutant (SOD1G85R) does not affect onset or survival.

In addition, levels of SOD1 activity do not correlate with disease in mice or humans; in fact, some mutant enzymes retain full dismutase activity. Finally, chronic increase in the levels of WTSOD1 (and dismutase activity) either has no effect on disease or accelerates it (99).

1.5.2 Proposed hypotheses for the toxicity of SOD1 mutants in ALS

Over the years, many proposals for ALS mechanisms that underlie the selective killing of upper and lower motor neurons have been put forward. The combination of genetic, pathological and biochemical post-mortem studies has fuelled four primary hypotheses for mechanisms that provoke or contribute to the disease (100):

1. *Oxidative damage*

One of the proposed functions acquired by mutations in SOD1 is the increased peroxidase activity. H_2O_2, normally a product of the superoxide disproportionation, is catalytically converted into highly reactive and toxic hydroxyl radical at Cu^{1+} ion in SOD1 mutant proteins, resulting in enzyme inactivation, oxidative modification of residues at or near the copper site, and loss of metal ions. Increased levels of hydroxyl radical have been reported in transgenic mouse expressing human SOD1 with the G93A mutation (37).

Another aberrant copper chemistry proposed in SOD1 mutant proteins involves a strong oxidant, peroxynitrite ($ONOO^-$). $ONOO^-$ forms from the reaction between nitric oxide (NO) and superoxide anion at a diffusion controlled rate. When SOD1 has no Zn ion bound, a Cu^{1+} ion in SOD1 is proposed to undergo one-electron reduction of molecular oxygen (O_2) to form superoxide anion, which further reacts with NO and leads to the peroxynitrite production. Given that many ALS-associated mutant SOD1 proteins have reduced affinity for Zn ion, an acquired toxic function of SOD1 by mutations may arise from the peroxynitrite chemistry including the tyrosine nitration (37).

Recently, however, aberrant copper chemistry has been questioned as a cause of the SOD1-linked familial ALS; disease symptoms have been found in the transgenic mouse overexpressing the copper-binding-site-null mutant SOD1, in which all four copper ligands (His 46, 48, 63, and 120) are mutated.

While increased oxidative stress is a major pathology found in ALS-model mice and ALS patients, the bulk of the evidence to date does not strongly support the idea that aberrant copper chemistry originating with mutant SOD1 proteins is responsible for the disease (41).

2. *Repetitive motor neuron firing and subsequent excitotoxic death due to mishandling of glutamate, the neurotransmitter that acts on both upper and lower motor neurons*

Glutamate-mediated excitotoxicity from repetitive firing and/or elevation of intracellular calcium by calcium-permeable glutamate receptors has long been implicated in neuronal death. Glutamate released from presynaptic terminals triggers action potentials in motor neurons by

diffusing across the synaptic cleft to activate specific receptors on the dendrites of the postsynaptic neuron. A key component of the mechanisms necessary to prevent repetitive firing is the rapid removal of synaptic glutamate by glutamate transporters. Five subtypes of transporter are known, but it is the glial glutamate transporter EAAT2 that is responsible for ~90% of the clearance for motor neurons (Fig. 8). Evidence of abnormalities in glutamate handling in ALS arose from the discovery of large increases in the levels of glutamate in the cerebrospinal fluid of ALS patients (81–83); a finding now reported in ~40% of sporadic ALS patients. Direct measurement of functional glutamate transport in ALS revealed a marked diminution in the affected brain regions, which was the result of a pronounced loss of the astroglial EAAT2 protein (100). Thus, glutamate excitotoxicity is likely to be an important contributor to neuronal death. Indeed, treatment with the glutamate release inhibitor riluzole is currently the only drug approved for treatment of ALS patients, although it extends survival for only two months on average (101).

3. *Axonal strangulation from neurofilamentous disorganization, an idea supported by the abnormal accumulation of neurofilaments as a pathological feature of many cases of sporadic and SOD1-mediated familial disease*

Another characteristic of ALS is the reduced activity of axonal transport, described first in patients with ALS (102) and more recently in transgenic mouse models of ALS (103) (Fig. 8). The anterograde and retrograde transport of molecules and organelles is a fundamental cellular process that is particularly important for the development, function and survival of motor neurons, which are among the largest and longest cells in the body. Although the molecular basis for this slowing is not fully elaborated, several authors suggest that aggregations of neurofilaments in the proximal axons (spheroids) might physically compromise the transport apparatus (102), at least for anterograde traffic (96).

4. *Toxicity from intracellular aggregates and/or failure of protein folding or degradation a common feature of ALS involving SOD1 mutations*

In the recent years, protein aggregation has been proposed as the most accredited ALS mechanism on the basis of the fact that Bunina body and Lewy body-like hyaline inclusion are found in motor neurons and astrocytes of sporadic and familial ALS patients, respectively (41, 96, 99, 104).

The protein aggregates found in SOD1-related familial ALS patients and transgenic mouse models are strongly immunoreactive to SOD1 (99, 105) (Fig. 7).

The obvious loss of motor neurons in the brain and spinal cord initially focused attention on how mutated SOD1 may act within motor neurons to provoke neuronal degeneration and death. However, as in almost all prominent examples of inherited human neurodegenerative diseases, the mutant gene products are expressed widely. In the case of SOD1, expression is ubiquitous, raising the possibility that the toxic cascade may be achieved wholly, or in part, by mutant SOD1 action in the adjacent non neuronal cells. It has in fact been proved that toxicity to motor neurons from SOD1 mutants is non cell autonomous, that is, it requires mutant damage not just within motor neurons but also to non neuronal cells (99).

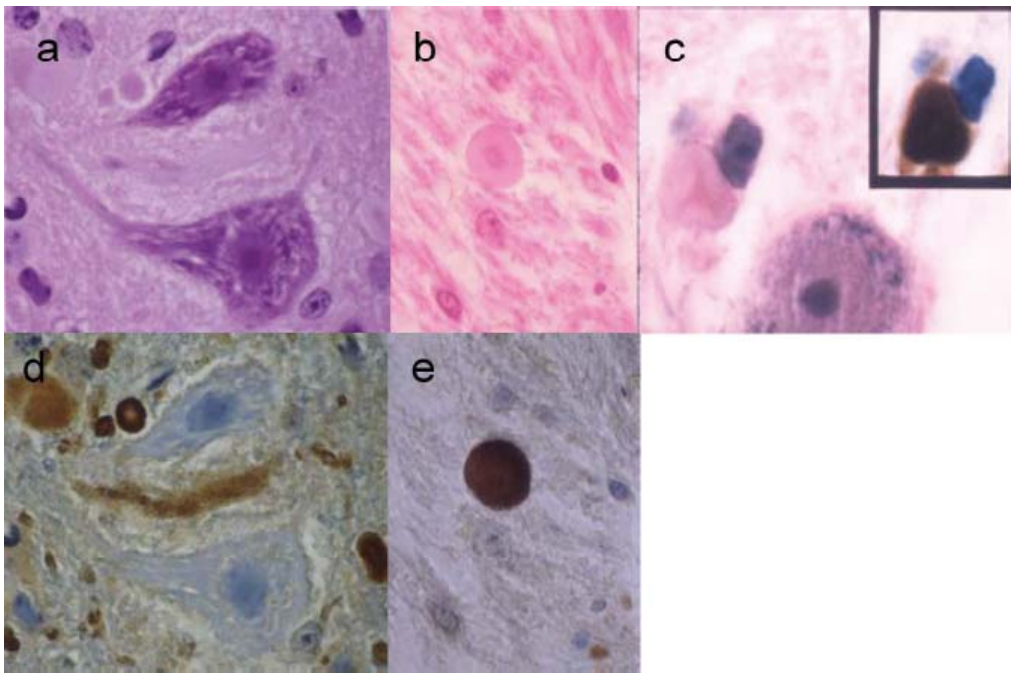

Fig. 7 SOD1 reactive inclusions in both motor neurons and astrocytes. (a) Motor neuron from a SOD1G85R ALS mouse. **(b)** Motor neuron from an ALS patient with SOD1 frameshift mutation at position 126. **(c)** Astrocyte from a SOD1G85R mouse. Top row **(a, b, c)** is stained with hematoxylin and eosin. Bottom row **(d, e)** and the insert in **(c)** represent the same sections stained with an antibody to SOD1. These inclusions are also immunoreactive with antibodies to ubiquitin (not shown). (Reprinted from Bruijn L. I., Miller T. M., Cleveland, D. W. (2004) Unraveling the mechanisms involved in motor neuron degeneration in ALS *Annu. Rev. Neurosci.* **27**, 723–749)

1.5.3 Net charge, subcellular localization and SOD1 aggregation

Most proteins possess a net surface charge (either positive or negative) at physiological pH, and the prevalence of net charge in biology has been proposed to function in part to prevent protein aggregation (106). In fact, decreasing the net charge on a protein usually leads to an increase in the rate of aggregation (107, 108).

Human SOD1 is predicted to have an isoelectric point (pI) of ~5.8 and to carry a net negative charge between 6 and 7 units at pH 7.4. Several ALS-associated SOD1 mutations decrease the net negative charge of SOD1 (Table 2), and this reduction in net charge could promote aggregation. Thus, ALS-associated SOD1 mutations such as D101N, D90A, N139K and E100K that are unlikely to promote SOD1 aggregation by destabilization of the native state or by inhibition of metal binding, might promote aggregation by decreasing the net negative charge of the SOD1 protein.

Furthermore, it is likely that the aggregation-promoting effects of some of the mutations that do result in native state destabilization or metal-binding inhibition are also compounded by a concomitant decrease in net charge. For example, the mutation G37R, which destabilizes SOD1, and the mutation H46R, which inhibits SOD1 metallation without destabilizing the native apo fold, both result in a decrease in the net negative charge of the SOD1 protein (86) (Table 2). Oliveberg and co-workers (109) have also pointed out that a better correlation between SOD1 variant stability and ALS patient survivability can be found when increases or decreases in net charge are taken into account. Mutations that decrease the net charge of a pathogenic protein are also prevalent in familial conditions associated with protein aggregation such as renal amyloidosis, early onset Alzheimer's disease and frontotemporal dementia with Parkinsonism (107).

The local intracellular pH or fluctuations in intracellular pH could also be a factor in SOD1 aggregation, not only because low pH can induce molten globule or partially folded states, but also because of the correlation between net charge and rate of aggregation. Protein aggregation has been observed, *in vitro*, to be fastest at pH values near the isoelectric point of the protein where the net charge is zero (110, 111). SOD1, in addition to being present in the cytosol, is also present in the intermembrane space of mitochondria (112) and, as recently reported, in the trans-Golgi network (113). Because these compartments are more acidic than the cytosol – the intermembrane space by as much as ~0.7 pH units (114) and the trans-Golgi network by up to 2 pH units (115) – SOD1 proteins that are localized in these areas can be expected to have a lower net charge and therefore to have a higher propensity to aggregate. Thus, it is possible that the aggregation propensity of SOD1 could depend on subcellular localization and local variations inside the cells.

1.5.4 Final event in ALS: A cascade of caspases which mediates motor neuron death

Although the primary toxicities of the familial ALS–linked mutations of SOD1 remain unresolved, the final event in the death cascade has been partially clarified. Apoptosis, or

programmed cell death, is thought to be responsible for the end stage of ALS. At this time, mitochondria release cytochrome c and apoptosis inducing factor (AIF) followed by activation of the caspase cascade (116, 117). Activation of caspase-1, one of the early events in the mechanism of toxicity of SOD1 mutants, occurs months prior to neuronal death and phenotypic disease onset. A central feature in cell death mediated by mutant SOD1 is the activation of caspase-3, one of the major cysteine-aspartate proteases responsible for degradation of many key cellular constituents in apoptotic cell death. Caspase-3 activation occurs in motor neurons and astrocytes, where it cleaves the astroglial excitatory amino acid transporter 2 (EAAT2), contemporaneous with the first stages of motor neuron death (99).

It has also been shown that amyotrophic lateral sclerosis-associated SOD1 mutant proteins bind and aggregate with the antiapoptotic factor Bcl2 in spinal cord mitochondria. When entrapped in inclusions, Bcl2 could be directly rendered non-functional. Entrapment and depletion of Bcl2 is supported by studies that show reduced levels of Bcl2 in SOD1 mice and patients with ALS (49).

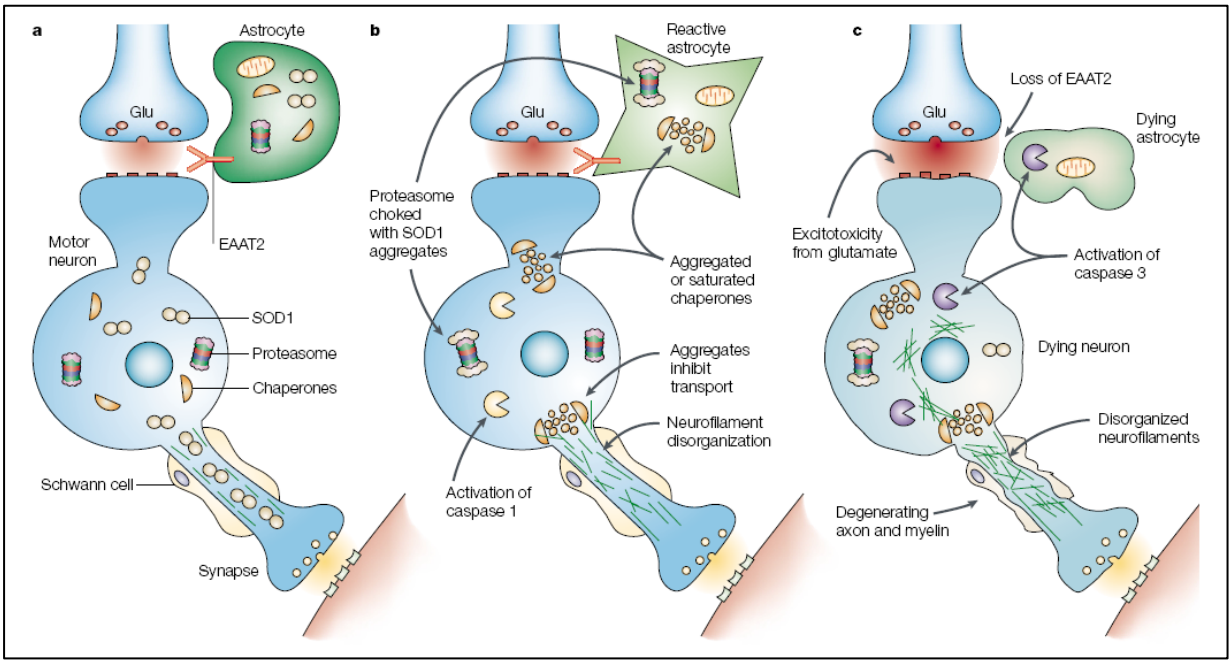

Fig. 8 The specificity of the toxic effect of SOD1 mutations on motor neurons arises from the convergence of several risk factors. (Reprinted from Cleveland D.W., Rothstein J.D. (2001) From Charcot to Lou Gehrig: deciphering selective motor neuron death in ALS *Nat. Rev. Neurosci.* **2,** 806–819)

Figure 8 give us an overall view of the toxicity given by the accumulation of SOD1 aggregates in motor neuronal cells and astrocytes.

(a) In normal cases a lower motor neuron receives signals to fire by the release of glutamate (Glu) from an upstream neuron, either an upper motor neuron or an interneuron. This signal is converted within the motor neuron into action potentials that stimulate the release of acetylcholine (orange) at its axon terminus, triggering muscle contraction.

(b) Accumulation of SOD1 aggregates in the motor neuronal cells triggers a loss of overall protein-folding chaperone activity and inhibits the removal of other damaged proteins by choking the 20S proteasome subunit having as a result the disorganisation of the axonal neurofilaments (inhibiting in this way the transport of components along the axon) and chronically activation of caspase-1.

(c) Inhibition of chaperone and proteasome activity, loss of axonal transport capacity and an accelerated SOD1-mutant burden force chronic deficits in motor neurons. Similar damage in astrocytes suppresses the accumulation and activity of glutamate transporters (EAAT2) that are necessary for recovering synaptic glutamate and for preventing repetitive motor neuron firing. Such disproportionate firing produces excessive calcium entry through calcium-permeable glutamate receptors, activating caspase-3, which serves as the executioner for motor neuron death through the degradation of key cellular components.

1.6 Aims and topics of the research

The propensity of a protein to aggregate is a complex property reflecting a collection of different biophysical and physicochemical parameters such as hydrophobicity, net charge, native state stability and intrinsic β-structure (95). Therefore, an observed increase in the rate of protein aggregation – for any given protein variant – is not always accompanied by a specific defect such as destabilization of the native state or a decrease in net charge but it is given by a combination of more parameters. There is, perhaps, no better example of this complexity than the mutations of SOD1 that cause ALS. This motley crew of variants numbers well over 100 and no single defect has been found to be common among all the mutants that have been studied so far.

The discovery of the relationship between SOD1 mutations and ALS (37) spurred intensive structural and biophysical analyses also in our laboratory, which aimed at revealing the molecular basis for this disease. My colleagues performed a deep study of human WTSOD1, both in the metalated and demetalated forms. When I joined the lab it has already been shown (118) that WTSOD1, when lacking both its metal ions, forms large, stable, soluble protein oligomers by intermolecular disulfide bonds, under physiological conditions. In order to identify, which cysteines were involved in the formation of these intermolecular disulfide bonds, I cloned and purified two SOD1 mutants: C6A, C111S. Negative oligomerization tests on both these mutant proteins proved the involvement of these two cysteines in apo WT protein oligomerization (118).

In order to test the validity of the mechanism proposed for WTSOD1 on its variants, eleven SOD1 mutants (T54R, V87M, G93A, G93D, V97M, I113F, I113T, L144F, D90A - pathogenic and L67V and I35T – non pathogenic) were also selected, cloned and purified in our laboratory (chapter 2.1.3). The mutations were chosen mainly on the basis of their structural location and character of the residue changes. The same characterizations performed for the WTSOD1 (by circular dichroism, optical, fluorescence, light scattering spectroscopies and size exclusion chromatography) were carried out for the mutant proteins in order to investigate their ability to form oligomers in conditions very close to the physiological ones. At this point of the research I contributed in showing that these eleven SOD1 mutants, only when they are in the metal-free form, undergo the same mechanism of oligomerization proposed for the WT metal-free protein (118). Moreover, in order to support the proposed mechanism, I cloned, expressed and studied the triple mutant [C6A, I113T, C111S]. This mutant, in its metal-free form, even though carrying one of the mutations inducing the fastest

oligomerization rate, did not oligomerize because of the absence of the two free cysteines Cys6 and Cys111.

We showed that the rates of oligomerization of SOD1 proteins carrying a single point mutation are different, but they eventually give rise to the same type of soluble oligomeric species only when Cys6 and Cys111 are present (119).

After we succeeded in obtaining these promising results our goal was to enter into the details of the oligomerization mechanism by looking for some structural and dynamic differences between WTSOD1 and its mutants. In particular, I focused my research investigations on the two pathogenic mutants (T54R and I113T), which showed the most diverse rates in the oligomerization process. Residue T54 is located at the SOD1 dimer interface, and in the T54R mutant, it is substituted by a positive residue, showing, in its apo form, the slowest aggregation rate. Residue I113 is located at the dimer interface as well, but, in the I113T variant, it is substituted by a hydrophilic residue, showing, in its apo form, the fastest aggregation rate compared to the apo WTSOD1 protein.

Before starting the structural and dynamic characterization of WTSOD1 and its mutants we had to improve the yield of expression for these proteins since, according to the protocol in use, the total amount of pure proteins obtained in minimal medium was very low (between 8 and 10 mg/L). In order to solve this problem, I cloned the *sod1* gene using the Gateway Technology (Invitrogen), which allows to readily insert it into a different set of expression plasmids codifying for various N-terminal fusion tags. It has already been reported (120) that, in many cases, the presence of these tags improve dramatically the solubility and the expression level of the proteins. Several constructs were expressed for the WTSOD1 protein (chapter 2.1.3) and the obtained results led us to choose the GB1-WTSOD1 fusion protein as the best candidate. I cloned then the mutant proteins in the new expression plasmid codifying for the selected N-terminal fusion tag and NMR and X-ray investigations of the purified proteins were undertaken as described in one of the following chapters (chapter 3.2).

Our new findings led us also to investigate different aspects of the oligomerization process of both apo WT and its ALS-related mutants. I started different and parallel projects, which involve both the characterization of specific ALS-related SOD1 mutants and issues more tightly associated with the oligomerization mechanism and structural aspects of the metal-free WT protein.

I am still in the process of completing a detailed biophysical and structural characterization as well as an investigation of the oligomerization propensity of apo D90A, which is the only SOD1 mutant showing a recessive hereditary pattern (chapter 3.3.1). I am

investigating the stability properties (guanidium-induced protein denaturation) of a slow oligomerizing mutant such as T54R in comparison with the WT protein in order to rationalize their oligomerization rates (chapter 3.3.2). Moreover, an investigation of the early steps of the oligomerization process is described as a work in progress in chapter 3.3.3., as well as preliminary data on the structural characterization of the dimeric metal-free form of WTSOD1 by Solid State NMR (SSNMR) spectroscopy is presented in chapter 3.3.4.

Reference List

1. Ross C.A., Poirier M.A. (2004) Protein aggregation and neurodegenerative disease *Nat Med.* **10 Suppl**, S10–S17. Review.

2. Taylor J.P., Hardy J., Fischbeck K.H. (2002) Toxic proteins in neurodegenerative disease *Science* **296,** 1991−1995.

3. Hardesty B., Kramer G. (2001) Folding of a nascent peptide on the ribosome *Prog. Nucleic Acid Res. Mol. Biol.* **66,** 41–66.

4. Bukau B., Horwich A. L. (1998) The Hsp70 and Hsp60 chaperone machines *Cell* **92,** 351−366.

5. Hartl F. U., Hayer-Hartl M. (2002) Molecular chaperones in the cytosol: from nascent chain to folded protein *Science* **295**, 1852–1858.

6. Chiti F., Dobson C.M. (2006) Protein misfolding, functional amyloid and human disease *Annu. Rev. Biochem.* **75,** 333–366.

7. Ellis, R. J. (2001) Macromolecular crowding: an important but neglected aspect of the intracellular environment *Curr. Opin. Struct. Biol.* **11,** 114–119.

8. Schubert U., Antón L.C., Gibbs J., Norbury C.C., Yewdell J.W., Bennink J.R. (2000) Rapid degradation of a large fraction of newly synthesized proteins by proteasomes *Nature* **404,** 770−774.

9. Hershko A., Ciechanover A. (1992) The ubiquitin system for protein degradation *Annu. Rev. Biochem.* **61,** 761−807.

10. Hershko A. (1997) Roles of ubiquitin-mediated proteolysis in cell cycle control *Curr. Opin. Cell Biol.* **9,** 788−799.

11. N. F. Bence, R. M. Sampat, R. R. Kopito (2001) Impairment of the ubiquitin-proteasome system by protein aggregation *Science* **292,** 1552−1555.

12. Dobson C. M. (2003) Protein folding and misfolding *Nature* **426,** 884−890.

13. Tan S. Y., Pepys M. B. (1994) Amyloidosis *Histopathology* **25,** 403–414.

14. Sunde M., Blake C. C. F. (1997) The structure of amyloid fibrils by electron microscopy and X-ray diffraction *Adv. Protein Chem.* **50,** 123–159.

15. Dobson C. M. (2001) The structural basis of protein folding and its links with human disease *Phil. Trans. R. Soc. Lond. B.* **356,** 133–145.

16. Dobson C. M. (1999) Protein misfolding, evolution and disease *Trends Biochem. Sci.* **24,** 329–332.

17. Fändrich M., Dobson C. M. (2002) The behaviour of polyamino acids reveals an inverse side-chain effect in amyloid structure formation *EMBO J.* **21,** 5682–5690.
18. Dobson C. M. (2003) Protein folding and disease: a view from the First Horizon Symposium *Nature Rev. Drug Discov.* **2,** 154–160.

19. True H. L., Lindquist S. L. (2000) A yeast prion provides a mechanism for genetic variation and phenotypic diversity *Nature* **407,** 477–483.

20. Chapman M. R. et al. (2002) Role of Escherichia coli curli operons in directing amyloid fiber formation *Science* **295,** 851–855.

21. Kelly J. W., Balch, W. E. (2003) Amyloid as a natural product *J. Cell Biol.* **161,** 461–462.

22. Nilsson M.R. (2004) Techniques to study amyloid fibril formation in vitro *Methods* **34,** 151–160.

23. Khurana R. , Uversky V.N. , Nielsen L. , Fink A.L. (2001) Is Congo red an amyloid-specific dye? *J. Biol. Chem.* **276,** 22715–22721.

24. Bousset L., Redeker V., Decottignies P., Dubois S., Le Marechal P., Melki R. (2004) Structural characterization of the fibrillar form of the yeast Saccharomyces cerevisiae prion Ure2p *Biochemistry* **43,** 5022–5032.

25. Serpell L.C., Sunde M., Benson M.D., Tennent G.A., Pepys M.B., Fraser P.E. (2000) The protofilament substructure of amyloid fibrils *J. Mol. Biol.* **300,** 1033–1039.

26. Sunde M., Blake C., (1997) The structure of amyloid fibrils by electron microscopy and X-ray diffraction *Adv. Protein Chem.* **50,** 123 – 159.

27. Harper J.D., Lieber C.M., Lansbury P.T. Jr. (1997) Atomic force microscopic imaging of seeded fibril formation and fibril branching by the Alzheimer's disease amyloid-beta protein *Chem. Biol.* **4,** 951–959.

28. Petkova A.T., Ishii Y., Balbach J.J., Antzutkin O.N., Leapman R.D., et al. (2002) A structural model for Alzheimer's beta -amyloid fibrils based on experimental constraints from solid state NMR *Proc. Natl. Acad. Sci. USA* **99,** 16742–16747.

29. Jaroniec C.P., MacPhee C.E., Astrof N.S., Dobson C.M., Griffin R.G. (2002) Molecular conformation of a peptide fragment of transthyretin in an amyloid fibril *Proc. Natl. Acad. Sci. USA* **99,** 16748–16753.

30. Ritter C., Maddelein M.L., Siemer A.B., Luhrs T., Ernst M., et al. (2005) Correlation of structural elements and infectivity of the HET-s prion *Nature* **435,** 844–848.

31. Makin O.S., Atkins E., Sikorski P., Johansson J., Serpell L.C. (2005) Molecular basis for amyloid fibril formation and stability *Proc. Natl. Acad. Sci USA* **102,** 315–320.

32. Nelson R., Sawaya M.R., Balbirnie M., Madsen A.O., Riekel C., et al. (2005) Structure of the cross-beta spine of amyloid-like fibrils *Nature* **435,** 773–778.

33. Charcot J. M., Joffory A. (1869) Deux cas d'atrophie musculaire progressive avec lesions de la substance grise et des faisceaux antero-lateraux de la moelle epiniere *Arch. Physiol. Neurol. Pathol.* **2,** 744–754.

34. Yoshida S., Mulder D. W., Kurland L. T., Chu C. P., Okazaki H. (1986) Follow-up study on amyotrophic lateral sclerosis in Rochester, Minn., 1925 through 1984 *Neuroepidemiology* **5,** 61–70.

35. Rowland L.P., Shneider N.A. (2001) Amyotrophic lateral sclerosis *N. Engl. J. Med.* **344,** 1688–1700.

36. Cleveland D.W., Rothstein J.D. (2001) From Charcot to Lou Gehrig: deciphering selective motor neuron death in ALS *Nat. Rev. Neurosci.* **2,** 806–819.

37. Rosen D. R. et al. (1993) Mutations in Cu/Zn superoxide dismutase gene are associated with familial amyotrophic lateral sclerosis *Nature* **362,** 59–62. **Reported the landmark discovery that mutations in SOD1 are a primary cause of familial ALS.**

38. McCord J.M., Fridovich I. (1969) Superoxide dismutase. An enzymic function for erythrocuprein (hemocuprein) *J. Biol. Chem.* **244,** 6049–6055.

39. Crapo J.D., Oury T., Rabouille C., Slot J.W., Chang L.Y. (1992) Copper, zinc superoxide dismutase is primarily a cytosolic protein in human cells *Proc. Natl Acad. Sci. USA* **89,** 10405–10409.

40. Chang L.Y., Slot J.W., Geuze H.J., Crapo J.D. (1988) Molecular immunocytochemistry of the CuZn superoxide dismutase in rat hepatocytes *J. Cell Biol.* **107,** 2169–2179.

41. Furukawa Y., O'Halloran T.V. (2006) Posttranslational modifications in Cu, Zn-superoxide dismutase and mutations associated with amyotrophic lateral sclerosis *Antioxi. Redox. Signal.* **8,** 847–867.

42. Kikuchi H., Almer G., Yamashita S., Guegan C., Nagai M., Xu Z., Sosunov A.A., McKhann G.M. II, Przedborski S. (2006) Spinal cord endoplasmic reticulum stress associated with a microsomal accumulation of mutant superoxide dismutase-1 in an ALS model *Proc. Natl. Acad. Sci. USA* **103,** 6025–6030.

43. Jaarsma D., Rognoni F., van Duijn W., Verspaget H.W., Haasdijk E.D., Holstege J.C. (2001) CuZn superoxide dismutase (SOD1) accumulates in vacuolated mitochondria in transgenic mice expressing amyotrophic lateral sclerosis-linked SOD1 mutations *Acta Neuropathol. (Berl.)* **102,** 293–305.

44. Okado-Matsumoto A., Fridovich I. (2001) Subcellular distribution of superoxide dismutases (SOD) in rat liver: Cu, Zn-SOD in mitochondria *J. Biol. Chem.* **276,** 38388–38393.

45. Higgins C.M., Jung C., Ding H., Xu Z. (2002) Mutant Cu, Zn superoxide dismutase that causes motoneuron degeneration is present in mitochondria in the CNS *J. Neurosci.* **22,** RC215.

46. Mattiazzi M., D'Aurelio M., Gajewski C.D., Martushova K., Kiaei M., Beal M.F., Manfredi G. (2002) Mutated human SOD1 causes dysfunction of oxidative phosphorylation in mitochondria of transgenic mice *J. Biol. Chem.* **277,** 29626–29633.

47. Vijayvergiya C., Beal M.F., Buck J., Manfredi G. (2005) Mutant superoxide dismutase 1 forms aggregates in the brain mitochondrial matrix of amyotrophic lateral sclerosis mice. *J. Neurosci.* **25,** 2463–2470.

48. Liu J., Lillo C., Jonsson P.A., Velde C.V., Ward C.M., Miller T.M., Subramaniam J.R., Rothstein J.D., Marklund S., Andersen P.M., et al. (2004) Toxicity of familial ALS-linked SOD1 mutants from selective recruitment to spinal mitochondria *Neuron* **43,** 5–17.

49. Pasinelli P., Belford M.E., Lennon N., Bacskai B.J., Hyman B.T., Trotti D., Brown R.H. Jr. (2004) Amyotrophic lateral sclerosis-associated SOD1 mutant proteins bind and aggregate with Bcl-2 in spinal cord mitochondria *Neuron* **43,** 19–30.

50. Vande Velde C., Miller T.M., Cashman N.R., Cleveland D.W. (2008) Selective association of misfolded ALS-linked mutant SOD1 with the cytoplasmic face of mitochondria *Proc. Natl Acad. Sci. USA* **105,** 4022–4027.

51. Parge H. E., Hallewell R. A., Tainer J. A. (1992) Atomic structures of wild-type and thermostable mutant recombinant human Cu, Zn superoxide dismutase *Proc. Natl. Acad. Sci. USA* **89,** 6109–6113.

52. Strange R. W., Antonyuk S., Hough M. A., Doucette P. A., Rodriguez J. A., P. Hart J., Hayward L. J., Valentine J. S. and Hasnain S. S. (2003) The structure of holo and metal-deficient wild-type human Cu, Zn superoxide dismutase and its relevance to familial amyotrophic lateral sclerosis *J. Mol. Biol.* **328,** 877–891.

53. Bertini I., Mangani S., Viezzoli M. S. (1998) in *Advanced Inorganic Chemistry*, ed. Sykes, A. G. (Academic Press, San Diego, CA, USA) **45,** 127-250.

54. Val Hart P.J., Balbirnie M.M., Ogihara N.L., Nersissian A.M., Weiss M.S., et al. (1999) A structure-based mechanism for copper-zinc superoxide dismutase *Biochemistry* **38,** 2167–78.

55. Val Hough M.A., Hasnain S.S. (2003) Structure of fully reduced bovine copper zinc superoxide dismutase at 1.15 A *Structure* **11,** 937–946.

56. Bordo D., Djinovic K., Bolognesi M. (1994) Conserved patterns in the Cu, Zn superoxide dismutase family *J. Mol. Biol.* **238,** 366–386.

57. Battistoni A., Rotilio G. (1995) Isolation of an active and heat-stable monomeric form of Cu, Zn superoxide dismutase from the periplasmic space of Escherichia coli *FEBS Lett.* **374,** 199–202.

58. Pacello F., Langford P.R., Kroll J.S., Indiani C., Smulevich G., Desideri A., Rotilio G., Battistoni A. (2001) A novel heme protein, the Cu, Zn-superoxide dismutase from Haemophilus ducreyi *J. Biol. Chem.* **276,** 30326–30334.

59. Spagnolo L., Toro I., D'Orazio M., O'Neill P., Pedersen J.Z., Carugo O., Rotilio G., Battistoni A., Djinovic–Carugo K. (2004) Unique features of the sodC-encoded superoxide dismutase from Mycobacterium tuberculosis, a fully functional copper-containing enzyme lacking zinc in the active site *J. Biol. Chem.* **279,** 33447–33455.

60. Tainer J. A., Getzoff E. D., Beem K. M., Richardson J. S., Richardson, D. C. (1982) Determination and analysis of the 2 A-structure of copper, zinc superoxide dismutase *J. Mol. Biol.* **160,** 181–217.

61. Fink R. C., Scandaliios J. G. (2002) Molecular evolution and structure-function relationships of the superoxide dismutase gene families in angiosperms and their relationship to other eukaryotic and prokaryotic superoxide dismutases *Arch. Biochem. Biophys.* **399,** 19–36.

62. Fukuhara R., Tezuka T., Kageyama T. (2002) Structure, molecular evolution, and gene expression of primate superoxide dismutases *Gene (Amst.)* **296,** 99–109.

63. Stanton J. L., Wilton S. D., Laing, N. G. (1996) Characterisation of the chicken Cu, Zn superoxide dismutase gene *DNA Seq.* **6,** 357–360.

64. Repock J. R., Frey H. E., Hallewell, R. A. (1990) Contribution of conformational stability and reversibility of unfolding to the increased thermostability of human and bovine superoxide dismutase mutated at free cysteines *J. Biol. Chem.* **265,** 21612–21618.

65. Fujiwara N., Nakano M., Kato S., Yoshihara D., Ookawara T., Eguchi H, Taniguchi N., Suzuki K. (2007) Oxidative modification to cysteine sulfonic acid of Cys111 in human copper-zinc superoxide dismutase *J. Biol. Chem.* **282,** 35933–35944.

66. Doucette P.A., Whitson L.J., Cao X., Schirf V., Demeler B., Valentine J.S., Hansen J.C., Hart P.J. (2004) Dissociation of human copper-zinc superoxide dismutase dimers using chaotrope and reductant. Insights into the molecular basis for dimer stability *J. Biol. Chem.* **279,** 54558–54566.

67. Lindberg M.J., Normark J., Holmgren A., Oliveberg M. (2004) Folding of human superoxide dismutase: disulfide reduction prevents dimerization and produces marginally stable monomers *Proc. Natl. Acad. Sci. USA* **101,** 15893–15898.

68. Arnesano F., Banci L., Bertini I., Martinelli M., Furukawa Y., O'Halloran T. V. (2004) The unusually stable quaternary structure of human SOD1 is controlled by both metal occupancy and disulfide status *J. Biol. Chem.* **279,** 47998–48003.

69. Valentine J. S., Doucette P. A., Potter S. Z. (2005) Copper-zinc superoxide dismutase and amyotrophic lateral sclerosis *Annu. Rev. Biochem.* **74,** 563–593.

70. Culotta V.C., Yang M., O'Halloran T.V. (2006) Activation of superoxide dismutases: putting the metal to the pedal *Biochim. Biophys. Acta.* **1763,** 747–758.

71. O'Halloran T. V., Culotta V. C. (2000) Metallochaperones, an Intracellular Shuttle Service for Metal Ions *J. Biol. Chem.* **275,** 25057–25060.

72. Rae T. D., Schmidt P. J., Pufahl R. A., Culotta V. C., O'Halloran T. V. (1999) Undetectable Intracellular Free Copper: The Requirement of a Copper Chaperone for Superoxide Dismutase *Science* **284,** 805–808.

73. Rae T. D., Torres A. S., Pufahl R. A., O'Halloran T. V. (2001) Mechanism of Cu, Zn-Superoxide Dismutase Activation by the Human Metallochaperone hCCS *J. Biol. Chem.* **276,** 5166–5176.

74. Lamb A. L., Torres A. S., O'Halloran T. V., Rosenzweig A. C. (2000) Heterodimer formation between superoxide dismutase and its copper chaperone *Biochemistry* **39,** 14720–14727.

75. Culotta V. C., Klomp L. W. J., Strain J., Casareno R. L. B., Krems B., Gitlin, J. D. (1997) The Copper Chaperone for Superoxide Dismutase *J. Biol. Chem.* **272,** 23469–23472.

76. Eisses J. F., Stasser J. P., Ralle M., Kaplan J. H., Blackburn N. J. (2000) Domains I and III of the human copper chaperone for superoxide dismutase interact via a cysteine-bridged Dicopper(I) cluster *Biochemistry* **39,** 7337–7342.

77. Furukawa Y., Torres A. S., O'Halloran T. V. (2004) Oxygen-induced maturation of SOD1: a key role for disulfide formation by the copper chaperone CCS *EMBO J.* **23,** 2872–2881.

78. Hwang C., Sinskey A. J., Lodish H. F. (1992) Oxidized redox state of glutathione in the endoplasmic reticulum *Science* **257,** 1496–1502.

79. Field L. S., Furukawa Y., O'Halloran T. V., Culotta V. C. (2003) Factors Controlling the Uptake of Yeast Copper/Zinc Superoxide Dismutase into Mitochondria *J. Biol. Chem.* **278,** 28052–28059.

80. Khare S.D., Caplow M., Dokholyan N.V. (2004) The rate and equilibrium constants for a multistep reaction sequence for the aggregation of superoxide dismutase in amyotrophic lateral sclerosis *Proc. Natl. Acad. Sci. USA* **101,** 15094–15099.

81. Hayward L.J., Rodriguez J.A., Kim J.W., Tiwari A., Goto J.J., Cabelli D.E., Valentine J.S., Brown Jr. R.H. (2002) Decreased metallation and activity in subsets of mutant superoxide dismutases associated with familial amyotrophic lateral sclerosis, *J. Biol. Chem.* **277,** 15923–15931.

82. Rodriguez J.A., Valentine J.S., Eggers D.K., Roe J.A., Tiwari A., Brown Jr. R.H., Hayward L.J. (2002) Familial amyotrophic lateral sclerosis-associated mutations decrease the thermal stability of distinctly metallated species of human copper/zinc superoxide dismutase, *J. Biol. Chem.* **277,** 15932–15937.

83. Malinowski D.P., Fridovich I. (1979) Subunit association and side-chain reactivities of bovine erythrocyte superoxide dismutase in denaturing solvents, *Biochemistry* **18,** 5055–5060.

84. Forman H.J., Fridovich I. (1973) On the stability of bovine superoxide dismutase. The effects of metals *J. Biol. Chem.* **248,** 2645–2649.
85. Weser U., Miesel R., Hartmann H. J., Heizmann W. (1989) Mummified enzymes, *Nature* **341,** 696.

86. Rodriguez J.A., Shaw B.F., Durazo A., Sohn S.H., Doucette P.A., Nersissian A.M., Faull K.F., Eggers D.K., Tiwari A., Hayward L.J., Valentine J.S. (2005) Destabilization of apoprotein is insufficient to explain Cu, Zn-superoxide dismutase-linked ALS pathogenesis *Proc. Natl. Acad. Sci. USA* **102,** 10516–10521.

87. Fridovich I. (1975) Superoxide dismutases *Annu. Rev. Biochem.* **44,** 147–159.

88. Kurobe N., Suzuki F., Okajima K., Kato K. (1990) Sensitive enzyme immunoassay for human Cu/Zn superoxide dismutase *Clin. Chim. Acta.* **187,** 11–20.

89. Lindenau J., Noack H., Possel H., Asayama K., Wolf G. (2000) Cellular distribution of superoxide dismutases in the rat CNS *Glia* **29,** 25–34.

90. Moriwaki Y., Yamamoto T., Suda M., Nasako Y., Takahashi S., Agbedana O.E., Hada T., Higashino K. (1993) Purification and immunohistochemical tissue localization of human xanthine oxidase *Biochim. Biophys. Acta.* **1164,** 327–330.

91. Cadenas E., Davies K.J. (2000) Mitochondrial free radical generation, oxidative stress, and aging *Free Radic. Biol. Med.* **29,** 222–230.

92. Tyler D.D. (1975) Polarographic assay and intracellular distribution of superoxide dismutase in rat liver *Biochem J.* 147, 493–504.

93. Asayama K., Burr I.M. (1985) Rat superoxide dismutases. Purification, labeling, immunoassay, and tissue concentration *J. Biol. Chem.* **260,** 2212–2217.

94. Pardo C.A., Xu Z., Borchelt D.R., Price D.L., Sisodia S.S., Cleveland D.W. (1995) Superoxide dismutase is an abundant component in cell bodies, dendrites, and axons of motor neurons and in a subset of other neurons *Proc. Natl. Acad. Sci. USA* **92,** 954–958.

95. Shaw B. F., Valentine, J. S. (2007) How do ALS-associated mutations in superoxide dismutase 1 promote aggregation of the protein? *Trends Biochem. Sci.* **32,** 78–85.

96. Pasinelli P., Brown R. H. (2006) Molecular biology of amyotrophic lateral sclerosis: insights from genetics. *Nat. Rev. Neurosci.* **7,** 710–723.

97. Andersen P.M., Nilsson P., Ala-Hurula V., Keranen M.L., Tarvainen I., et al. (1995) *Nat. Genet.* **10,** 61–66.

98. Jonsson P.A., Backstrand A., Andersen P.M., Jacobsson J., Parton M., et al. (2002) *Neurobiol. Dis.* **10,** 327–333.

99. Bruijn L. I., Miller T. M., Cleveland D. W. (2004) Unraveling the mechanisms involved in motor neuron degeneration in ALS *Annu. Rev. Neurosci.* **27,** 723–749.

100. Cleveland D.W., Rothstein J.D. (2001) From Charcot to Lou Gehrig: deciphering selective motor neuron death in ALS *Nat. Rev. Neurosci.* **2,** 806–819.

101. Miller R.G., Mitchell J.D., Lyon M., Moore D.H. (2003) Riluzole for amyotrophic lateral sclerosis (ALS)/motor neuron disease (MND) *Amyotroph. Lateral. Scler. Other Motor Neuron Disord.* **4,** 191–206.

102. Sasaki S., Iwata M. (1996) Impairment of fast axonal transport in the proximal axons of anterior horn neurons in amyotrophic lateral sclerosis *Neurology* **47,** 535–540.

103. Sasaki S., Warita H., Abe K., Iwata M. (2005) Impairment of axonal transport in the axon hillock and the initial segment of anterior horn neurons in transgenic mice with a G93A mutant SOD1 gene *Acta Neuropathol. (Berl.)* **100,** 48–56.

104. Bruijn L.I., Houseweart M.K., Kato S., Anderson K.L., Anderson S.D., Ohama E., Rea ume A. G., Scott R. W. and Cleveland D. W. (1998) Aggregation and motor neuron toxicity of an ALS-linked SOD1 mutant independent from wild-type SOD1 *Science* **281,** 1851–1854.

105. Shibata N., Asayama K., Hirano A., Kobayashi M. (1996) Immunohistochemical study on superoxide dismutases in spinal cords from autopsied patients with amyotrophic lateral sclerosis *Dev. Neurosci.* **18,** 492–498.

106. Gitlin I., Carbeck J.D., Whitesides G.M. (2006) Why are proteins charged? Networks of charge–charge interactions in proteins measured by charge ladders and capillary electrophoresis *Angew. Chem. Int. Ed. Engl.* **45,** 3022–3060.

107. Chiti F., Calamai M., Taddei N., Stefani M., Ramponi G., Dobson C.M. (2002) Studies of the aggregation of mutant proteins in vitro provide insights into the genetics of amyloid diseases *Proc. Natl. Acad. Sci. USA* **99,** 16419–16426.

108. Calamai M., Taddei N., Stefani M., Ramponi G., Chiti F. (2003) Relative influence of hydrophobicity and net charge in the aggregation of two homologous proteins *Biochemistry* **42,** 15078–15083.

109. Lindberg M.J., Byström R., Boknäs N., Andersen P.M., Oliveberg M. (2005) Systematically perturbed folding patterns of amyotrophic lateral sclerosis (ALS)-associated SOD1 mutants *Proc. Natl. Acad. Sci. USA* **102,** 9754–9759.

110. J.P. Schmittschmitt and J.M. Scholtz (2003) The role of protein stability, solubility, and net charge in amyloid fibril formation *Protein Sci.* **12,** 2374–2378.

111. Zhu M., Souillac P.O., Ionescu-Zanetti C., Carter S.A., Fink A.L. (2002) Surface-catalyzed amyloid fibril formation *J. Biol. Chem.* **277,** 50914–50922.

112. Sturtz L.A., Diekert K., Jensen L.T., Lill R., Culotta V.C. (2001) A fraction of yeast Cu, Zn-superoxide dismutase and its metallochaperone, CCS, localize to the intermembrane space of mitochondria. A physiological role for SOD1 in guarding against mitochondrial oxidative damage *J. Biol. Chem.* **276,** 38084–38089.

113. Urushitani M., Sik A., Sakurai T., Nukina N., Takahashi R., Julien J.-P. (2006) Chromogranin-mediated secretion of mutant superoxide dismutase proteins linked to amyotrophic lateral sclerosis *Nat. Neurosci.* **9,** 108–118.

114. Porcelli A.M., Ghelli A., Zanna C., Pinton P., Rizzuto R., Rugolo M. (2005) pH difference across the outer mitochondrial membrane measured with a green fluorescent protein mutant *Biochem. Biophys. Res. Commun.* **326,** 799–804.

115. Paroutis P., Touret N., Grinstein S. (2004) The pH of the secretory pathway: measurement, determinants, and regulation *Physiology (Bethesda)* **19,** 207–215.

116. Zoratti M., Szabo I. (1995) The mitochondrial permeability transition *Biochim. Biophys. Acta.* **1241,** 139–176.

117. Jiang D., Sullivan P.G., Sensi S.L., Steward O., Weiss J.H. (2001) $Zn^{(2+)}$ induces permeability transition pore opening and release of pro-apoptotic peptides from neuronal mitochondria *J. Biol. Chem.* **276,** 47524–47529.

118. Banci L., Bertini I., Girotto S., Martinelli M., Vieru M., Whitelegge J., Durazo A., Valentine J. S. (2007) Metal-free superoxide dismutase forms amyloid-like oligomers: A possible general mechanism for familial ALS *Proc. Natl. Acad. Sci. USA* **104,** 11263–11267.

119. Banci L., Bertini I., Boca M., Girotto S., Martinelli M., Valentine J. S., Vieru, M. (2008) SOD1 and amyotrophic lateral sclerosis: Mutations and Oligomerization *Plos ONE* **3,** e1677.

120. Hammarstrom M, Woestenenk EA, Hellgren N, Hard T, Berglund H (2006) Effect of N-terminal solubility enhancing fusion proteins on yield of purified target protein. *J Struct Funct Genomics* **7,** 1–14.

2

Materials and Methods

2.1 Cloning techniques

2.1.1 Gene cloning

Isolation of sufficient amounts of protein from native sources is often impossible owing to low yields, culturing difficulties of the organism and instability during purification. Therefore, protein production from cloned recombinant DNA is normally the method of choice to obtain the desired protein. The cloning strategy has to be carefully designed, since it will influence the behaviour of the target protein in terms of yield, solubility, folding, etc. Although protein expression is no longer considered a major limiting step and protein purification techniques have improved dramatically in the past years, the problem of producing soluble proteins for purification is still a major concern.

Many years ago it was discovered that some affinity tags are able to enhance the solubility of some of the partner proteins to which they are attached (1). Even if the number of fusion partners is increasing progressively during the years none of these tags work universally with each partner protein. The best way to maximize the probability of obtaining a soluble and correctly folded target protein is to proceed with a parallel cloning and expression of it with a high number of fusion partners.

Anyway, the experience shows that in some cases the classic approach of expressing the native protein without any tag results the most successful one. While the latter classical approache do not require further sub cloning, 'fusion partners' impact on protein solubility leads to sub cloning of the gene of interest in a library of expression vectors that becomes laborious when handling a large number of genes.

Another cloning strategy used in our laboratory is the Gateway® Technology from Invitrogen. The Gateway® Technology is a universal cloning method that takes advantage of the site-specific recombination properties of bacteriophage lambda (2) to provide a rapid and highly efficient way to move our gene of interest into multiple vector systems.

In order to express the gene of interest using the Gateway® Technology the following steps have to be performed:

1. cloning of the gene (which is a blunt-end PCR product) into one of the pENTR/TOPO vectors to generate an entry clone.

2. generation of an expression construct by performing an LR recombination reaction between the entry clone and a Gateway destination vector of choice (Fig. 9)

3. introduction of the expression construct into the appropriate host (*e.g.* bacterial, mammalian, yeast, insect) and expression of the recombinant protein.

This cloning method is faster, due to the higher reaction efficiency and to the fact that only sequencing of the entry clone is required, and most of all, the destination vectors are compatible with one single entry clone making the parallel approach easier.

On the basis of the former considerations, in our laboratory, we usually clone each protein with the classic methods to express the protein in the native form and with Gateway system (Invitrogen) in order to express it with different N-terminal fusion tags (e.g. 6xHis-tag, TRX, GST, MBP, periMBP and GB1).

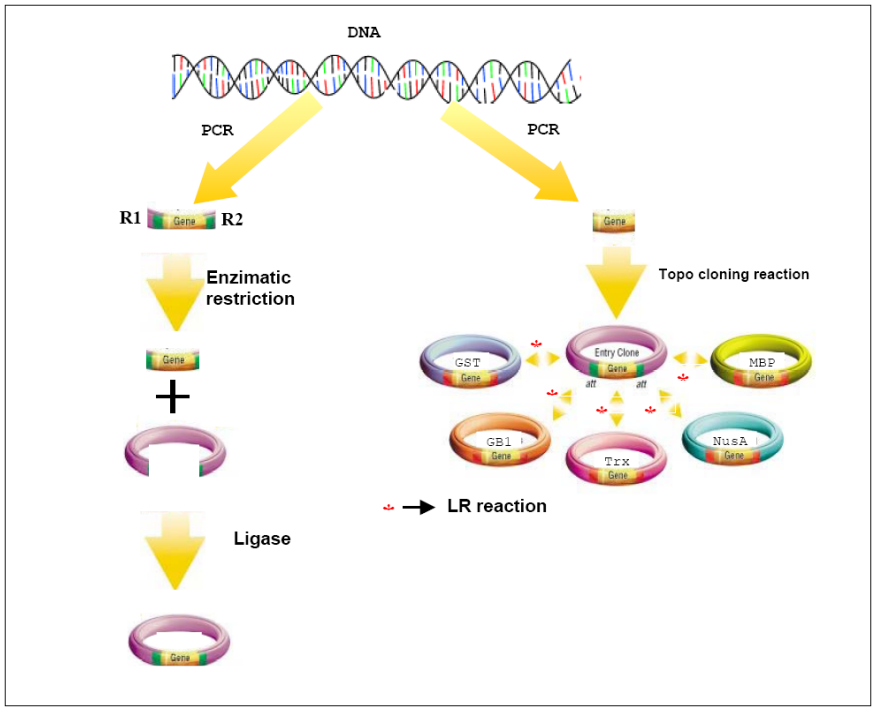

Fig. 9 Schematic comparison between the Classic and the Gateway cloning technology. Theoretically, parallel cloning is possible in both the cases but the Gateway system results faster due to the higher reaction efficiency and less sequencing demand since only the starting pENTR should be sequence verified.

2.1.2 Site-directed mutagenesis

The functional analysis of a protein often requires the generation of a number of single or multiple amino acid variants of the wild type gene. Site-directed mutagenesis is a technique for carrying out vector modification and characterizing the dynamic, complex relationships between protein structure and function. The basic procedure utilizes a supercoiled double-stranded DNA vector with an insert of interest (the gene of interest) and two synthetic oligonucleotide primers containing the desired mutation (Fig 10). The primers, each complementary to opposite strands of the vector, are extended during temperature cycling by a

high fidelity DNA polymerase (*Pfu Turbo*, Stratagene). Extension of the oligonucleotide primers generates a mutated plasmid. After PCR reaction the product is treated with an endonuclease specific for methylated and hemimethylated DNA, *Dpn* I. This enzyme is used to digest the parental DNA template and thus select only the mutation-containing synthesized DNA; this happens because DNA isolated from almost all *E. coli* strains is dam methylated and therefore susceptible to endonuclease digestion. The vector containing the desired mutations is then transformed into XL1-Blue supercompetent cells and subsequently subjected to sequencing analysis.

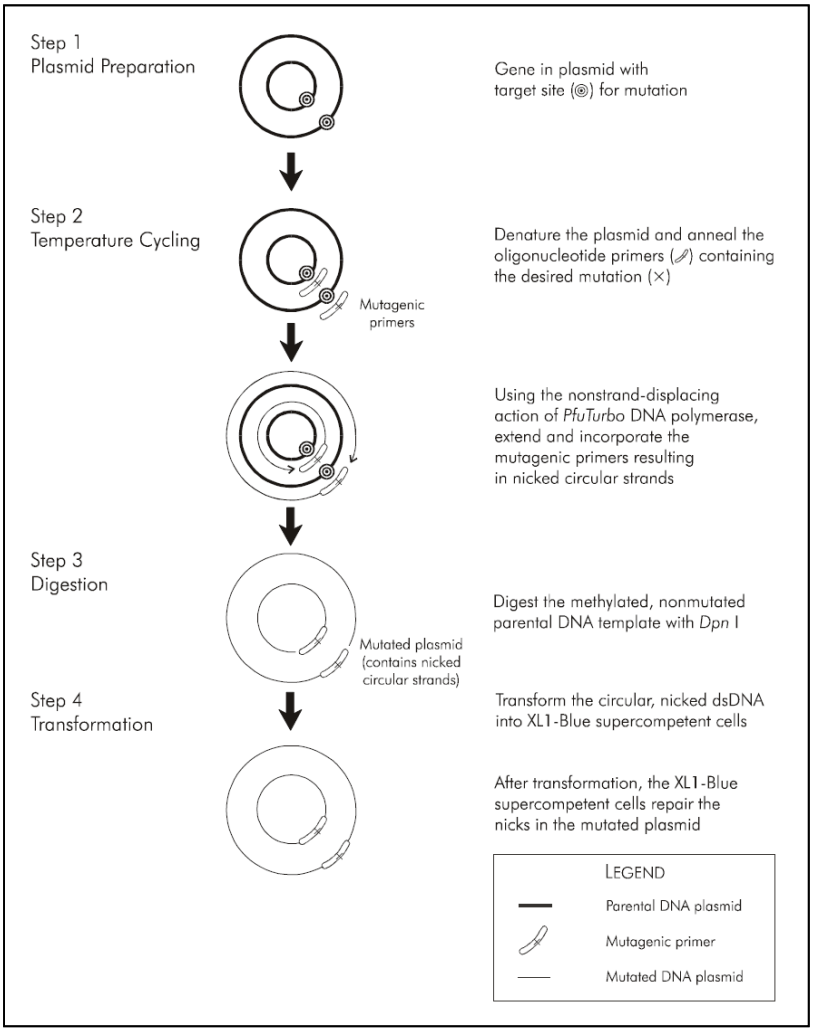

Fig. 10 Overview of the QuikChange® site-directed mutagenesis method. (Reprinted from QuikChange® site-directed mutagenesis instruction manual)

2.1.3 Cloning and site-directed mutagenesis of *sod1* gene

During this PhD thesis, the following WTSOD1 mutants were cloned using the classical approach: I35T, D90A, C6A and C111S. Mutations were performed in pPSOD-Iq plasmid

using a QuikChange™ site-directed mutagenesis kit (Stratagene). The plasmids were propagated and purified by MINI KIT (Invitrogen) and the sequences were verified.

In order to improve the yield of expression and the folding properties of WTSOD1 and some of its mutants obtained with the classic method, the *sod1* gene was cloned by PCR and inserted in Gateway pENTR/TEV/D-TOPO plasmid (Invitrogen). The plasmid was propagated and purified by MINI KIT (Invitrogen) and the sequence was verified. The LR recombination reaction was performed in order to transfer the *sod1* gene from pENTR/TEV/D-TOPO plasmid into different pDest plasmids (pDEST14, pDEST24, pETG20A, pETG30A, pDEST-HisMBP, pDEST-periHisMBP, and pTH34) suitable for protein expression and codifying for various N-terminal fusion tags (6xHis, TRX, GST, MBP and GB1) (Fig. 11). The most efficient expression and purification system was conferred from the small-size fusion partner GB1.

Mutations were performed in the pTH34 plasmid codifying for the GB1 fusion tag, which was chosen as the best candidate, using a QuikChange™ site-directed mutagenesis kit (Stratagene).

Also the pTH34 plasmids containing the following mutations: T54R, I113T, C6A, C111S, C111Y and the triple mutant [C6A, I113T, C111S] were propagated and purified by MINI KIT (Invitrogen) and the sequences were verified.

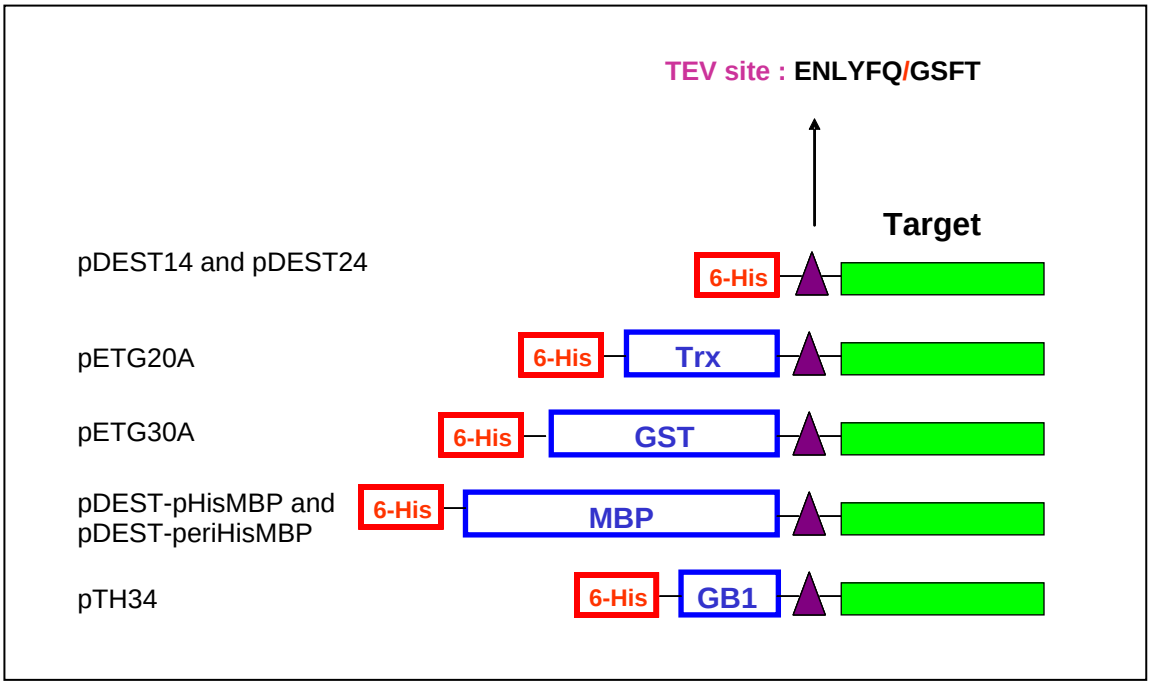

Fig. 11 Different pDest plasmids codifying for various N-terminal fusion tags.

2.2 Protein expression

The variables in a protein expression experiment can be divided into two groups: genetic and environmental. Genetically encoded variables that affect protein expression include the sequence of the open reading frame, the choice of promoter, codon usage, mRNA secondary structure and addition of fused tags. Environmental variables include host strain, growth medium and induction parameters, *e.g.* temperature, IPTG concentration and duration of induction step.

At the moment, several host systems are available for protein expression, including bacteria, yeast, plants, fungi, insect and mammalian cells. The choice is strongly dependent upon the specific requirements for the final product, since it will affect not only the protein expression, but also the subsequent purification.

Unfortunately, many proteins belonging to interesting families, especially the human proteins, are extremely difficult to be produced as soluble proteins in the Gram-negative bacterium *Escherichia coli,* which often represents the first choice as an expression system, since it is the easiest, quickest and cheapest one. Even if in the recent years, the increasing knowledge of additives can assist the "in vitro" refolding process, and numerous proteins have been refolded into their active forms, yet the successful rate of this strategy is very low. Considerable efforts are currently underway to make alternative hosts more accessible and affordable, and eukaryotic systems including mammalian, yeast and insect cell expression are becoming easier and less expensive to be used (3, 4). Cell-free protein synthesis has also great potential for overcoming some of the problems of soluble and membrane proteins expression, but it still remains a work in progress for the time being (5). However, especially for NMR purpose, which requires the production of high yield of labelled ^{15}N and ^{13}C samples, the *E.coli* expression system is nowadays, the most widely used.

Many efforts are currently focused on the optimization of the *E.coli* expression system. Factors such as reduced temperature (6), changes in the *E.coli* expression strain (7), different promoters or induction conditions (8) and co-expression of molecular chaperones and folding modulators (9) have all been examined and, in some specific cases, they led to enhancements of soluble protein production.

In our laboratory, the main system for protein expression is given by different strains of *E. coli* like BL21(DE3)Gold, Rosetta(DE3)pLysS, Rosetta2(DE3), Origami(DE3)pLysS, Origami2(DE3), etc.

At first, expression and solubility screening on a small scale (1-10 ml LB) are usually performed using different *E. coli* strains available in our laboratory and inducing protein expression at two different temperatures (37ºC and 25ºC). The results are checked on SDS polyacrilamide gel (SDS-PAGE) and, on the basis of these data, it is decided whether or not proceeding to the scale-up and testing the expression in minimal medium (M9). This kind of approach allows to explore a large set of expression conditions and to identify the one, which gives the best yield of soluble protein. A second screening is sometimes performed in order to refine expression conditions or, in the case in which all the tests are negative, to redefine the strategy modifying some or all variables, in particular the most influencing ones, such as the choice of bacterial strain, the induction times, the kind of vectors and expression promoters used. If the main part of the protein is produced in the insoluble fraction, an alternative approach is to try an in-vitro refolding screening with different additives in order to obtain a folded and soluble protein. The last choice is to redesign the expressed protein domains or to switch to other expression system.

2.2.1 SOD1 protein expression

T54R, V97M, I113T (the cloning and the preliminary expression tests for these 3 mutants were already done when I joined the lab) I35T, D90A, C6A and C111S native SOD1 mutated proteins, cloned using the classical approach, were expressed in *E. coli* BL21(DE3)Gold. The cells were grown in LB medium in shaking flaks at 37°C until they reached the OD_{600} = 0.6. After induction with 0.7mM IPTG cells were left overnight at the same temperature (37°C).

The GB1-WTSOD1 and GB1-SOD1 mutated proteins were instead over expressed in the *E. coli* Origami pLysS strain (Novagen). The fusion proteins were obtained by growing the cells in minimal medium, in shaking flasks at 37ºC until OD_{600} = 0.7 and then induced with 0.7mM IPTG and left overnight at 25ºC.

The ^{15}N-labeled, ^{15}N- ^{13}C-labeled proteins were obtained by growing the cells in M9 containing 3g/l ^{13}C-Glucose and 1g/l ^{15}N-(NH4)2SO4 and following the above mentioned protocol.

2.2.2 SOD1 protein extraction

Depending on the location of the expression, the protein has to be brought into solution by breaking the cells containing it. There are several methods to achieve this: repeated freezing and thawing, sonication, homogenization by pressure or permeabilization by organic solvents. The method of choice depends on how fragile the protein is and how sturdy the cells are.

For the native SOD1 mutated proteins the extraction from cells periplasma was done by osmotic shock. The proteins were isolated in a 20mM Tris, 150mM NaCl, 0.1mM EDTA, 5mM dithiothreitol (DTT) buffer at pH=8. After incubation for 30 minutes at 37ºC, the proteins were centrifuged at 165,000 × g for 20 minutes. Supernatants were dialyzed against a 20mM Tris, 1mM DTT buffer in order to be loaded on the anionic exchange column.

The GB1-WTSOD1 and GB1-SOD1 mutated proteins were instead isolated from cells cytoplasm by sonication in binding buffer (20mM Tris, 500mM NaCl and 5mM Imidazol) at pH=8.00 and centrifuged at 165,000 × g for 20 minutes.

2.3 Protein purification

Protein purification presents also a number of challenges particularly in the presence of many other contaminant proteins. Separation of one protein from all others is typically the most laborious aspect of protein purification. All the purifications involve several chromatographic steps performed exploiting differences in protein size, physical, chemical and biological properties and binding affinity. The purification strategy depends mainly upon the location of the expressed protein within the host. In fact, the protein can be transported in the periplasmic space or expressed like a soluble or insoluble (inclusion bodies) protein within the cytoplasm. In each case the isolation can be performed with a variety of different techniques. Ion exchange and size exclusion chromatography are commonly used to purify proteins expressed in their native states. The purification of the recombinant proteins with the specific affinity tags is usually done by affinity techniques. Immobilized metal ion affinity chromatography (IMAC) is currently the most commonly used technique which exploits the interaction between transition metal ions (generally, Zn^{2+} or Ni^{2+}) and side-chains of specific amino acids (mainly histidine) on the protein. In some cases, solubility tags have been combined with simple His-tag, allowing the fusion partner to maintain its solubilizing functionality and the His-tag its efficiency as an affinity tag.

For the recombinant proteins, enzymatic digestion with a specific protease is necessary to remove the fusion partner from the target protein and a second IMAC purification is generally

performed in order to separate the two proteins. AcTEV, Factor Xa, Thrombin, Prescission Protease, recombinant Enterokinase are some examples of proteases that are normally used for the cleavage of fusion proteins. The protease specific recognition site is selected and cloned in the vector codifying for the protein sequence at the cloning step. For each protease/fusion protein pilot experiments should be done to define the most suitable conditions.

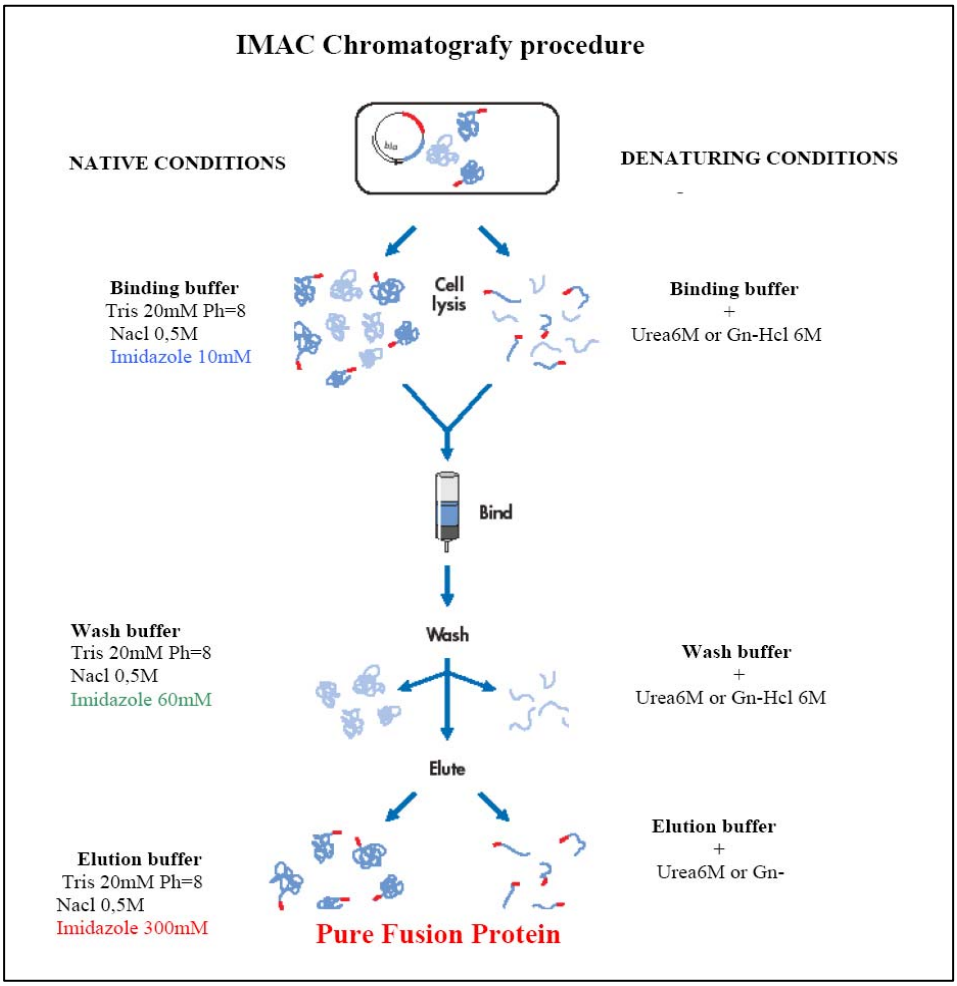

Fig. 12 General purification procedure of a typical His-tagged proteins. (Reprinted from Qiagen handbook for expression and purification of His-tagged proteins)

2.3.1 SOD1 purification

Native SOD1 mutated proteins were purified by Fast Performance Liquid Chromatography (FPLC) using anionic exchange and/or gel filtration techniques. In the first step, proteins were loaded onto a DEAE FF (Amersham Biosciences) anion exchange column and eluted during increasing salt gradient, using chromatographic buffers with 1 mM DTT each. Proteins were typically eluted in two different peaks, one at low salt concentration (around 60mM) and the other at higher salt concentration, thus suggesting the presence of two

differently charged species. The first purification was followed by a size exclusion chromatography when it was necessary.

GB1-WTSOD1 and GB1-SOD1 mutated proteins purification was performed by IMAC using a nickel chelating (Ni^{2+}) column (His-Trap) (Armersham Bioscience). The protein was eluted in 20mM Tris, 150mM NaCl and 300mM imidazol, pH=8.0. After concentration the sample was loaded on a PD-10 desalting column in order to exchange the buffer in 50mM Tris, 0.5mM EDTA, 1mM DTT, pH=8.0. GB1 tag was cleaved with 2µl of AcTEV protease/1mg of fusion protein (Invitrogen, Carlsbad, CA) under overnight incubation at room temperature. The protease digestion was followed by a second IMAC purification in order to separate the protein from the fusion partner. At this point, WTSOD1 and SOD1 mutants, which were initially fused with GB1 tag, lacking the 6xHis fusion parter, do not bind any more the chelating column, while, the GB1 tag is eluted at 300mM of imidazole. Proteins purity was checked on a 17% SDS-PAGE and protein concentration was determined by optical spectroscopy; the extinction coefficient at 265 nm for SOD1 is 15900 $M^{-1}cm^{1}$.

2.4 Sample preparation

Copper-zinc superoxide dismutase is one of the most stable globular proteins studied so far. Structural investigations have been established that the enzyme stability is due to a combination of different factors, including the intrinsic stability of the eight-stranded β barrel fold, the close packing of the hydrophobic interfaces between the subunits, the presence of intramolecular disulfide bond and the active site stabilization induced by metal ions (10–12).

Metal free WTSOD1 (apo form) and its mutants were obtained according to a previously published protocol (13) with some small differences. The proteins buffer was exchanged using PD-10 desalting column (protein concentration was usually around 3 mg/ml). The modified procedure implies two buffer exchanges in 50mM acetate, 10mM EDTA, pH=3.8 followed by 3 days of incubation at 4ºC. A further overnight exchange in the same buffer with 100mM NaCl was then performed, followed by the last two exchanges in 20mM phosphate buffer, pH=7.

WTSOD1 protein was reconstituted with both zinc and copper ions (Cu_2, Zn_2) SOD1 according to the procedure described below (14). (E_2, Zn_2) SOD1 was obtained by addition of one equivalent of zinc per subunit in a 50 mM acetate buffer, pH=5.0 followed by 12 hours incubation at room temperature. This form was further reconstituted with copper in a 20mM

Tris buffer pH=8.0 resulting in (Cu_2, Zn_2) SOD1. The SOD1 mutant proteins were reconstituted with zinc only by addition to the apo-form of two equivalents of zinc per subunit in 20 mM Tris buffer, pH=8.0. Metal content of these various forms of SOD1 was checked by inductively coupled plasma mass spectrometry (ICP-MS) using a Thermo Jarrell Ash Atomscan Model 25 Sequential inductively coupled spectrometer.

Polyethylene glycol (PEG)/pH, $(NH)_4SO_4$/pH screenings using the vapour diffusion technique vapour were performed in order to obtain SOD1 crystals suitable for X-ray diffraction. Crystals of apo SOD1 (WT, T54R, I113T and D90A) were obtained at 288K from solutions containing 0.1 M MES (pH=6.5) or 0.1 M HEPES (pH=7.0), 20% PEG 3350. The final protein concentration was in all cases 0.1 mM.

2.5 Biophysical characterizations

Once obtained a pure protein, several studies can be done in order to characterize it. First of all, mass spectroscopy analysis is performed in order to verify the protein identity and understand if the sequence has the N-terminal methionine. Solubility and stability of the proteins, at high concentrations, generally represent an indication of a good folding. Before proceeding to the preparation of labelled samples the degree of "foldedness" is estimated by ^{1}H-NMR and circular dichroism spectroscopy. The latter technique could be suitable also to evaluate the thermal stability. Size exclusion chromatography coupled with multiangle light scattering is performed in order to determine the aggregation state of the protein in solution. The metal content is analyzed by atomic absorption measurements. Disulfide status could be checked by SDS−PAGE after modification with 4-acetamido 4' maleimidylstilbene-2, 2'-disulfonic acid, or more accurately, by mass spectroscopy after modification with iodoacetamide.

Once we are sure that the produced proteins are stable, a more complete set of biophysical and biochemical characterizations can be performed according to the particular research problem and system under investigation.

2.5.1 Circular Dichroism

Circular Dichroism (CD) is an excellent method to analyze protein and nucleic acid secondary structure in solution and it can be used to follow the changes in folding as a function of temperature or denaturant. CD is a phenomenon occurring when asymmetrical molecules

interact with circularly polarized light, thus absorbing left and right hand circularly polarized light with different absorption coefficients. In proteins the major optically active groups are the amide bonds of the peptide backbone, typically disposed in highly ordered arrays such as α-helices or β-pleated sheets. In dependence of the orientation of the peptide bonds in the arrays, given by the symmetry of its disposition, optical transitions are differently split by exciton splitting, thus yielding characteristic spectral profiles for each of the three basic secondary structures of a polypeptide chain (α-helical, β-sheet or random-coil structures). A protein consisting of these elements will therefore display a spectrum that can be deconvoluted into the tree individual contributions; for this purpose several mathematical methods have been developed, all of them relying on the assumption that the spectrum of a protein can be represented by a linear combination of the spectra of its secondary structural elements, plus a noise term which includes the contribution of aromatic chromophores.

Circular dichroism spectroscopy is particularly good to:

· determine whether a protein is folded, and if so, characterizing its secondary structure and the structural family to which it belongs.

· compare the structures of a protein obtained from different sources (e.g. species or expression systems) or comparing structures for different mutants of the same protein.

· study the conformational stability of a protein under stress (thermal stability, pH stability, and stability to denaturants) and how this stability is altered by buffer composition or addition of stabilizers.

· determine whether protein-protein interactions alter the conformation of protein.

2.5.2 Fluorescence

Fluorescence spectroscopy is a type of electromagnetic spectroscopy, using a beam of light, which analyzes fluorescence from a sample. Given its extremely high sensitivity and selectivity, it is an important investigational tool in many areas including material sciences, analytical sciences, and across a broad range of chemical, biochemical and medical research. It has become an essential investigational technique allowing detailed, real-time observation of the structure and dynamics of intact biological systems. The pharmaceutical industry uses it heavily and it has become a dominating technique in biochemistry and molecular genetics.

Fluorescence is the result of a three-stage process that occurs in certain molecules (generally polyaromatic hydrocarbons or heterocycles) called fluorophores or fluorescent dyes. A fluorescent probe is a fluorophore designed to localize within a specific region of a biological specimen or to respond to a specific stimulus. The process responsible for the

fluorescence of fluorescent probes and other fluorophores is illustrated by the simple electronic-state diagram (Jablonski diagram) shown in (Fig. 13).

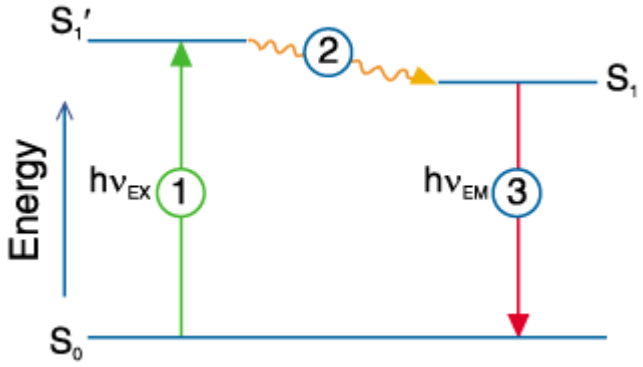

Fig. 13 Jablonski diagram illustrating the processes involved in the creation of an excited electronic singlet state by optical absorption and subsequent emission of fluorescence. The labeled stages 1, 2 and 3 are explained in the adjoining text.

Excitation (stage 1). A photon of energy $h\nu_{EX}$ is supplied by an external source such as an incandescent lamp or a laser and absorbed by the fluorophore, creating an excited electronic singlet state (S_1').

Excited-State Lifetime (stage 2). The excited state exists for a finite time (typically 1–10 nanoseconds). During this time, the fluorophore undergoes conformational changes and is also subject to a multitude of possible interactions with its molecular environment. These processes have two important consequences. First, the energy of S_1' is partially dissipated, yielding a relaxed singlet excited state (S_1) from which fluorescence emission originates. Second, not all the molecules initially excited by absorption return to the ground state (S_0) by fluorescence emission. Other processes such as collisional quenching, fluorescence resonance energy transfer (FRET) and intersystem crossing may also depopulate S_1. The fluorescence quantum yield, which is the ratio of the number of fluorescence photons emitted (stage 3) to the number of photons absorbed (stage 1), is a measure of the relative extent to which these processes occur.

Fluorescence Emission (stage 3). A photon of energy $h\nu_{EM}$ is emitted, returning the fluorophore to its ground state S_0. Due to energy dissipation during the excited-state lifetime, the energy of this photon is lower, and therefore of longer wavelength, than the excitation photon $h\nu_{EX}$.

Indeed, proteins, with aromatic amino acids are “intrinsically” fluorescent when excited by UV light. The three amino acid residues that are primarily responsible for the inherent

fluorescence of proteins are tryptophan, tyrosine and phenylalanine. These residues have distinct absorption and emission wavelengths and differ in the quantum yields (Table 3).

Table 3. Fluorescent characteristic of the aromatic amino acids.

	Absorption		**Fluorescence**	
Amino Acid	Wavelength(nm)	Absorption	Wavelength(nm)	Quantum Yield
Tryptophan	280	5,600	348	0.20
Tyrosine	274	1,400	303	0.14
Phenylalanin	257	200	282	0.04

Protein fluorescence is generally excited at 280 nm or at longer wavelengths, usually at 295 nm. In the first case, we obtain the excitation of both tryptophan and tyrosine residues but, due to tryptophan's large absorptivity, the fluorescence spectrum usually resembles that of tryptophan. In the second case, using an excitation wavelength of 295 nm we can obtain a selective excitation of the tryptophan. The fluorescence of the aromatic residues varies in a somewhat unpredictable manner in various proteins. The quantum yield may be either increased or decreased by the folding. Accordingly, a folded protein can have either greater or less fluorescence than the unfolded form. The intensity of fluorescence is not very informative in itself. The magnitude of intensity, however, can be used as a probe of the perturbation of the folded state.

The fact that protein conformal transitions, corresponding to the transition between different states, like folded and unfolded, oxidized and reduced, are generally characterized by different fluorescence intensities (15) was exploited in order to determine the relative stability of this states under different conditions. Progressive protein unfolding in guanidinium chloride (16), or a disulfide bond red-ox potential (17) are some examples of interesting protein properties that can be monitored in this way. Moreover, proteins can be covalently labelled with various fluorophores, thus producing fluorescent protein conjugates. The emission from these attached tags is called "extrinsic" fluorescence**.** Tagging a protein with fluorescent labels is an important and valuable tool for protein characterization.

ThioflavinT (ThT) fluorescence is a commonly used method to monitor fibril formation. This method is particularly attractive since ThT fluoresces only when bound to fibrils. The reaction between the protein and ThT is completed within 1 minute and ThT does not interfere with aggregation. Free ThT has excitation and emission maxima at 350 nm and

450 nm, respectively. However, upon binding to fibrils the excitation and emission change to 450 nm and 485 nm, respectively (18). The structure of ThT has a hydrophobic end with a dimethylamino group attached to a phenyl group, linked to a more polar benzothiazole group containing the polar N and S. This combination of polar and hydrophobic regions creates the possibility for thioflavin T molecules to form micelles in aqueouse solution, with hydrophobic interiors and the positively charged N pointing toward the solvent. The benzothiazole moiety is a combination of a hydrophobic phenyl ring linked to a thiazole ring with positively charged nitrogen. ThT micelles binding involves hydrogen bond formation between charged nitrogen in the thiazole group to fibrils (19).

In the present work, ThT fluorescence spectroscopy was used in order to investigate the tendency of the apo, copper depleted and fully metallated, human WTSOD1 and some of its mutants to form fibrillar aggregates under incubation in condition close to the physiological ones (100μM and 37°C) .

2.5.3 Reaction with 4-acetamido 4' maleimidylstilbene-2, 2'-disulfonic acid (AMS)

AMS is a reagent that covalently reacts with free thiol groups, and its molecular weight is about 500 Da; it therefore modifies protein mobility when it runs in a SDS-PAGE. This iodoacetamide derivate has high water solubility and is readily conjugated to thiols.

The number of free cysteines in WTSOD1 and its mutants were monitored on a SDS-PAGE according to the following protocol. 10ul samples containing 2-4% SDS, 10μM protein, 100μM AMS were prepared. After incubation for 1h at 37°C and addition of FSB3X without DTT the samples were run on SDS-PAGE. Samples prepared following the same procedure, but without the addition of AMS were used as reference.

2.5.4 Light scattering

Laser light scattering is a “non-invasive” technique that provides the absolute molecular weight (MW) and size of macromolecules in solution; the amount of light scattered is directly proportional to the product of the weight-average molar mass and the concentration of the macromolecule. Thus monitoring the size of a protein molecule is a way of observing the structure changes which may happen over time, pH, ionic strength, and it also provides information about the oligomeric state of the protein. Since laser light scattering provides the MW average for all molecules in solution it is generally useful to utilize it coupled with the gel filtration technique.

In this work, SOD1 aggregation was monitories by gel filtration and light scattering. 100 µl aliquots of the incubated proteins at 37ºC were periodically taken and analyzed by gel filtration on Superdex 75 HR 10/30 (Amersham Biosciences) at room temperature. The column was preequilibrated with 20 mM potassium phosphate, pH=7.0, and the flow rate was 0.6 ml/min. The chromatogram, which monitors the species formed during incubation, was obtained by monitoring the absorbance at 280 nm. 20µl aliquots of the incubated proteins at 37ºC were also periodically taken and analyzed by gel filtration on G2000SW$_{XL}$ and G4000SW$_{XL}$ (Tosoh Bioscience) columns at room temperature. The columns were preequilibrated with 20 mM potassium phosphate, pH=7.0, and the flow rates were 0.7 and 1 ml/min respectively. The chromatogram, which monitors the species formed during incubation, was obtained by monitoring the absorbance at 280 nm.

While Superdex 75 HR 10/30 is a semi-preparative gel filtration columns, the G2000/4000SW$_{XL}$ are analytical ones. Their void volumes are 75 kDa, 150 kDa and 7000 kDa respectively. The Superdex column was used when a separation of the dimer from the rest of the oligomeric species was necessary for further analysis. The G2000SW$_{XL}$ analytical column was used to monitor the very initial steps of the oligomerization process while the successive time points, in which a larger oligomer, with MW higher than 150 kDa, was formed, were better observed with the G4000SW$_{XL}$ column.

The G2000SW$_{XL}$ and G4000SW$_{XL}$ columns were also connected to a light scattering spectrometer. The online multiangle light scattering (MALS) detector (DAWN EOS, Wyatt Technology, Santa Barbara, CA) and differential refractive index (DRI) detector (Optilab DRI, Wyatt Technology) setup was used to measure the light scattered as a function of angle and absolute protein concentration of fractions eluting from the size-exclusion chromatography column. The Zimm/Debye approximations were used in the Astra software (Wyatt Technology) to estimate molar mass. Data were fit using a second-order polynomial. The analysis was performed for each one of the 20µl aliquots periodically taken from the incubation batches so as to monitor the increase in molecular weight of the soluble species formed during aggregation.

2.6 Structural characterization

Determination of protein structure is a top priority for complete understanding of proteins role and function. There are many techniques suitable to study different structural aspects of

cellular components, but two techniques allow a resolution at the level of distinguishing individual atoms: X-ray crystallography and Nuclear Magnetic Resonance (NMR).

2.6.1 X-ray crystallography

X-ray crystallography uses the diffraction pattern of X-rays, which are shot through a crystal. The pattern is determined by the electron density within the crystal. The diffraction is the result of an interaction between the high energy X-rays and the electrons in the atom. The electrons get activated and their relaxation to the initial energy state emits new X-rays. Bundles of such waves can be enhanced if they are in phase, and they get cancelled out if they are out of phase. Therefore, the diffraction of parallel X-rays from an object containing thousands of unit molecules arranged in a regular lattice, results in the enhancement and cancellation of the diffracted waves. A resulting pattern of this vectorial process can be correlated with the distribution of the electrons in the crystal.

X-ray crystallography requires the growth of protein crystals up to 100/300 micron in size from a highly purified protein source. The most time consuming process on the path to determining molecular structure is protein crystallization. This involves screening a large number of buffer conditions until the ones ideal to induce protein crystallization are found. Once a well-diffracting crystal (< 2.5Å) is obtained the structure determination can proceed quickly especially if the structural model of a protein with good sequence homology to the unknown one has already been determined.

X-ray structures are high resolution structures enabling resolutions of the order of 1Å. Yet they depict a static structure, the result of a technique which requires large, stable protein crystals, within which each protein unit is lined up in a regular lattice. It was soon recognized that these static structures didn't really help explaining function because the structures are mostly the average of millions of identical units. 'Loose' structural parts like surface loops often failed to be resolved leaving some protein structures incomplete. The development of nuclear magnetic resonance techniques, NMR, was also used to overcome such kind of problems.

2.6.2 NMR spectroscopy

NMR measurements are carried out in solution under conditions that can be as close as possible to the physiological state. Some times even if crystal structures are available,

additional data in solution are needed to determine the potential biological function of the protein. NMR is not only capable of solving protein structures to atomic resolution but it also has the unique ability of accurately measure the dynamic properties of proteins and can also supply information on protein folding and on intra-, as well as, intermolecular interactions. Furthermore, the analysis through NMR spectroscopy easily allows the characterization under several, different experimental conditions, such as different ionic strength and pH. A protein sample characterized by a good circular dichroism spectrum, a good ^{1}H-NMR or better a good ^{1}H-^{15}N HSQC spectrum and if it is stable in time, has high probability to be suitable for NMR structural characterization.

Nuclear magnetic resonance spectroscopy, which was first used to determine the three-dimensional structure of a protein in 1985 (20, 21), relies on the fact that some atomic nuclei, such as hydrogen, are intrinsically magnetic. In a magnetic field, these magnetic nuclei can adopt states of different energy. Applying radio-frequency radiation can induce the nuclei to flip between these energy states, which can be measured and depicted in the form of a spectrum.

The NMR properties of a nucleus – such as the energy difference between the orientations and therefore the frequency at which that nucleus absorbs energy – depends on its chemical environment. Magnetic nuclei are affected by each other as well as the applied field, both through chemical bonds and over short distances through space. This can be exploited to assign resonance signals to particular nuclei in a complex structure, and derive constraints for the distances that separate them.

The steps towards NMR structure determination can be summarized as follows: preparation of the protein solution, NMR measurements, assignment of NMR signals to individual atoms in the molecule, identification of conformational constraints (e.g. distances between hydrogen atoms), calculation of the 3D structure on the basis of the experimental constraints. NMR spectra of biological macromolecules contain hundreds or even thousands of resonance lines which cannot be resolved in conventional one-dimensional spectra (1D). In fact, the interpretation of NMR data requires correlations between different nuclei, which are implicitly contained in 1D spectrum but often are difficult to extract. Multidimensional NMR spectra provide both, increased resolution and correlations which are easy to analyze.

During its relatively short history, protein NMR already has undergone several transformations that have extended its size limit (Fig. 14) (22, 23). These transformations were brought about by technical advances in NMR spectroscopy and by progress in protein labeling schemes. The assignment of resonance initially were accomplished by analyzing two-

dimensional homonuclear spectra, limiting the size of proteins suitable for NMR studies under 10 kDa because of spectral complexity. The subsequent availability of uniformly $^{15}N/^{13}C$-labeled proteins produced in bacteria led to the development of the so-called triple resonance experiments in the late 1980s and early 1990s. These multidimensional heteronuclear experiments establish sequential connections of backbone resonance on the basis of the larger and more uniform heteronuclei through-bond couplings instead of through-space couplings that vary greatly in intensity depending on the local conformation. In addition, the NMR signals have been spread effectively into additional ^{15}N and/or ^{13}C dimensions, alleviating spectral degeneracy. These advances, together with the later incorporation of pulsed field gradients, extended the range of proteins suitable for NMR to 25 kDa. ^{2}H labeling of proteins has contributed greatly to the field of protein NMR. By substituting the nonexchangeable protons with deuterons, the relaxation time of heteronuclear signals are prolonged, resulting in narrowed linewidth and a dramatic increase in resolution and sensitivity. This has increased the size limit of protein NMR to 35 kDa (22).

In the latest nineties, the availability of higher field magnets (^{1}H frequency of 800 MHz) has allowed the development of new experimental improvements such as TROSY-type experiments (22), which show significantly narrower linewidth and higher sensitivity.

New recently developed experiments, in combination with extensive protein deuteration, have successfully been used for the detection of amide resonances in systems up to 900 kDa (23). New improvements of the experimental as well as technological aspects of NMR are constantly increasing the protein size limit observable through this technique with the aim of making most proteins accessible to NMR analysis.

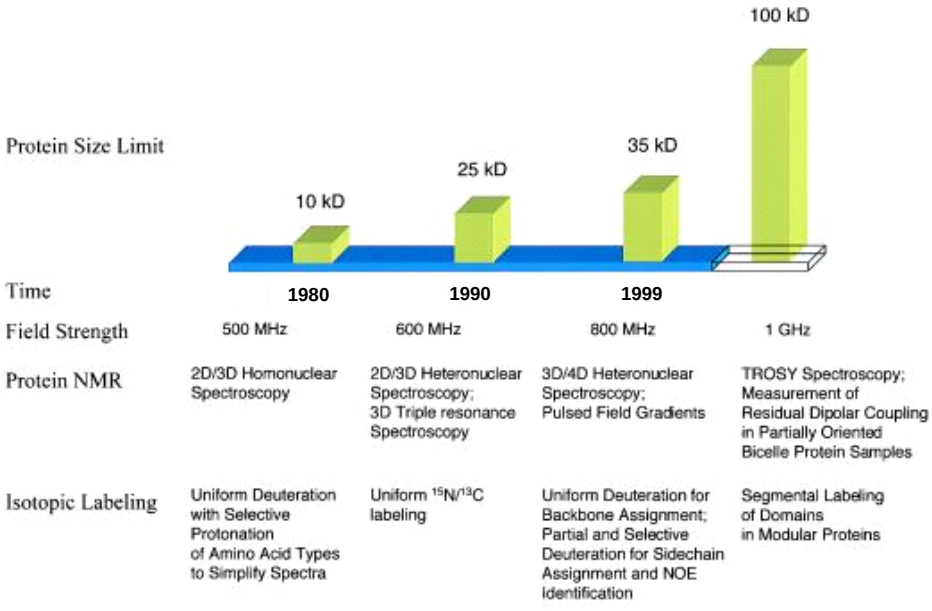

Fig. 14 Advances in NMR spectroscopy and isotopic labeling have extended the size limit of protein NMR.

Reference List

1. Kapust R.B., Waugh D.S. (1999) Escherichia coli maltose-binding protein is uncommonly effective at promoting the solubility of polypeptides to which it is fused *Protein. Sci.* **8,** 1668–1674.

2. Landy A. (1989) Dynamic, structural, and regulatory aspects of lambda site-specific recombination *Ann. Rev. Biochem.* **58,** 913–949.

3. Holz C., Hesse O., Bolotina N., Stahl U., Lang C. (2002) A micro-scale process for high-throughput expression of cDNAs in the yeast Saccharomyces cerevisiae *Protein Expression & Purification* **25,** 372–378.

4. Boettner M., Prinz B., Holz C., Stahl U., Lang C. (2002) High-throughput screening for expression of heterologous proteins in the yeast Pichia pastoris *Journal of Biotechnology* **99,** 51–62.

5. Klammt C., Schwarz D., Lohr F., Schneider B., Dotsch V., Bernhard F. (2006) Cell-free expression as an emerging technique for the large scale production of integral membrane protein *FEBS J.* **273,** 4141–4153.

6. Hammarstrom M., Hellgren N., Van Den Berg S., Berglund H., Hard T. (2002) Rapid screening for improved solubility of small human proteins produced as fusion proteins in Escherichia coli *Protein Sci.* **11,** 313–321.

7. Miroux B., Walker J.E. (1996) Over-production of proteins in Escherichia coli: mutant hosts that allow synthesis of some membrane proteins and globular proteins at high levels *J, Mol. Biol.* **260,** 289–298.

8. Qing G., Ma L.C., Khorchid A., Swapna G.V., Mal T.K., Takayama M.M., Xia B., Phadtare S., Ke H., Acton T. (2004) Cold-shock induced high-yield protein production in Escherichia coli *Nat. Biotechnol.* **22,** 877–882.

9. De Marco A., De Marco V. (2004) Bacteria co-transformed with recombinant proteins and chaperones cloned in independent plasmids are suitable for expression tuning *J. Biotechnol*. **109,** 45–52.

10. Banci L., Bertini I., Cramaro F., Del Conte R., Viezzoli M.S. (2002) The solution structure of reduced dimeric copper zinc superoxide dismutase. The structural effects of dimerization *Eur. J.Biochem.* **269,** 1905–1915.

11. Fisher C.L., Cabelli D.E., Tainer J.A., Hallewell R.A., and Getzoff E.D. (1994) The role of arginine 143 in the electrostatics and mechanism of Cu, Zn superoxide dismutase: computational and experimental evaluation by mutational analysis *Proteins* **19,** 24–34.

12. Bertini I., Mangani S., Viezzoli M. S. (1998) in *Advanced Inorganic Chemistry*, ed. Sykes A. G. (Academic Press, San Diego, CA, USA) **45,** 127–250.

13. Valentine J.S., Pantoliano M.W., McDonnell P.J., Burger A.R., Lippard S.J. (1979) pH-dependent migration of copper(II) to the vacant zinc-binding site of zinc-free bovine erythrocyte superoxide dismutase *Proc. Natl. Acad. Sci. USA* **76,** 4245–4249.

14. Beem K.M., Rich W.E., Rajagopalan K.V. (1974) Total reconstitution of copper-zinc superoxide dismutase *J. Biol. Chem.* **249,** 7298–7305.

15. Holmgren A. (1972) Tryptophan fluorescence study of conformational transitions of the oxidized and reduced form of thioredoxin *J. Biol. Chem.* **247,** 1992–1998.

16. Tsou C. L. (1995) Inactivation precedes overall molecular conformation changes during enzyme denaturation *Biochim. Biophys. Acta* **1253,** 151–162.

17. Haugstetter J., Blicher T., Ellgaard L., (2005) Identification and characterization of a novel thioredoxin-related transmembrane protein of the endoplasmic reticulum *J. Biol. Chem.* **280,** 8371–8380.

18. LeVine H. 3rd (1993) Thioflavine T interaction with synthetic Alzheimer's disease beta-amyloid peptides: detection of amyloid aggregation in solution *Protein Sci.* **3,** 404–410.

19. Krebs M.R., Bromley E.H., Donald A.M. (2005) The binding of thioflavin-T to amyloid fibrils: localisation and implications *J. Struct. Biol.* **149,** 30–37.

20. Williamson R.L., Kwiram A.L. (1984) Optically detected magnetic resonance in lysozyme: evidence for three phosphorescent TRP residues *Biochem. Biophys. Res. Commun.* **125,** 974–979.

21. Kaptein R., Zuiderweg E.R., Scheek R.M., Boelens R., van Gunsteren W.F. (1985) A protein structure from nuclear magnetic resonance data. lac repressor headpiece *J. Mol. Biol.* **182,** 179–182.

22. Hongtao Yu (1999) Extending the size limit of protein nuclear magnetic resonance *Proc. Natl. Acad. Sci. USA* **96,** 332–334.

23. Fiaux J., Bertelsen E.B., Horwich A.L., Wüthrich K. (2002) NMR analysis of a 900K GroEL GroES complex *Nature* **418,** 207–211.

3

Results

3.1

SOD1 and amyotrophic lateral sclerosis: mutations and oligomerization

Lucia Banci, Ivano Bertini, Mirela Boca, Stefania Girotto, Manuele Martinelli, Joan Selvester Valentine, Miguela Vieru

OPEN ACCESS Freely available online

PLoS one

SOD1 and Amyotrophic Lateral Sclerosis: Mutations and Oligomerization

Lucia Banci[1,2], Ivano Bertini[1]*, Mirela Boca[1], Stefania Girotto[1], Manuele Martinelli[1], Joan Selverstone Valentine[3], Miguela Vieru[1]

1 Magnetic Resonance Center (CERM), Department of Chemistry, University of Florence, Florence, Italy, **2** FiorGen Foundation, Florence, Italy, **3** Department of Chemistry and Biochemistry, University of California Los Angeles, Los Angeles, California, United States of America

Abstract

There are about 100 single point mutations of copper, zinc superoxide dismutase 1 (SOD1) which are reported (http://alsod.iop.kcl.ac.uk/Als/index.aspx) to be related to the familial form (fALS) of amyotrophic lateral sclerosis (ALS). These mutations are spread all over the protein. It is well documented that fALS produces protein aggregates in the motor neurons of fALS patients, which have been found to be associated to mitochondria. We selected eleven SOD1 mutants, most of them reported as pathological, and characterized them investigating their propensity to aggregation using different techniques, from circular dichroism spectra to ThT-binding fluorescence, size-exclusion chromatography and light scattering spectroscopy. We show here that these eleven SOD1 mutants, only when they are in the metal-free form, undergo the same general mechanism of oligomerization as found for the WT metal-free protein. The rates of oligomerization are different but eventually they give rise to the same type of soluble oligomeric species. These oligomers are formed through oxidation of the two free cysteines of SOD1 (6 and 111) and stabilized by hydrogen bonds, between beta strands, thus forming amyloid-like structures. SOD1 enters the mitochondria as demetallated and mitochondria are loci where oxidative stress may easily occur. The soluble oligomeric species, formed by the apo form of both WT SOD1 and its mutants through an oxidative process, might represent the precursor toxic species, whose existence would also suggest a common mechanism for ALS and fALS. The mechanism here proposed for SOD1 mutant oligomerization is absolutely general and it provides a common unique picture for the behaviors of the many SOD1 mutants, of different nature and distributed all over the protein.

Citation: Banci L, Bertini I, Boca M, Girotto S, Martinelli M, et al (2008) SOD1 and Amyotrophic Lateral Sclerosis: Mutations and Oligomerization. PLoS ONE 3(2): e1677. doi:10.1371/journal.pone.0001677

Editor: Sotirios Koutsopoulos, Massachusetts Institute of Technology, United States of America

Received October 26, 2007; **Accepted** January 17, 2008; **Published** February 27, 2008

Funding: This work was supported by the European Community "Understanding Protein Misfolding and Aggregation by NMR" (UPMAN) Grant LSHG-CT-2004-512052 (11/1/04–10/31/07), by MIUR PRIN-2005 2005039878 and by Marie Curie Host Fellowship for Early Stage Research Training MEST-CT-2004-504391 "NMR in Inorganic Structural Biology." It also was supported by National Institutes of Health Grants DK46828 and NS049134 (to J.S.V.).

Competing Interests: The authors have declared that no competing interests exist.

*E-mail: bertini@cerm.unifi.it

Introduction

Amyotrophic lateral sclerosis (ALS) is a neurological disease that causes the death of motor neurons with consequent muscular paralysis [1]. Although it is predominantly a sporadic disease, 10% of the ALS cases are described as familial (fALS). A link between fALS and mutations in the SOD1 gene was first suggested in 1993 [2], and over 100 fALS-linked mutations, distributed throughout the SOD1 gene, are now associated with approximately 20% of the fALS cases [1,3,4]. The pathogenicity of SOD1 mutants has been demonstrated to be due to the gain of a toxic function and not to the loss of the normal function. Thus SOD1 knock-out mice do not show any ALS symptoms, whereas transgenic mice, expressing, for example, the fALS associated mutant G93A human SOD1, develop the symptoms, despite expression of endogenous mouse SOD1 [1,5]. Studies of the properties of the isolated ALS-mutant SOD1 proteins have *not* revealed the nature of their toxic properties. Some of the mutations differently affect protein stabilities, metal ion affinities and SOD1 activities, while others do not [3,6,7,8]. Thus the molecular mechanisms by which the mutations cause fALS are currently unknown.

Protein aggregates and inclusions are a common pathological feature of many neurological disorders such as Huntington's, Alzheimer's and Parkinson's diseases [9]. In these neurodegenerative diseases, misfolding, aggregation, and precipitation of proteins seem to be directly related to neurotoxicity. The finding of proteinaceous aggregates containing SOD1 in motor neurons of postmortem fALS patients and transgenic mice was therefore a major advance in the field since it suggested that aggregation of SOD1 is related to the pathology of SOD1-linked fALS [10]. As in the other neurodegenerative diseases, it appears unlikely that the visible SOD1-containing inclusions themselves are toxic; rather their presence suggests that smaller, soluble high molecular weight oligomeric precursor species containing SOD1 are being generated *in vivo* [11].

Eukaryotic copper, zinc superoxide dismutase (SOD1) is a 32-kDa homodimeric metalloenzyme, found predominantly in the cytosol, but also in the mitochondrial intermembrane space, nucleus, and peroxisomes. Each of the two subunits of SOD1 forms an eight-stranded Greek key β-barrel and contains an active site that binds a catalytic copper ion (binding residues: His46, His48, His63 and His120) and a structural zinc ion (binding residues: His63, His71, His80 and Asp83). Its functional role is that of catalyzing the dismutation of superoxide radical to dioxygen and hydrogen peroxide [12,13]. The mature, correctly folded and enzymatically active form of SOD1 is obtained *in vivo* through several post-translational modifications: acquisition of

zinc and copper ions, disulfide bond formation, and dimerization [3,14,15]. Attention has been focused on how mutations could affect these steps of SOD1 maturation. We have recently shown that wild type (WT) human SOD1, when lacking both its metal ions, forms large, stable, soluble, amyloid-like protein oligomers in solutions exposed to air, under physiological conditions (37°C, pH 7, and 100 μM protein concentration) [16]. Oligomerization was shown to occur through a combination of oxidation of Cys 6 and Cys 111 and formation of amyloid-like interactions between beta strands, as judged by the ability of the oligomers to bind the amyloid-binding dye thioflavin T (ThT), a benzothiazole dye that exhibits increases in fluorescence intensity upon binding to amyloid fibers [17].

The next question therefore was to discover whether fALS-linked mutations in SOD1 oligomerize through the same, common mechanism and, if so, whether this mechanism can be proposed as generally associated to the ALS pathology.

With this aim, we selected a number of mutants, most of which related to fALS. All of them were characterized in the apo and zinc-reconstituted states with respect to their ability to form soluble large molecular weight oligomers. Just as in the WT SOD1, we found that demetallation is the key factor for fALS-mutant SOD1 oligomerization and that intersubunit disulfide bonds involving the free Cys residues, Cys6 and Cys111, as well as formation of ThT-binding non-covalent interactions, uniquely characterize the soluble oligomeric species formed. This sheds a new light on the entire story of ALS and its familial cases. It may be suggested that metal-free SOD1 itself is a cause of ALS and that a number of mutants associated with fALS may be more prone to oligomerization *in vivo*. We found that all of the fALS mutant SOD1 proteins tested, just like WT SOD1, form these high molecular weight oligomers, and that some, but not all, of the fALS mutant SOD1 proteins form them at remarkably fast rates.

Results

We have recently reported that apo WT SOD1 gives rise to soluble oligomers under aerobic conditions when the protein is kept at 37°C and at a concentration and pH close to physiological, i.e., 100 μM and pH 7. The resulting soluble oligomers are formed by intermolecular disulfide covalent bonds and by non-covalent interactions between beta strands, forming amyloid-like structures capable of binding ThT [16].

The SOD1 mutants (figure 1), which are reported to be linked to fALS disease, were selected following the criteria indicated in Table 1. We selected mutants spread over the entire protein: some of the mutations are located at the subunit-subunit interface, some add a positively charged residue, others substitute an hydrophobic residue with an hydrophilic one, or some produce a simple side chain size variation. Other mutations are on residues either located on secondary structural elements, namely β strands, or just outside them, with change to residues favoring a helical conformation. We also selected a mutation, on a residue in a loop, which introduces a negative charge in the hydrophobic core of the protein. Finally, we introduced two mutations not reported to be related to fALS. Each of these mutant proteins was analyzed with respect to its behavior toward oligomerization, and correlations were sought between the mutant behavior, the nature of the mutation, and its location on the sequence. We purposely introduced the mutations on the "real" WT SOD1 and not on the thermostable form where the two free cysteines (6 and 111) are changed to alanine and serine, respectively (so-called AS SOD1) [18]. This is an essential condition as we have shown that the presence of these two cysteines is the key for SOD1 oligomerization [16].

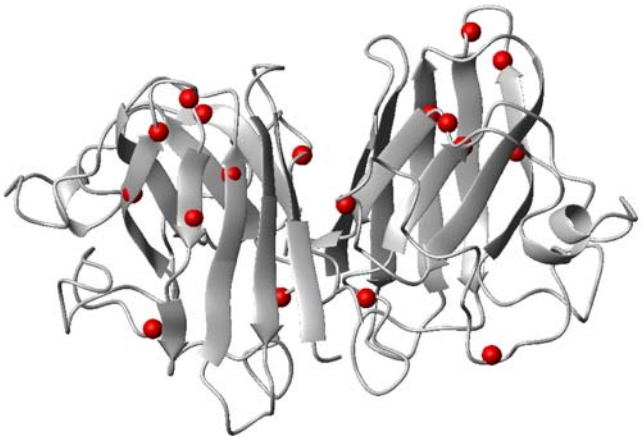

Figure 1. SOD1 investigated mutations. Location of the investigated mutations (red spheres) mapped on the (Cu,Zn) WT SOD1 structure (pdb-ID 1l3n).
doi:10.1371/journal.pone.0001677.g001

Each of the mutants, in the zinc-reconstituted as well as in the apo form, retained the dimeric quaternary structure, as assessed by gel filtration chromatography, which also demonstrated the absence of any significant amount of high molecular weight species. Circular dichroism (CD) spectra on both metallated and apo proteins indicated that the secondary structure present in WT SOD1 was fully conserved in all of the mutants. It has been shown previously that reduction of the intramolecular disulfide bond of apo WT SOD1 causes complete monomerization [15]. We therefore inferred, from the dimeric state of the apo form of all the mutant proteins, that the intrasubunit disulfide bond was intact. For some of the mutants (T54R, V97M and I113T), the folded state of the proteins and the intact disulfide bond were also experimentally confirmed from their ^{1}H-^{15}N HSQC NMR spectra since their cysteine residues 57 and 146 have shifts very close to those observed for oxidized WT SOD1, but far from those of reduced WT.

Optical and fluorescence spectroscopies, the latter with the use of the ThT, coupled with gel chromatography, showed that the zinc-bound proteins did not give rise to any oligomeric species

Table 1. Mutants studied in this work and their criteria of selection

Mutations	Criteria of choice
Thr54Arg	Dimer interface, charge change to positive amino acid
Val87Met	Amino acid with α propensity within β strand
Asp90Ala	Amino acid at the protein surface
Gly93Ala	Amino acid with α propensity just outside β strand
Gly93Asp	Charge variation (to negative residue) on buried amino acid
Val97Met	Amino acid with α propensity within β strand
Ile113Phe	Dimer interface, still hydrophobic amino acid
Ile113Thr	Dimer interface, change to hydrophilic amino acid
Leu144Phe	Amino acid with decreased α propensity just outside β strand
Ile35Thr	Non-ALS mutation located on the only SOD1 β strand without mutations; mutation from polar hydrophobic amino acid to non-polar hydrophilic amino acid
Leu67Val	Non-ALS mutation on a pathogenic site located on the zinc-binding loop

doi:10.1371/journal.pone.0001677.t001

when they are incubated at pH 7, 37°C, 100 μM concentration, for periods of time longer than a month. The absence of formation of any large molecular weight species was confirmed by gel filtration chromatography. Consistently, turbidity at 400 nm showed no insoluble precipitate. These data indicate that, similar to WT SOD1 [16], the zinc-bound forms of any SOD1 mutant are stable even under prolonged incubation at 37°C.

By contrast, the behavior of the metal-free (apo) form was dramatically different. Upon incubation at 37°C in the air, a progressive increase in ThT-binding fluorescence was observed for the apo form of all the mutants. Figure 2 shows the ThT-binding behavior of the eleven SOD1 mutants, together with that of apo WT SOD1, over a period of more than one year. The temperature dependence of this process was tested for incubations ranging from 15 to 40°C. While at 15°C the oligomerization process is much slower starting after 5–6 days, in the range 36–40°C a difference of one degree Celsius almost doubles the detected rates (data not shown). When a reducing agent such as DTT was added to the solutions of the mutants (tested for T54R, V87M, D90A, G93A, V97M, I113T and L144F), the oligomeric species were destroyed, leading to monomeric species, thus showing that the oligomerization occurs through disulphide bonds. The soluble oligomers, which appear to have a similar amyloid-like structure, as judged by their ThT-binding behavior, are stabilized by H-bond interactions between beta strands of SOD1 subunits. To test further for the existence of these non-covalent interactions, GdnHCl, a cauthropic agent that breaks hydrogen bonds, was added to the oligomers. For each of the mutants tested (T54R, V87M, D90A, I113F, I113T and L144F), the ThT-binding fluorescence was quenched in few minutes, whereas gel filtration of the resulting solutions showed that high-molecular-weight species remained present. While the loss of ThT-binding ability is due to the disruption of the amyloid-like structure of the oligomeric assemblies, the persistence of the oligomeric state is due to the covalent disulfide bonds between the free cysteines of the monomeric subunits.

The rates of oligomerization and consequently of fluorescence increase, is found to depend on the nature of the mutation, being for some mutants strikingly different from that of apoWT SOD1. In particular, three mutants (G93A, V97M and I113T) showed a very

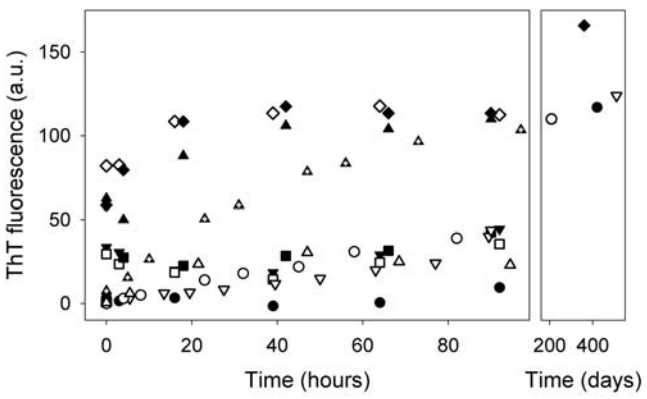

Figure 2. Formation of ThT-binding structures when apo SOD1 mutants and WT are incubated at 37°C. Fluorescence due to ThT binding to SOD1 mutants (presented as arbitrary units, A.U.) for apo T54R SOD1 (•); apo L67V SOD1 (Δ), apo D90A SOD1 (∇), apo I113F SOD1 (□), apo V87M SOD1 (▼), apo WT SOD1 (O), apo L144F SOD1 (■), apo I35T SOD1 (▲), apo V97M SOD1 (▲), apo G93A SOD1 (◇), apo I113T SOD1 (♦), during the incubation of the samples at 37°C. Apo G93D SOD1 mutant is not reported because the oligomeric species formed precipitates after about 30 hours of incubation.
doi:10.1371/journal.pone.0001677.g002

fast initial rate of oligomerization, more than twice that of WT SOD1. I35T, a mutant not currently linked to fALS, showed a significantly slower rate of oligomer formation than these three, but the rate was still higher relative to the WT SOD1 protein. The other mutants showed rates of oligomer formation very similar to apo WT SOD1 or, in one case, i.e., T54R SOD1, slightly lower than it. Thus the rates of aggregation for the fALS mutant proteins studied can be divided in two groups, some with rates of oligomerization very similar to that of apo WT SOD1 and three others much faster, with one, non-ALS mutant SOD1 oligomerizing at an intermediate rate. It is important to stress that in no case did a human SOD1 apoprotein fail to form soluble, high molecular weight oligomers. Repeated trials of each of the mutants also established that the kinetics of oligomer formation were highly reproducible as monitored by increases in ThT fluorescence. The data for T54R, D90A, I113T SOD1, and WT SOD1 apoproteins are shown in figure S1.

It is not only the location of the mutation, but also the nature of the amino acid substitution that determines the oligomerization rate. For example, mutation of Ile113 induces a very fast rate of oligomerization, much faster than WT, when is substituted with Thr, but close to that of WT when Ile is replaced by Phe.

Similar oligomerization behavior is also observed for the two mutants, up to now not reported to be involved in ALS. The I35T mutant, located in $\beta 3$ strand, showed a fast increase in ThT fluorescence (figure 2), and therefore in the rate of oligomerization, as also evidenced by the gel chromatographic analysis (data not shown), while the other mutant here investigated, L67V, ologomerizes with a slower rate, similarly to WT SOD1. The oligomerization of mutants I35T and L67V, in their apo forms, supports our mechanism suggesting that the process would take place for any mutation only when the protein is in the apo form, but not in the zinc-bound form, as we have extensively verified.

In any case, it is important to note that, despite the different aggregation rates, the fluorescence limits at very long times (about 1 year) are similar, indicating the formation of very large molecular weight oligomers for WT and all of the mutant SOD1 proteins studied (figure 2 and figure S1).

The pattern of oligomerization, detected through fluorescence, was paralleled by gel filtration data. The data for the two mutants with the two extreme oligomerization rates, as observed in the fluorescence experiments, (I113T and T54R) are shown in figures 3 and 4. After about 100 hours, while I113T was mostly in high molecular weight states, even if not yet as the final, highest molecular weight ones, mutant T54R was still essentially all in the dimeric state. Gel filtration data also indicated that the final status (after about one year) contains a distribution of high MW species, up to the column cut off (7×10^6 Da). The presence of intermediate MW species is also observed during the long period of the aggregation process; they eventually evolve towards the final very high MW species. Multi-angle light scattering analyses of the samples along the oligomerization process also showed that the average molecular weight was increasing as a function of time (figure 3, Table S1), with a decrease of the fraction of the dimeric species and the increase of that of the oligomers. The increase in ThT-fluorescence and that in molecular weight from light scattering go in parallel, with a linear correlation between the fraction of aggregated specie (non-dimer) and the ThT-binding fluorescence at each period of incubation (figure 5). This correlation indicates that similar increase in fluorescence corresponds to similar increase in oligomeric species. Multi-angle light scattering data of samples after long periods of incubation, when they reach a steady state condition, provide very similar average molecular weights for all the mutants (of the order of 10^6 Da), indicating that the oligomers eventually have essentially the same size, independently of the rate of aggregation.

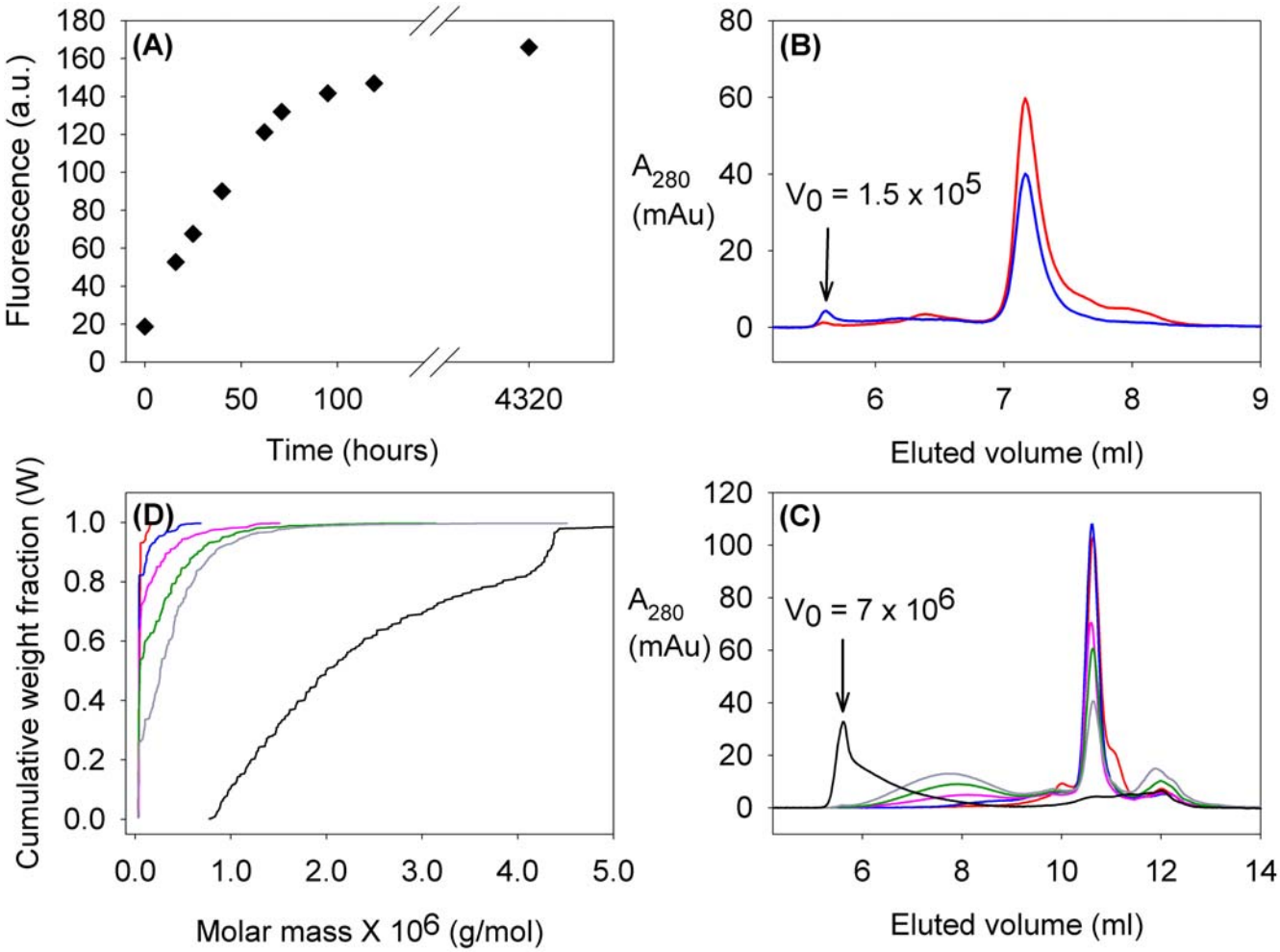

Figure 3. Formation of oligomeric structures when apo I113T SOD1 mutant is incubated at 37°C. (A) Fluorescence due to ThT binding to SOD1 mutants (presented as arbitrary units, A.U.) for apo I113T SOD1 during the incubation of the samples at 37°C. Panels **(B)** and **(C)** shows the size exclusion chromatograms on a G2000SW_{XL} and a G4000SW_{XL} Tosoh columns respectively, corresponding to the samples analyzed by light scattering. The void volume is labeled V_0. **(D)** Variation in species distribution during incubation of apo I113T SOD1. Each curve shows the molecular weight distribution detected by light scattering for the sample after different incubation times at 37°C. In all four panels the samples can be identified according to the following colors: before incubation (—), after 16 hours (—), 40 hours (—), 62 hours (—), 4 days (—) and 6 months (—) of incubation at 37°C.
doi:10.1371/journal.pone.0001677.g003

Discussion

It is now well assessed that, in neuronal tissues of SOD1-linked fALS patients, visible protein aggregates are present that contain aggregated SOD1 and that these aggregates are essentially associated to mitochondria [19,20]. What is still not understood are the factors and the mechanisms inducing this aggregation. fALS-related SOD1 mutations have been found distributed all over the entire protein and of every possible nature (i.e. charge reversal, charge increase or decrease, from hydrophobic to hydrophilic, different residue size, etc.) with no reasonable correlation/rational between the mutation and the ability to give rise to aggregates. It was already suggested that metal-deficient forms of SOD1 mutants might have a role in fALS [21,22] but no general relation has been suggested up to now between lack of metal ion and protein aggregation.

Our data on WT SOD1 and on its mutants would then suggest a general feature in the relation between SOD1 and ALS: the apo protein, before it is metalated, is susceptible to oligomerization. Lack of oligomer formation for the metallated proteins shows that metallation is a key factor to inhibit oligomerization. SOD1 or its mutants enter mitochondria as demetallated [23,15] and, as such, may undergo an abundant oxidation and consequently oligomerization on the way to maturity i.e. before metal binding.

Therefore, independent of the presence and of the nature of the mutation, factors that prevent SOD1 from being efficiently and quickly metalated could lead to protein oligomerization and consequently to disease onset. While it has been shown that the metal-loaded forms of most of the mutant SOD1's are stable and hardly lose the metal ions once metalated as also holds for WT SOD1 [24], several ALS mutations have instead the largest effect on the most immature forms of SOD1; some mutations destabilize the metal-free and disulfide-reduced polypeptide to the point that these forms are unfolded at physiological temperatures [7,25].

Not all fALS-related mutants enhance the oligomerization process. Actually most of them behave quite similarly to apo WT (figure 2). Only three mutants, out of the eleven investigated, show a significant increase in the initial oligomerization rates compared to the WT protein. We therefore suggest that the presence of a mutation and its location and type would only modulate the rate of

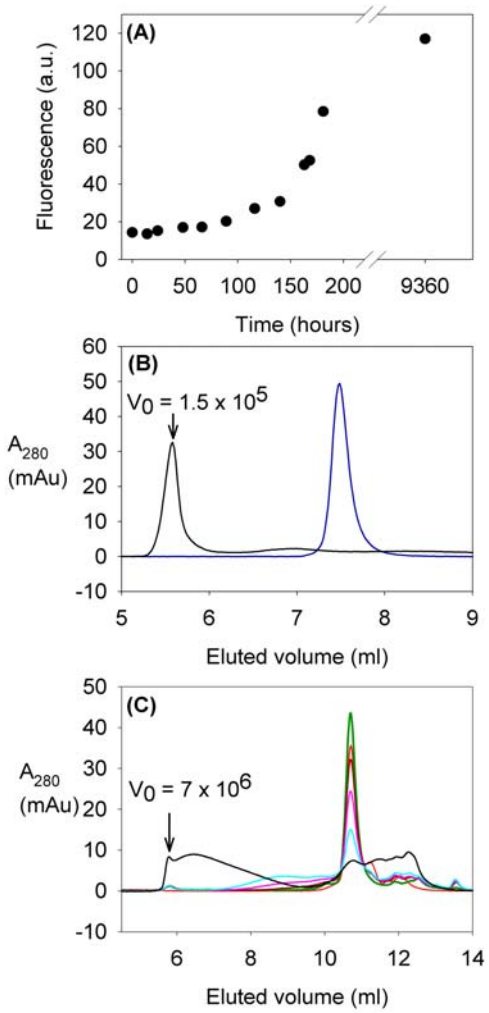

Figure 4. Formation of oligomeric structures when apo T54R SOD1 mutant is incubated at 37°C. (A) Fluorescence due to ThT binding to SOD1 mutants (presented as arbitrary units, A.U.) for apo T54R SOD1 during the incubation of the samples at 37°C. Panels **(B)** and **(C)** shows the size exclusion chromatograms on a G2000SW_{XL} and a G4000SW_{XL} Tosoh columns respectively, corresponding to the samples analyzed by light scattering. The void volume is labeled V_0. In all four panels the samples can be identified according to the following colors: before incubation (—), after 66 hours (—), 4.8 days (—), 6.8 days (—),7.5 days (—), and 13 months (—) of incubation at 37°C. In panel **(B)** the zinc reconstituted sample (—) is also reported.
doi:10.1371/journal.pone.0001677.g004

the aggregation process. This modulation could occur in two ways: 1) the mutation could influence the local structural and dynamical properties of the apo state, exposing areas of the protein that make it prone to oligomerization through disulfide bond formation between the free cysteines of different SOD1 molecules [16]. The lack of metal ions leads, indeed, to a more disordered SOD1 structure, thus making the free cysteines more exposed, solvent accessible, and less structurally constrained than in the metallated form, as observed in the solution structure of the apo form of a stable monomeric species, characterized by a dramatic increase in protein flexibility, with regions experiencing random coil structural features. This acquired freedom could be affected differently by the various mutations. 2) the mutations could modulate the rate of metalation. If the protein remained for an abnormally long period of time in the apo state, our results suggest that the SOD1 apoprotein, WT or mutant, would be more prone to aggregation.

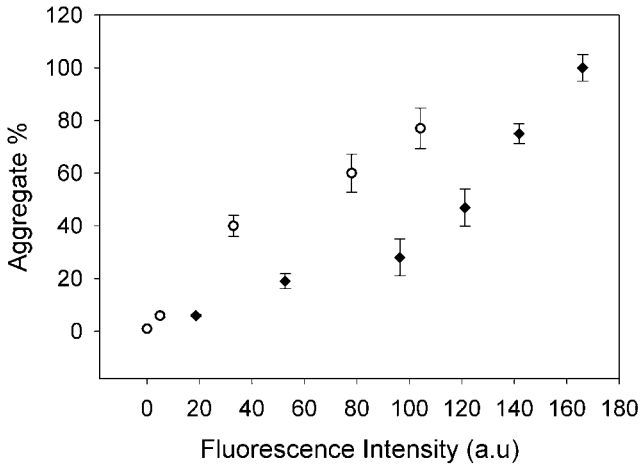

Figure 5. Correlation between percentage of aggregated species and ThT-binding fluorescence. Percentage of aggregated species (non-dimer), determined by light scattering measurements, *vs* ThT-binding fluorescence for apo WT SOD1 (O) and apo I113T SOD1 (♦) during the incubation of the samples at 37°C. Error bars are derived from the molecular mass errors of the light scattering experiments.
doi:10.1371/journal.pone.0001677.g005

The aggregation process we observe is strongly sensitive to temperature and obviously to the redox conditions of the environment. Because of the involvement of disulfide bond formation, an oxidative stress would be expected to favor the process, while a reducing environment would prevent aggregation. Indeed, it has been suggested that the redox state of the cell may play a role in the aggregation process [26]. SOD1 is mainly present in two different cell compartments, i.e. cytoplasm and mitochondria, where it independently acquires metal ions. These two cell compartments have quite different redox properties, which could further modulate the aggregation process *in vivo*. It has been proposed that an important toxic property of most mutSOD1s derives from their high level of accumulation in mitochondria in an aggregated state with cross-linked mutSOD1s and that this localization is caused by the aberrant reactivity of cysteines driven by the more oxidizing redox environment of these mitochondria [26]. Recent studies suggest that a non-physiological intermolecular disulfide bond between cysteines at positions 6 and 111 of mutant SOD1 is important for high molecular weight aggregate formation in cells [27].

Our results show that WT, as well as all the SOD1 mutants here studied, form similar high molecular weight oligomers when these proteins, in the apo dimeric form with the intramolecular disulfide bonds intact, are kept in conditions very close to the physiological ones (figure 6). The finding that WT and all the mutants, independently of the nature and location of the mutation, undergo the same type of oligometization suggest a general, unifying picture of SOD1 aggregation that could operate when either wild type or mutant SOD1 proteins are in the metal-free state. Although we cannot exclude other mechanisms in SOD1-linked familial ALS, the one proposed here has the strength of explaining how a large and diverse set of SOD1 mutant proteins all could lead to disease through the same mechanism.

Despite our efforts to build up a correlation between our results and the severity of the disease, the data on the latter are few. The number of cases documented, in particular for the mutations reported by us, is not exhaustive and broad enough to build up a relationship. Still our approach has the potentiality to establish such correlation as soon as enough data become available.

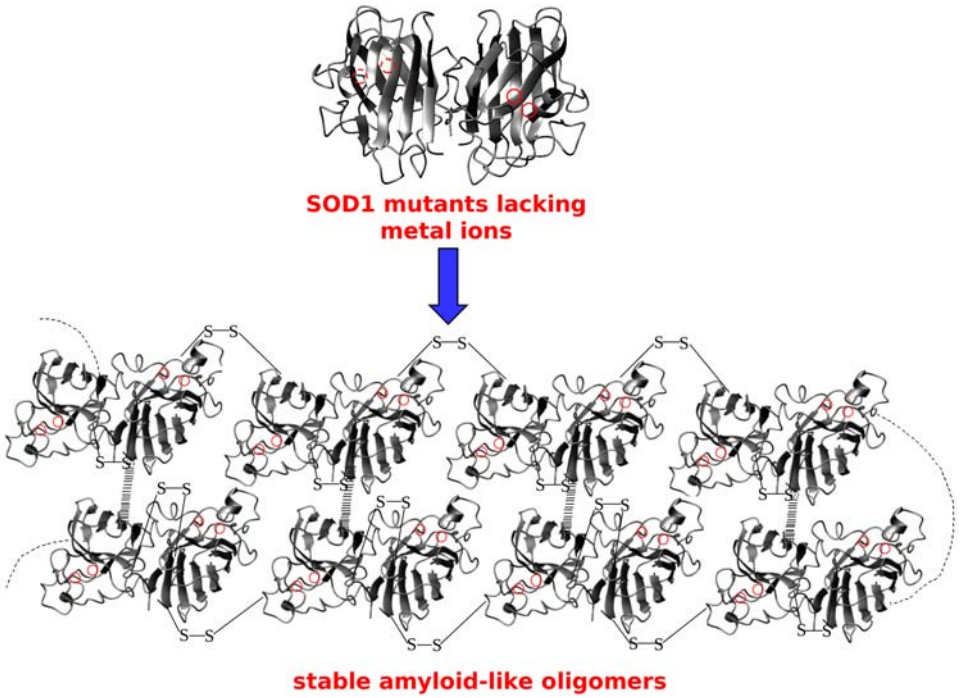

Figure 6. Mutants SOD1 aggregation. Formation of soluble oligomers occuring when apo WT SOD1 protein is kept close to physiological conditions for an extended period of time. In the absence of metal ions, SOD1 proteins form abnormal disulfide cross-links though the two free cysteines (Cys 6 and Cys 111) and noncovalent associations with other SOD1 monomers or dimers.
doi:10.1371/journal.pone.0001677.g006

Materials and Methods

Sample Preparation—WT SOD1 and its mutants were expressed in the *Escherichia coli* BL21(DE3) strain. Mutations were performed using a QuikChange^{TM} site-directed mutagenesis kit (Stratagene). The proteins, obtained from cells grown in LB medium, were isolated by osmotic shock in a 20 mM Tris, 5 mM dithiothreitol (DTT) buffer at pH 8. After incubation for 30 minutes at 37°C, the proteins were centrifuged at 40000 rpm for 20 minutes. Supernatants were purified following a reported procedure [28] modified by the addition of 1 mM DTT to each chromatographic buffer. The proteins obtained with this procedure contained substoichiometric amounts of the metal ions (Table S2). The metal ions were completely removed, at 25°C, to prepare the demetallated (apo) form, according to previously published protocols [29], and the zinc reconstituted forms were prepared, as well, as previously described [15]. Metal content of the various forms of SOD1 was checked by inductively coupled plasma mass spectrometry (ICP-MS) using a Thermo Jarrell Ash Atomscan Model 25 Sequential inductively coupled spectrometer (Table S2). The dimeric state of the apo form of the mutants at time zero of the incubation was checked through gel filtration chromatography.

Spectroscopic characterization—Protein samples were 100 μM in SOD1 concentration (as dimer) in 20 mM phosphate buffer at pH 7. The proteins were incubated at 37°C to mimic physiological conditions. Optical and fluorescence spectroscopies, coupled with gel filtration chromatography, were used to monitor the formation of oligomeric species at these sample conditions. The analysis were carried out in both the zinc-bound and apo forms of the proteins.

Far-UV CD spectra (190–250 nm) of SOD1 were recorded on JASCO J-810 spectropolarimeter. A cell with a path length of 1 mm was used for the measurement, and the parameters were set as follows: bandwidth, 2 nm; step resolution, 1 nm; scan speed, 20 nm/min; and response time, 2 s. Each spectrum was obtained as the average of four scans. The protein concentration was typically around 8–10 μM. Prior to the calculation of the mean residue molar ellipticity, all of the spectra were corrected by subtracting the contributions from the buffer. Spectra were then smoothed using adjacent averaging or Fast Fourier transform filter. Quantitative estimations of the secondary structure contents were made using the DICROPROT software package [30].

Fluorescence was followed with Thioflavin T, (ThT) probe, which specifically binds to amyloid-like structures [17]. Free ThT has excitation and emission maxima at 350 nm and 450 nm, respectively. However, upon binding to amyloid-like oligomers, the excitation and emission maxima change to 450 and 485 nm, respectively. 54 μl aliquots of sample were added to 646 μl of a 215 μM ThT solution in a 20 mM phosphate buffer at pH 7. The solution fluorescence emission was measured, over time of incubation,with a Cary 50 Eclipse Spectrophotometer supplied with a Single cell Peltier thermostatted cell holder regulated at 37°C. The background fluorescence spectrum of the buffer was subtracted. The excitation wavelength was 446 nm (bandwidth 10 nm) and the emission was recorded at 480 nm (bandwidth 10 nm). Fluorescence intensity at 483 nm was plotted against time of incubation.

Turbidity was measured at 400 nm to detect possible formation of insoluble precipitate. Solution turbidity was measured as apparent absorbance at 400 nm using a Cary UV-visible spectrophotometer. Experiments were performed by diluting 120 μl of the incubation SOD1 stock solution into 280 μl of 20 mM phosphate buffer at pH 7. A 1 cm quartz cuvette was used. Instrumental detection limit was 0.001 at 400 nm.

NMR data were acquired at 288 and 298 K on a 700 or a 900 Bruker spectrometer operating at proton nominal frequencies of 700.13 and 900.13 MHz, respectively. A triple resonance Cryoprobe equipped with pulsed field gradients along the *z*-axis was used. The two-dimensional ^{1}H-^{15}N HSQC spectra, performed to monitor

the folding of the protein mutants, were collected on 100 μM samples of ^{15}N-labeled E,E- and E,Zn-hSOD1^{SS} mutant proteins in 20 mM sodium phosphate buffer (pH 7).

Monitoring SOD1 Aggregation by Gel Filtration and Light Scattering—100 μl aliquots of the incubated proteins at 37°C were periodically taken and analyzed by gel filtration on Superdex 75 HR 10/30 (Amersham Biosciences) at room temperature. The column was preequilibrated with 20 mM potassium phosphate, pH 7.0, and the flow rate was 0.6 ml/min. The chromatogram, which monitors the species formed during incubation, was obtained by monitoring the absorbance at 280 nm. 20 μl aliquots of the incubated proteins at 37°C were also periodically taken and analyzed by gel filtration on G2000SW$_{XL}$ and G4000SW$_{XL}$ (Tosoh Bioscience) columns at room temperature. The columns were preequilibrated with 20 mM potassium phosphate, pH 7.0, and the flow rates were 0.7 and 1 ml/min respectively. The chromatogram, which monitors the species formed during incubation, was obtained by monitoring the absorbance at 280 nm. A species, present in small amount, was observed in the chromatographic spectra of mutants I113T and T54R, eluting after about 12.0 ml. This species might be due to a fragment from some degradation, which takes place during the aggregation process. We can exclude that it is due to a monomeric species either folded or unfolded as they elute only slightly later than the dimeric species (folded) or even earlier than it (unfolded) (data not shown). Further studies are underway to elucidate this issue.

While Superdex 75 HR 10/30 is a semi-preparative gel filtration columns, the G2000/4000SW$_{XL}$ are analytical ones. Their void volumes are 75 kDa, 150 kDa and 7,000 kDa respectively. The Superdex column was used when a separation of the dimer from the rest of the oligomeric species was necessary for further analysis. The G2000SW$_{XL}$ analytical column was used to monitor the very initial steps of the oligomerization process while the successive time points, in which a larger oligomer, with MW higher than 150 kDa, was formed, were better observed with the G4000SW$_{XL}$ column.

The G2000SW$_{XL}$ and G4000SW$_{XL}$ columns were also connected to a light scattering spectrometer. The online multi-angle light scattering (MALS) detector (DAWN EOS, Wyatt Technology, Santa Barbara, CA) and differential refractive index (DRI) detector (Optilab DRI, Wyatt Technology) setup was used to measure the light scattered as a function of angle and absolute protein concentration of fractions eluting from the size-exclusion chromatography column. The Zimm/Debye approximations were used in the Astra software (Wyatt Technology) to estimate molar mass. Data were fit using a second-order polynomial. The analysis was performed for each one of the 20 μl aliquots periodically taken from the incubation batches so as to monitor the increase in molecular weight of the soluble species formed during aggregation.

Supporting Information

Figure S1 Formation of ThT-binding structures when apo SOD1 mutants and WT are incubated at 37 °C. Fluorescence due to ThT binding to SOD1 mutants (presented as arbitrary units, A.U.) for apo T54R SOD1 (• apo D90A SOD1 (Ñ), apo I113T SOD1 (♦) and apo WT SOD1 (O), during the incubation of the samples at 37 °C. Error bars are standard deviations values obtained from two/three repeats of the experiments.
Found at: doi:10.1371/journal.pone.0001677.s001 (0.34 MB DOC)

Table S1 Light Scattering analysis. ThT binding fluorescence, as well as species distribution (dimer and aggregate) and average molecular weights of the aggregated species, as detected by light scattering measurements, of apo I113T SOD1 after different periods of incubation.
Found at: doi:10.1371/journal.pone.0001677.s002 (0.02 MB DOC)

Table S2 Extraction from *E. coli* cells and metal reconstitution with zinc. The metal contents of the proteins are shown as equivalents of each metal per enzyme dimer.
Found at: doi:10.1371/journal.pone.0001677.s003 (0.02 MB DOC)

Author Contributions

Conceived and designed the experiments: LB IB SG JS. Performed the experiments: MB SG MM MV. Analyzed the data: LB IB MB SG MM JS MV. Wrote the paper: LB IB SG JS.

References

1. Bruijn LI, Miller TM, Cleveland DW (2004) Unraveling the mechanisms involved in motor neuron degeneration in ALS. Annu Rev Neurosci 27: 723–749.
2. Rosen DR (1993) Mutation in Cu,Zn superoxide dismutase gene are associated with familial amyotrophyc lateral sclerosis. Nature 362: 59–62.
3. Valentine JS, Doucette PA, Potter SZ (2005) Copper-Zinc Superoxide Dismutase and Amyotrophic Lateral Sclerosis. Annu Rev Biochem 74: 563–593.
4. Andersen PM (2006) Amyotrophic lateral sclerosis associated with mutations in the CuZn superoxide dismutase gene. Curr Neurol Neurosci Rep 6: 37–46.
5. Tu PH, Raju P, Robinson KA, Gurney ME, Trojanowski JQ, et al. (1996) Transgenic mice carrying a human mutant superoxide dismutase transgene develop neuronal cytoskeletal pathology resembling human amyotrophic lateral sclerosis lesions. Proc Natl Acad Sci U S A 93: 3155–3160.
6. Valentine JS, Hart PJ (2003) Misfolded CuZnSOD and amyotrophic lateral sclerosis. Proc Natl Acad Sci U S A 100: 3617–3622.
7. Lindberg MJ, Bystrom R, Boknas N, Andersen PM, Oliveberg M (2005) Systematically perturbed folding patterns of amyotrophic lateral sclerosis (ALS)-associated SOD1 mutants. Proc Natl Acad Sci U S A 102: 9754–9759.
8. Furukawa Y, O'Halloran TV (2005) Amyotrophic Lateral Sclerosis Mutations Have the Greatest Destabilizing Effect on the Apo- and Reduced Form of SOD1, Leading to Unfolding and Oxidative Aggregation. J Biol Chem 280: 17266–17274.
9. Taylor JP, Hardy J, Fischbeck KH (2005) Toxic proteins in neurodegenerative disease. Science 296: 1991–1995.
10. Bruijn LI, Houseweart MK, Kato S, Anderson KL, Anderson SD, et al. (1998) Aggregation and motor neuron toxicity of an ALS-linked SOD1 mutant independent from wild-type SOD1. Science 281: 1851–1854.
11. Ross CA, Poirier MA (2006) Protein Aggregation and Neurodegenerative Disease. Nat Med 10: S10–17.
12. Fridovich I (1978) The biology of oxygen radicals. Science 201: 875–879.
13. Bertini I, Mangani S, Viezzoli MS (1998) Advanced Inorganic Chemistry. San Diego: Academic Press. pp 127–250.
14. Culotta VC, Yang M, O'Halloran TV (2006) Activation of superoxide dismutases: putting the metal to the pedal. Biochim Biophys Acta 1763: 747–758.
15. Arnesano F, Banci L, Bestini I, Martinelli M, Furukawa Y, et al. (2004) The unusually stable quaternary structure of human SOD1 is controlled by both metal occupancy and disulfide status. J Biol Chem 279: 47998–48003.
16. Banci L, Bertini I, Durazo A, Girotto S, Gralla EB, et al. (2007) Metal-free superoxide dismutase forms soluble oligomers under physiological conditions: a possible general mechanism for familial ALS. Proc Natl Acad Sci U S A 104: 11263–11267.
17. Krebs MR, Bromley EH, Donald AM (2005) The binding of thioflavin-T to amyloid fibrils: localisation and implications. J Struct Biol 149: 30–37.
18. Banci L, Bertini I, Cabelli DE, Hallewell RA, Tung JW, et al. (1991) A characterization of copper/zinc superoxide dismutase mutants at position 124 - Zinc-deficient proteins. Eur J Biochem 196: 123–128.
19. Ohi T, Nabeshima K, Kato S, Yazawa S, Tacheki S (2004) Familial amyotrophic lateral sclerosis with His46Arg mutation in Cu/Zn superoxide dismutase presenting characteristic clinical features and Lewy body-like hyaline inclusions. J Neurol Sci 225: 19–25.
20. Pasinelli P, Belford ME, Lennon N, Bacskai BJ, Hyman BT, et al. (2004) Amyotrophic Lateral Sclerosis-associated SOD1 mutant proteins bind and aggregate with Bcl-2 in spinal cord mitochondria. Neuron 43: 19–30.
21. Stathopulos PB, Rumfeldt JAO, Scholz GA, Irani RA, Frey HE, et al. (2003) Cu/Zn superoxide dismutase mutants associated with amyotrophic lateral sclerosis show enhanced formation of aggregates in vitro. Proc Natl Acad Sci U S A 100: 7021–7026.

22. Tiwari A, Xu Z, Hayward LJ (2005) Aberrantly increased hydrophobicity shared by mutants of Cu,Zn-superoxide dismutase in familial amyotrophic lateral sclerosis. J.Biol.Chem. 280: 29771–29779.
23. Field LS, Furukawa Y, O'Halloran TV, Culotta VC (2003) Factors controlling the uptake of yeast copper/zinc superoxide dismutase into mitochondria. J.Biol.Chem. 278: 28052–28059.
24. Potter SZ, Valentine JS (2003) The perplexing role of copper-zinc superoxide dismutase in amyotrophic lateral sclerosis (Lou Gehrig's disease). J Biol Inorg Chem. 8: 373–380.
25. Lindberg MJ, Tibell L, Oliveberg M (2002) Common denominator of Cu/Zn superoxide dismutase mutants associated with amyotrophic lateral sclerosis: Decreased stability of the apo state. Proc Natl Acad Sci U. S. A 99: 16607–16612.
26. Ferri A, Cozzolino M, Crosio C, Nencini M, Casciati A, et al. (2006) Familial ALS-superoxide dismutases associate with mitochondria and shift their redox potentials. Proc Natl Acad Sci U S A 103: 13860–13865.
27. Niwa J, Yamada S, Ishigaki S, Sone J, Takahashi M, et al. (2007) Disulfide Bond Mediates Aggregation, Toxicity, and Ubiquitylation of Familial Amyotrophic Lateral Sclerosis-linked Mutant SOD1. J Biol Chem 282: 28087–28095.
28. Banci L, Benedetto M, Bertini I, Del Conte R, Piccioli M, et al. (1998) Solution structure of reduced monomeric Q133M2 Copper, Zinc Superoxide Dismutase. Why is SOD a dimeric enzyme? Biochemistry 37: 11780–11791.
29. McCord JM, Fridovich I (1969) Superoxide dismutase. Enzymic function for erythrocuprein. J Biol Chem 244: 6049–6055.
30. Deleage G, Geourjon C (1993) An interactive graphic programme for calculating the secondary structures content of proteins from circular dichroism spectrum. Comp Appl Biosc 9: 197–199.

3.2

Apo SOD1 and its mutants: structural and dynamic aspects related to oligomerization

Lucia Banci, Ivano Bertini, Mirela Boca, Vito Calderone, Francesca Cantini, Stefania Girotto, Miguela Vieru

Submitted

Classification: Biological Sciences/Biophysics

Apo SOD1 and its mutants: structural and dynamic aspects related to oligomerization

Lucia Banci[1,2], Ivano Bertini[1*], Mirela Boca[1], Vito Calderone[1], Francesca Cantini[1], Stefania Girotto[1], Miguela Vieru[1]

[1] Magnetic Resonance Center (CERM) and Department of Chemistry – University of Florence, Via L. Sacconi 6, 50019 Sesto Fiorentino, Italy

[2] FiorGen Foundation, Via Luigi Sacconi 6, 50019 Sesto Fiorentino, Italy

*To whom correspondence should be addressed:

Prof. Ivano Bertini, Magnetic Resonance Center CERM and Department of Chemistry, University of Florence, Via L. Sacconi 6, Sesto Fiorentino, ITALY 50019. Tel.: +39-055-4574272; Fax: +39-055-4574271; E-mail: ivanobertini@cerm.unifi.it

The number of text pages: 18

The number of figures: 4

The number of tables: 0

Data deposition: Protein Data Bank accession codes 3ECU, 3ECV, 3ECW for apo WT, apo I113T and apo T54R SOD1 structures, respectively.

Abstract

The structural and dynamical properties of the metal free form of WT human SOD1 and its fALS-related mutants, T54R and I113T, were characterized both in solution, through NMR, and in the crystal, through X-ray diffraction. We found that all three X-ray structures show significant structural disorder in two loop regions which are, at variance, well defined in the fully metalated structures. Interestingly, the apo state crystallizes only at low temperatures, while all three proteins, in the metalated form, crystallize at any temperature suggesting that crystallization selects one of the most stable conformations among the manifold adopted by the apo form in solution. Indeed, NMR experiments show that the protein in solution is highly disordered sampling a large range of conformations. The large conformational variability of the apo state allows the free reduced cysteine Cys6 to become highly solvent accessible in solution, while it is essentially buried in the metalated state as well as in the crystal structures. Such solvent accessibility, together with that of Cys111, accounts for the tendency to oligomerization of the metal free state. The present results suggest that the investigation of the solution state coupled with that of the crystal state can provide major insights into SOD1 pathway towards oligomerization in relation to fALS.

Over 100 different variants of human copper-zinc superoxide dismutase ((Cu_2 Zn_2) SOD, SOD1) have been identified and linked to the neurodegenerative disease familial amyotrophic lateral sclerosis (fALS) by a gain-of-function mechanism (1, 2). Although the mechanism of the toxicity is unknown, aberrant SOD1 protein oligomerization has been strongly implicated in disease causation (3, 4). Several recent publications have presented compelling evidence that *in vivo* abnormal disulfide-crosslinking of ALS-mutant SOD1 plays a role in this oligomerization (5–7), and disulfide-linked SOD1 multimers, which are presumed to be components of higher molecular weight species or intermediates (7), have been detected mainly in mitochondria of neuronal tissues of SOD1-linked fALS patients and transgenic mice (8–10).

Wild type (WT) human SOD1 is an exceptionally stable, homodimeric 32kDa protein, located mainly in the cytoplasm, but also present in the peroxisomes, in the mitochondrial intermembrane space and in the nucleus of eukaryotic cells (11–13). Each subunit of the dimer binds one copper (binding residues: His46, His48, His63 and His120) and one zinc ion (binding residues: His63, His71, His80 and Asp83) and folds as an eight-stranded Greek-key β-barrel that is stabilized by an intra-subunit disulfide bond (Cys57, Cys146) near the active site (14). *In vivo,* in the highly reducing cytoplasm environment, the existence of this intrasubunit disulfide bond points to its very low reduction potential. WT human SOD1 actually contains four cysteine residues per monomer. Besides the two cysteines involved in the formation of the intramolecular disulfide bond, two reduced cysteines Cys6 and Cys111 are located on β strand 1 and loop VI respectively. Among the loops connecting the eight β strands, two have structural and functional role. The electrostatic loop (loop VII, residues 121–144) contains charged residues that contribute to guide the negatively charged superoxide substrate towards the catalytic copper site. The long zinc loop (loop IV, residues 49–84) contains all the zinc binding residues including His63, which acts as a ligand to both metals (14).

We have recently reported (15, 16) that oxidized WTSOD1 and several of its mutants, only when they are in the metal free form, give rise, *in vitro*, to soluble oligomers under aerobic conditions when the proteins are kept at 37°C and at a concentration and pH close to physiological, i.e., 100μM and pH=7.0. The resulting soluble oligomers are formed by intermolecular disulfide covalent bonds, involving Cys6 and Cys111, and by non-covalent interactions between β strands, forming amyloid-like structures capable of binding ThT (15, 16). The rates of protein oligomerization are different for the various mutants, but eventually they give rise to the same type of soluble oligomeric species.

SOD1 enters the mitochondria in the metal free (apo) state (17, 18) and mitochondria are cellular compartments where oxidative stress may easily occur. The soluble oligomeric species, formed by the apo form of both WTSOD1 and its mutants through an oxidative process, might represent the precursor toxic species, whose existence would also suggest a common mechanism for ALS and fALS.

In order to investigate the mechanism for SOD1 oligomerization, a detailed study of the protein behaviour in the absence of metals is required. The structural and dynamical features of the metal free state of SOD1 for both WT and some ALS-related mutants were here characterized both in solution, through NMR, and in the crystal, through X-ray diffraction. We found that the metal free state is significantly disordered in the crystal for two pathogenic SOD1 mutants as already reported for the WT protein (19, 20), at variance with what observed in the metalated state. In solution, the highly disordered and dynamical metal free state allows the free cysteines to become accessible for oxidation and subsequent oligomerization, at variance with what occurs in the metal-bound form.

Results and Discussion

In the present study we characterized the metal free form (apo) of WTSOD1 and of two, ALS-related mutants with two extreme behaviors in terms of oligomerization rates: T54R oligomerizes with rates slightly slower than WTSOD1 while I113T has an oligomerization rate more than twice that of WTSOD1 (16).

In the crystal structures of the metal free form of WTSOD1 and of its mutants T54R and I113T, the asymmetric unit contains two biologically relevant dimers. While one has a very well defined electron density throughout the entire sequence, the other dimer has clear breaks in the electron density in the regions encompassing residues 68–78 (loop IV) and 125–140 (loop VII). Overall, the structures are very similar to each other. Only few minor local differences in terms of conformation, buried surface areas and residues involved in H-bond interactions are detected **(Table S1**). Peculiar for apo T54R SOD1 is a mutation-related hydrogen bond, which is formed at the dimer interface, i.e. between NH2 of Arg54 of each monomer and OD1 of Asn19 of the other monomer in the same dimer. This interaction might lead to a partial stabilization of the dimeric state with respect to the WT protein and might correlate with the slightly slower oligomerization rates for apo T54R compared to the WT protein (16), as oligomerization presumably occurs through monomerization (21). The free Cys6, in all three apo SOD1 structures, is essentially buried due to the constraints imposed by two H-bonds with Ile18, while the other free cysteine, Cys111, has a considerably high (75%) solvent exposed side chain (thiol group).

The three structures here determined clearly resemble the already available partially apo (20% zinc in one of the two dimers) WTSOD1 structure (PDB code 1HL4) (20). Similarly, also the same electron density breaks were found in only one of the two dimers. On the contrary, the fully metalated ((Cu_2, Zn_2); holo) structures of both WTSOD1 (PDB code 1HL5, (20)) and I113T SOD1 mutant (PDB code 1UXL, (22)) show a well defined electron density throughout the entire sequence for each dimer present in the asymmetric unit. The backbone RMSD between the holo and apo form of both WT and I113T SOD1 is about 0.45 Å. The main structural differences between the holo and apo states are observed in the loops connecting the β strands, where the electron density is broken in one of the dimers in the structures of the apo state. Similar electron density breaks were also observed for the structure of the apo state of the H46R SOD1 mutant (23), the only, up to now published structure of a completely metal free SOD1 mutant. On the contrary, the structures of ALS-related SOD1 mutants, in the fully metalated state are very similar to each other, and particularly well ordered throughout the sequence (22–27).

WTSOD1 and its mutants T54R and I113T, in the apo state, form a continuous, extended arrangement of β-barrels stacked up along a direction (crystallographic *b*-axis) perpendicular to the dimer interface; orthogonal to this direction, the β-strands form a zig-zag array of filaments. This behaviour is similar to that already observed for 1HL4 (20) and is common to amyloid-like fibrils (28).

The comparison between the structures of WTSOD1 and ALS-related mutants was unable to shed light on the structural basis of different behaviors between WT and pathogenic mutants, although pointing at some conformational disorder as a consequence of the lack of metal ions. At this stage, therefore, a characterization of the apo state in solution of WTSOD1 and its mutants is necessary.

The ^{1}H-^{15}N HSQC spectra of the apo forms of both WTSOD1 and of the two pathological mutants i.e. T54R and I113T, have reduced signal dispersion with respect to those of the metalated form (**Figure 1**) indicating that some parts of the protein do not have a well defined conformation. High protein instability as well as strong tendency to form high molecular weight oligomers (15) prevented us from collecting the triple resonance NMR experiments necessary to achieve a specific resonance assignment. Therefore a protein sample analysis aiming at finding the best compromise between protein stability towards oligomerization and line broadening effects led us to acquire all the spectra at 0.6 mM protein concentration and 288K. In these experimental conditions, dimeric apo SOD1 is stable for periods of time long enough to collect some of the triple resonance NMR experiments necessary to achieve an almost complete sequence specific resonance assignment (see Material and Methods section). More than one sample was needed, however, to complete NMR data collection. Unfortunately, the I113T mutant is too unstable and oligomerizes so fast to prevent further analysis, beyond recording a simple ^{1}H-^{15}N HSQC spectrum.

Through the NMR experiments, 68% of the backbone atoms (N, HN and Cα) were assigned for apo WTSOD1. The non assigned peaks were all clustered in the central part of the HSQC spectrum, thus experiencing severe resonance overlap; they were mainly located in loops connecting the β strands, in particular in loop IV which contains most of the metal binding residues. This spectral pattern was already observed in the apo state of a monomeric form of SOD1 obtained through residue mutations at the subunit-subunit interface (19). Further mutation of the two free cysteines (6 and 111) (AS WTSOD1) in the monomeric form prevented oligomerization, allowing to reach a much higher protein concentration; this combined with the half molecular weight led to a more complete assignment, which was here used for comparison purposes.

From the analysis of the assigned chemical shift resonances it appears that some of the secondary structural elements present in the holo protein exist also in the metal free state, while β strands 4, 5, and 7, are much shorter. The NH-NH long range NOEs are present within one of the two β sheets, which form the SOD1 β barrel, i.e. that formed by β1, β2, β3, β6, while they are essentially missing in the other β sheet, which contains some of the metal ligand residues (**Figure 2**). From the analysis of the NOESY spectrum, it appears also that most of the long range ^{1}H-^{1}H NOEs, involving side chain protons, are missing even within the secondary structural elements.

Combined chemical shift variations of backbone amide moieties between the dimeric apo SOD1 and its fully metallated form (**Figure 3a**) reflect significant structural changes in loop VII, similarly to what already observed for the monomeric apo SOD1 form (19). Furthermore, a number of NH groups in this loop show, mainly at low temperature, another set of signals with lower intensity due to a minor conformation or a group of fast exchanging conformers in slow exchange with the rest of the conformations. Analysis of the chemical shift variations between the apo state of the monomeric and dimeric forms of SOD1 (**Figure 3b**) confirms that the absence of metal ions similarly affects the two forms. The only few detected differences can be ascribed to the mutation of the two free cysteines residues (C6A and C111S) and of two interface residues (F50E, G51E), these four mutations being present only in this "artificial" monomeric form.

We have recently shown (15) that oligomerization of apo SOD1 involves oxidation of the two free cysteines (6 and 111) with the formation of inter-subunit disulfide bonds, thus linking a high number of protein molecules in high molecular weight species. In the X-ray structure of apo WTSOD1 and of apo T54R and I113T, Cys6 and Cys111 appear as reduced, while Cys57 and 146 are oxidized. The actual oxidation state of the four cysteines (Cys6, 57, 111 and 146), in the dimeric form of apo SOD1, was also investigated by NMR on a ^{13}C, ^{15}N, ^{2}H Cys sample. The shift of the Cβ nuclei confirmed the presence of two oxidized (Cys146 and Cys57, ~ 43.9 and ~ 35.1 ppm respectively) and two reduced (Cys6 and Cys111, ~ 27.7 and ~ 24.03 ppm respectively) cysteine residues (**Figure S1**). At low temperature, double forms, possibly due to *cis-trans* intrasubunit disulfide bond isomerization, were detected for the Cβ carbon signals of both Cys57 and 146. Broadening of the Cys146 NH signal as well as disappearance of the NH signal of Cys57 at high temperatures (data not shown) support this hypothesis, already observed for disulfide bond isomerization in other systems (29).

The dynamical properties of apo dimeric SOD1 are also dramatically affected by the absence of the metals (**Figure 4**). The ^{15}N relaxation rates of backbone NHs, measured in the

temperature range 288–310K, are consistent with the protein being essentially only in the dimeric state, with its tumbling rate increasing with decreasing temperature. The relaxation rates and $^{15}N\{^{1}H\}$-NOEs, which are homogeneous in the β strand structures, are sizably altered in the loop regions. In particular, the electrostatic loop VII has, at 298K, lower than average R_2, higher than average R_1 values and lower $^{15}N\{^{1}H\}$-NOEs, which become even negative at 310K, indicating that the relative residues experience motions faster than the overall protein tumbling, i.e. faster than nanosecond. Internal motions in the subnanosecond time scale were also observed for loop VII in monomeric apo SOD1 (19), confirming that the absence of metal ions similarly affects the dynamical properties of both monomeric and dimeric apo forms. The spectral features in solution for loop VII suggest that this region, as well as the non assigned residues located in the other loop regions, sample a wide range of conformations which interconvert each other very fast on the chemical shift time scale (i.e. $>10^{-3}s^{-1}$), confirming that the absence of the metals dramatically affects the protein dynamic properties. This is also consistent with the much lower values of the $^{15}N\{^{1}H\}$-NOEs detected for apo versus metalated form.

Consistent with the increased flexibility of the apo form with respect to the metalated ones, the solvent accessibility of the former is dramatically higher with respect to the latter. Indeed, the overall number of NH protons exchanging fast with the bulk solvent, as measured from H_2O/D_2O exchange processes, is much higher than in the metalated state. In the apo form, after twenty minutes the sample has been dissolved in D_2O, about sixty residues were completely exchanged while only about thirty are exchanged in the metalated one. Indeed, the increased protein flexibility of the apo state makes larger regions of the protein more solvent exposed and the solvent exchange process more efficient.

Particularly striking with respect to the oligomerization process which the apo state is undergoing at physiological conditions (15), is the solvent exposure of the free cysteines (Cys6 and Cys111). While Cys111 is highly solvent exposed in both protein forms, Cys6 has a dramatically different solvent accessibility (**Figure S2**). In the metalated form its NH is essentially buried and protected from the solvent and indeed its NH signal is still present after five days in D_2O. On the contrary, in the apo form it completely disappears after only four hours. Also, the NH signals of adjacent residues (4–8, β strand l) all disappear in four hours, suggesting a high solvent accessibility of the region around the free Cys6. The highly solvent accessibility of Cys6 and of the region around is observed in the T54R mutant as well, which has the same behavior of WTSOD1, i.e. the metalated form is rigid and solvent protected,

while the lack of metal ions makes this region and the entire protein highly dynamic and accessible to the solvent.

All the features described here indicate that the apo state of SOD1 in solution is characterized by a distribution of conformations, particularly for β strands 4 and 5 and loop VII.

Analogous behavior was observed in the superoxide dismutase-like protein from *Bacillus subtilis* (30), where its NMR properties indicate a conformational mobility for most of the protein, characterized by defined secondary-structure elements and a dynamic tertiary structure, at variance with the X-ray crystal structure of the same protein, which shows a well ordered tertiary structure.

The overall studies here presented for the apo state of SOD1 and its mutants in solution also explain the behaviour of these proteins with respect to crystallization. Crystallization trials were performed at two different temperatures on both the apo and metalated forms of WTSOD1 and the two mutants (**Table S2**), i.e. at 288K, which is the temperature at which the crystals discussed above were obtained, and at 310K, which is the temperature at which the oligomerization studies were carried out (15, 16). Crystals of the apo state of WTSOD1 and of the two mutants can be obtained at 288K only, while crystals for the metalated forms of WTSOD1 and the mutants were obtained at both temperatures. This indicates that temperature has a major influence on the crystallization of the apo state while it is almost negligible on the metalated one. This overall behaviour is consistent with the dynamic properties and conformational disorder of the apo state. As the protein is intrinsically disordered and samples a range of conformations, at higher temperatures the interconversion among them is faster and new conformations could be sampled, thus making the lowest energy state less populated and therefore lowering the probability of crystallization. A decrease in temperature slows down the interconversion process among the various conformations and increases the population of the most stable states, which can therefore crystallize. Mutations do not seem to affect the chance of obtaining crystals at either temperatures.

Concluding remarks

We have recently shown (15) that oligomerization of apo SOD1 involves oxidation of the two free cysteines (6 and 111) with the formation of inter-subunit disulfide bonds, thus linking a high number of protein molecules in high molecular weight species. Someone suggested that the formation of SOD1 aggregates are the consequence of both covalent disulfide cross-linking and non-covalent interactions (31), while others proposed that extensive disulfide cross-linking

is not required for the formation of mutant SOD1 aggregates (32). Recent studies showed the importance of non-physiological intermolecular disulfide bond between cysteines 6 and 111 in mutant SOD1 for high molecular weight aggregate formation and also for protein ubiquitylation and neurotoxicity, which are all dramatically reduced when the pertinent cysteines are replaced (33). Nevertheless, there is a general agreement on a critical role played by cysteines 6 and 111, particularly the latter, in the modulation of human SOD1 aggregation (31–33).

We have shown that only the lack of metal ions makes SOD1 oligomerization possible (15). The reason for the dramatic different behavior of apo and metalated forms of SOD1 is now better understood. Indeed, the solvent exposure of the reduced cysteines changes dramatically from the metallated form to the apo one. Only in the latter state a free cysteine can bind another one of a different monomer to form the soluble oligomer. The crystal structures, on the contrary, are not informative on this respect as they clearly represent only one of the multiple conformations taken in solution by the protein. Consistently, the apo form of both WT and the mutants fail to crystallize at physiological temperature due to the high disorder and internal mobility.

The information obtained from the NMR spectra indicate that in solution apo WTSOD1 samples a range of conformations, highly disordered in some parts. Higher temperatures accelerate exchange among these conformations and could populate new ones. This behaviour explains why only the disordered, partially unfolded, metal free state has a dramatic protein flexibility which makes accessible conformations prone to oligomerize, while the rigid structure of the metalated protein is unable to do it.

Overall the present extensive structural and dynamical characterization of the apo state of WTSOD1 and some of its mutants showed that the lack of metal ions and the subsequent protein flexibility allows the free cysteines (Cys6 and Cys111) to become exposed and therefore ready to get oxidized and to form the disulfide bonds which give rise to the soluble oligomers.

Materials and Methods

Protein expression and purification

The *sod1* gene was cloned by PCR and inserted in Gateway pENTR/TEV/D-TOPO plasmid (Invitrogen). The plasmid was propagated and purified by MINI KIT (Invitrogen) and the sequence was verified. The LR recombination reaction was performed in order to transfer the *sod1* gene from pENTR/TEV/D-TOPO plasmid into pTH34 plasmid codifying for GB1 fusion tag. Mutations were performed using a QuikChange^{TM} site-directed mutagenesis kit (Stratagene). WTSOD1 and mutant proteins were over expressed in the *Escherichia coli* Origami pLysS strain (Novagen). The fusion proteins were obtained by growing the cells in minimal medium, in shaking flasks at 37 ºC until OD_{600} = 0.7 and then induced with 0.7 mM IPTG for twelve hours at 25 ºC. Proteins were isolated by sonication in a 5mM imidazol buffer at pH=8.0 and centrifuged at 165,000 × g for 20 minutes. Purification was performed by affinity chromatography using a nickel chelating (His-Trap) column (Armersham Bioscience) and by digestion with AcTEV protease. Protein purity was checked on a 17% polyacrilamide gel and concentration was determined by optical spectroscopy. The metal free protein was prepared according to previously published protocols (34). Zinc reconstitution was carried out as described in (17).

The ^{15}N-labeled, ^{13}C-, ^{15}N-labeled proteins were obtained by growing cells in minimal medium containing 3g/l ^{13}C-Glucose and 1g/l ^{15}N-$(NH_4)_2SO_4$ and induced at 25°C overnight. The deuterium enriched protein (^{13}C-, ^{2}H-, ^{15}N- labelled WT SOD1) was expressed under similar conditions except for the growth of the *E. coli* strain, which was carried out in minimal medium containing 90% (volume) of deuterated water ($^{2}H_2O$, D_2O). In order to obtain 80% of deuterium incorporation into WTSOD1 protein, the *E. coli* cells were subjected to growth conditions of increasing D_2O content.

To produce (^{13}C, ^{2}H, ^{15}N)Cys-selectively labeled protein, WTSOD1 was also expressed in a cysteine auxotrophic *E. coli* strain, BL21(DE3)cysE according to an already published protocol (35).

Crystallization, data collection and structure solution

Crystals of metal free SOD1 (WT, T54R and I113T) were obtained using the vapour diffusion technique at 288K from 0.1 mM protein solutions containing 0.1 M MES (pH=6.5) or 0.1 M HEPES (pH=7.0), 20% PEG 3350.

The metal free WT and I113T SOD1 crystal diffraction patterns were measured with a PX-Ultra copper sealed tube source (Oxford Diffraction) equipped with an Onyx CCD

detector, whereas the diffraction pattern of the metal free T45R mutant was measured using synchrotron radiation at BW7A beamline (DESY, Hamburg, Germany). All datasets were collected at 100K and the crystals used for data collection were cryo-cooled using 20% ethylene glycol in the mother liquor. Apo WT and apo I113T SOD1 crystals diffracted to 1.9 Å resolution while apo T54R SOD1 diffracted to 2.1 Å; they all belong to the spacegroup C2 with four molecules (two functional dimers) in the asymmetric unit, a solvent content of about 50% and a mosaicity of 0.8°–0.9°.

All data were processed using the program MOSFLM (36) and scaled using the program SCALA (37). **Table S2** shows the data collection and processing statistics for all datasets.

The structures were solved using the molecular replacement technique with the program MOLREP (38, 39); the model used for the WT dataset was 1HL5 whereas the two mutants were solved using the apo WT as the template. The isotropic refinement was carried out using REFMAC5 (40) on all datasets. In between the refinement cycles the models were subjected to manual rebuilding by using XtalView (41). Water molecules have been added by using the standard procedures within the ARP/WARP suite (42). The stereochemical quality of the refined models was assessed using the program Procheck (43). The Ramachandran plot is in all cases of good quality.

The three crystal structures are deposited in the Protein Data Bank (accession codes 3ECU, 3ECV, 3ECW for apo WT, apo I113T and apo T54R SOD1 structures, respectively).

NMR experiments

NMR spectra were acquired at 288K on Avance 900 Bruker spectrometer equipped with cryogenically-cooled probe. Resonance assignments of apo WTSOD1 form were performed through conventional multi-dimensional NMR techniques based on triple resonance experiments summarized in **Table S1**.

The dynamic properties of the apo dimeric form of WTSOD1 were directly sampled through ^{15}N relaxation measurements. ^{15}N longitudinal and traverse relaxation rates and $^{15}N\{^{1}H\}$-NOEs were recorded at 288, 298 and 310K at 500 MHz, using a protein concentration of about 0.6 mM. R_1 and R_2 relaxation rates were obtained by fitting the cross peak volumes (I), measured as a function of the relaxation delay, to a single exponential decay as described in the literature (44). Heteronuclear NOE values were calculated as the ratio of peak volumes in spectra recorded with and without saturation. In all experiments the water signal was suppressed with the 'water flipback' scheme (45).

The average backbone ^{15}N longitudinal R_1 and transversal R_2 relaxation rates and $^{15}N\{^{1}H\}$-NOEs values were 0.64 ± 0.04 s^{-1}, 34.0 ± 1.6 s^{-1} and 0.70 ± 0.03, respectively at

288K, 0.81 ± 0.05 s^{-1}, 27.1 ± 1.2 s^{-1} and 0.72 ± 0.03 at 298 K and 1.15 ± 0.06 s^{-1}, 19.4 ± 0.9 s^{-1} and 0.75 ± 0.03 at 310K. A correlation time for protein tumbling (τ_c) of 22.6 ± 1.9 ns at 298K was estimated from the R_2/R_1 ratio excluding those residues exhibiting below-average $^{15}N\{^1H\}$-NOEs values and those experiencing conformational processes. The result is consistent with that obtained with the HYDRONMR program for apo WTSOD1 being only in a dimeric state.

H_2O/D_2O exchange properties were analyzed on samples obtained by diluting concentrated apo SOD1 and (Zn_2, Zn_2) SOD1 solutions, for WT and the T54R proteins, rapidly with ^2H_2O to a final $^2H_2O/H_2O$ ratio of 0.90. H/D exchange rates were investigated through a series of ^1H-^{15}N HSQC experiments performed from 20 minutes after dilution up to five days.

Acknowledgments

We thank Marie-Paule Strub for providing us the cysteine-auxotrophic strain BL21(DE3)cysE. This work was supported by the European Community "Understanding Protein Misfolding and Aggregation by NMR" (UPMAN) Grant LSHG-CT-2004-512052 (11/1/04–10/31/07), by MIUR - FIRB "Fondo per gli Investimenti della Ricerca di Base" Grant - RBLA032ZM7 (12/09/05 -12/09/10) , by Ente Cassa di Risparmio di Firenze "Relazione varianti proteiche strutturali-malattie genetiche" and "Basi molecolari di patologie umane correlate a disfunzioni della catena respiratoria" and by Marie Curie Host Fellowship for Early Stage Research Training MEST-CT-2004-504391 "NMR in Inorganic Structural Biology".

Reference List

1. Valentine J. S., Doucette P. A., Potter S. Z. (2005) Copper-zinc superoxide dismutase and amyotrophic lateral sclerosis *Annu. Rev. Biochem.* **74**, 563–593.

2. Bruijn L. I., Miller T. M., Cleveland D. W. (2004) Unraveling the mechanisms involved in motor neuron degeneration in als *Annu. Rev. Neurosci.* **27**, 723–749.

3. Jonsson P. A., Ernhill K., Andersen P. M., Bergemalm D., Brannstrom T., Gredal O., Nilsson P., Marklund S. L. (2004) Minute quantities of misfolded mutant superoxide dismutase-1 cause amyotrophic lateral sclerosis *Brain* **127**, 73-88.

4. Wang J., Xu G., Borchelt D. R. (2006) Mapping superoxide dismutase 1 domains of non-native interaction: roles of intra- and intermolecular disulfide bonding in aggregation *J. Neurochem.* **96**, 1277–1288.

5. Jonsson P. A., Graffmo K. S., Andersen P. M., Brannstrom T., Lindberg M., Oliveberg M., Marklund S. L. (2006) Disulphide-reduced superoxide dismutase-1 in CNS of transgenic amyotrophic lateral sclerosis models *Brain* **129**, 451–464.

6. Deng H. X., Shi Y., Furukawa Y., Zhai H., Fu R., Liu E., Gorrie G. H., Khan M. S., Hung W. Y., Bigio E. H. *et al.* (2006) Conversion to the amyotrophic lateral sclerosis phenotype is associated with intermolecular linked insoluble aggregates of sod1 in mitochondria *Proc. Natl. Acad. Sci. U. S. A* **103**, 7142–7147.

7. Furukawa Y., Fu R., Deng H. X., Siddique T., O'Halloran T. V. (2006) Disulfide cross-linked protein represents a significant fraction of ALS-associated Cu, Zn-superoxide dismutase aggregates in spinal cords of model mice *Proc. Natl. Acad. Sci. U. S. A* **103**, 7148-7153.

8. Pasinelli P., Belford M. E., Lennon N., Bacskai B. J., Hyman B. T., Trotti D., Brown R. H. Jr. (2004) Amyotrophic lateral sclerosis-associated sod1 mutant proteins bind and aggregate with Bcl-2 in spinal cord mitochondria *Neuron* **43**, 19–30.

9. Ohi T., Nabeshima K., Kato S., Yazawa S., Takechi S. (2004) Familial amyotrophic lateral sclerosis with his46arg mutation in Cu/Zn superoxide dismutase presenting characteristic clinical features and lewy body-like hyaline inclusions *J. Neurol. Sci.* **225**, 19–25.

10. Ferri A., Cozzolino M., Crosio C., Nencini M., Casciati A., Gralla E. B., Rotilio G., Valentine J. S., Carri M. T. (2006) Familial ALS-superoxide dismutases associate with mitochondria and shift their redox potentials *Proc. Natl. Acad. Sci. U. S. A* **103**, 13860-13865.

11. Fridovich I. (1997) Superoxide anion radical ($O_2^{\cdot-}$), superoxide dismutases, and related matters *J. Biol. Chem.* **272**, 18515–18517.

12. Okado-Matsumoto A., Fridovich I. (2001) Subcellular distribution of superoxide dismutases (sod) in rat liver: Cu, Zn-sod in mitochondria *J. Biol. Chem.* **276**, 38388-38393.

13. Sturtz L. A., Diekert K., Jensen L. T., Lill R., Culotta V. C. (2001) A fraction of yeast Cu, Zn-superoxide dismutase and its metallochaperone, CCS, localize to the intermembrane space of mitochondria *J. Biol. Chem.* **276**, 38084–38089.

14. Bertini I., Mangani S., Viezzoli M. S. (1998) in *Advanced Inorganic Chemistry*, ed. Sykes, A. G. (Academic Press, San Diego, CA, USA), 127–250.

15. Banci L., Bertini I., Girotto S., Martinelli M., Vieru M., Whitelegge J., Durazo A., Valentine J. S. (2007) Metal-free superoxide dismutase forms amyloid-like oligomers: A possible general mechanism for familial ALS *Proc. Natl. Acad. Sci. USA* **104**, 11263–11267.

16. Banci L., Bertini I., Boca M., Girotto S., Martinelli M., Valentine J. S., Vieru M. (2008) SOD1 and amyotrophic lateral sclerosis: Mutations and Oligomerization *Plos ONE* **3**, e1677.

17. Arnesano F., Banci L., Bertini I., Martinelli M., Furukawa Y., O'Halloran T. V. (2004) The unusually stable quaternary structure of human sod1 is controlled by both metal occupancy and disulfide status *J. Biol. Chem.* **279**, 47998–48003.

18. Field L. S., Furukawa Y., O'Halloran T. V., Culotta V. C. (2003) Factors controlling the uptake of yeast copper/zinc superoxide dismutase into mitochondria *J. Biol. Chem.* **278**, 28052–28059.

19. Banci L., Bertini I., Cramaro F., Del Conte R., Viezzoli M. S. (2003) Solution structure of apo Cu, Zn superoxide dismutase: role of metal ions in protein folding *Biochemistry* **42**, 9543–9553.

20. Strange R. W., Antonyuk S., Hough M. A., Doucette P. A., Rodriguez J. A., Hart P. J., Hayward L. J., Valentine J. S., Hasnain S. S. (2003) The structure of holo and metal-deficient wild-type human Cu, Zn superoxide dismutase and its relevance to familial amyothrophic lateral sclerosis *J. Mol. Biol.* **28**, 877–882.

21. Rakhit R., Crow J. P., Lepock J. R., Kondejewski L. H., Cashman N. R., Chakrabartty A. (2004) Monomeric Cu, Zn-superoxide dismutase is a common misfolding intermediate in the oxidation models of sporadic and familial amyotrophic lateral sclerosis *J. Biol. Chem.* **279**, 15499–15504.

22. Hough M. A., Grossmann J. G., Antonyuk S. V., Strange R. W., Doucette P. A., Rodriguez J. A., Whitson L. J., Hart P. J., Hayward L. J., Valentine J. S. *et al.* (2004) Dimer destabilization in superoxide dismutase may result in disease-causing properties: structures of motor neuron disease mutants *Proc. Natl. Acad. Sci. USA* **101**, 5976–5981.

23. Elam J. S., Taylor A. B., Strange R., Antonyuk S., Doucette P. A., Rodriguez J. A., Hasnain S. S., Hayward L. J., Valentine J. S., Yeates T. O. *et al.* (2003) Amyloid-like filaments and water-filled nanotubes formed by sod1 mutant proteins linked to familial ALS *Nat. Struct. Biol.* **10**, 461–467.

24. Hart P. J., Liu H., Pellegrini M., Nersissian A. M., Gralla E. B., Valentine J. S., Eisenberg D. (1998) Subunit asymmetry in the three-dimensional structure of a human Cu, Zn-sod mutant found in familial amyotrophic lateral sclerosis *Protein Sci* **7**, 545–555.

25. Cardoso R. M., Thayer M. M., DiDonato M., Lo T. P., Bruns C. K., Getzoff E. D., Tainer J. A. (2002) Insights into Lou Gehrig's disease from the structure and instability of the A4V mutant of human Cu, Zn superoxide dismutase *J. Mol. Biol.* **324**, 247–256.

26. DiDonato M., Craig L., Huff M. E., Thayer M. M., Cardoso R. M., Kassmann C. J., Lo T. P., Bruns C. K., Powers E. T., Kelly J. W. *et al.* (2003) ALS mutants of human superoxide dismutase form fibrous aggregates via framework destabilization. *J. Mol. Biol.* **332**, 601–615.

27. Cao X., Antonyuk S. V., Seetharaman S. V., Whitson L. J., Taylor A. B., Holloway S. P., Strange R. W., Doucette P. A., Valentine J. S., Tiwari A. *et al.* (2008) Structures of the G85R variant of sod1 in familial amyotrophic lateral sclerosis *J. Biol. Chem.* **283**, 16169–16177.

28. Serag A. A., Altenbach C., Gingery M., Hubbell W. L., Yeates T. O. (2002) Arrangement of subunits and ordering of beta-strands in an amyloid sheet *Nat. Struct. Biol* **9**, 734–739.

29. Otting G., Liepinsh E., Wuthrich K. (1993) Disulfide bond isomerization in bpti and bpti (G36S): An NMR study of correlated mobility in proteins *Biochemistry* **32**, 3571–3582.

30. Banci L., Bertini I., Calderone V., Cramaro F., Del Conte R., Fantoni A., Mangani S., Quattrone A., Viezzoli M. S. (2005) A prokaryotic superoxide dismutase paralog lacking two Cu ligands: from largely unstructured in solution to ordered in the crystal *Proc. Natl. Acad. Sci. USA* **102**, 7541–7546.

31. Cozzolino M., Amori I., Pesaresi M. G., Ferri A., Nencini M., Carri M. T. (2008) Cysteine 111 affects aggregation and cytotoxicity of mutant Cu, Zn-superoxide dismutase associated with familial amyotrophic lateral sclerosis *J. Biol. Chem.* **283**, 866–874.

32. Karch C. M., Borchelt, D. R. (2008) A limited role for disulfide cross-linking in the aggregation of mutant sod1 linked to familial amyotrophic lateral sclerosis *J. Biol. Chem.* **283**, 13528–13537.

33. Niwa, J., Yamada, S., Ishigaki, S., Sone, J., Takahashi, M., Katsuno, M., Tanaka, F., Doyu, M. & Sobue, G. (2007) Disulfide bond mediates aggregation, toxicity, and ubiquitylation of familial amyotrophic lateral sclerosis-linked mutant sod1 *J. Biol. Chem.* **282**, 28087–28095.

34. McCord J. M., Fridovich I. (1969) Superoxide dismutase. Enzymic function for erythrocuprein *J. Biol. Chem.* **244**, 6049–6055.

35. Strub M. P., Hoh F., Sanchez J. F., Strub J. M., Bock A., Aumelas A., Dumas C. (2003) Selenomethionine and selenocysteine double labeling strategy for crystallographic phasing *Structure* **11**, 1359–1367.

36. Leslie A. G. W. (1991) in *Molecular data processing*, eds. Moras D., Podjarny A. D., Thierry J. C. (Oxford University Press, Oxford), 50–61.

37. Evans P. R. (1993) "Data Reduction", Proceedings of CCP4 Study Weekend. Data Collection & Processing, 114–122.

38. Vagin A., Teplyakov A. (2000) An approach to multi-copy search in molecular replacement *Acta Crystallogr. D. Biol. Crystallogr.* **56**, 1622–1624.

39. Vagin A., Teplyakov A. (1997) Molrep: an automated program for molecular replacement *J. Appl. Crystallogr.* **30**, 1022–1025.

40. Murshudov G. N., Vagin A. A., Dodson E. J. (1997) Refinement of macromolecular structures by the maximum-likelihood method *Acta Crystallogr. D. Biol. Crystallogr.* **53**, 240–255.

41. McRee D. E. (1992) "Xtalview: a visual protein crystallographic software system for xii/xview" *J. Mol. Graphics* **10**, 44–47.

42. Lamzin V. S., Wilson K. S. (1993) Automated refinement of protein models *Acta Crystallogr. D. Biol. Crystallogr.* **49**, 129–147.

43. Laskowski R. A., MacArthur M. W., Moss D. S., Thornton J. M. (1993) Procheck: a program to check the stereochemical quality of protein structures *J. Appl. Crystallogr.* **26**, 283–291.

44. Mandel M. A., Akke M., Palmer A. G. III (1995) Backbone dynamics of *Escherichia Coli* ribonuclease hi: correlations with structure and function in an active enzyme *J. Mol. Biol.* **246**, 144–163.

45. Grzesiek S., Bax A. (1993) The importance of not saturating H_2O in protein NMR. Application to sensitivity enhancement and noe measurements *J. Am. Chem. Soc.* **115**, 12593–12594.

Figure legends

Figure 1

^{1}H-^{15}N HSQC spectra of a) (Zn_2, Zn_2) WTSOD1 and b) apo WTSOD1. Spectra recorded at 298K, 0.1mM protein concentration, pH7.

Figure 2

Secondary structural elements (red) based on the chemical shift index analysis for the apo WTSOD1 protein. Backbone long range NOEs (blue sticks) determined from 15N-edited NOESY spectra. The locations of the free cysteines Cys6 and Cys111 are represented by green and yellow spheres respectively.

Figure 3

Combined chemical shift variations of backbone amide resonances between a) dimeric apo WT SOD1 and dimeric (Cu_2, Zn_2) AS WTSOD1; b) dimeric apo WTSOD1 and monomeric apo AS WTSOD1. The combined chemical shift variations $\Delta_{avg}(HN)$ were calculated as $[((\Delta H)^2 + (\Delta N/5)^2)/2]^{1/2}$, where ΔH and ΔN are chemical shift differences for ^{1}H and ^{15}N, respectively.

Figure 4

Backbone $^{15}N(H)$ relaxation parameters and heteronuclear ^{1}H-^{15}N NOEs for apo WTSOD1 at 288K (a), 298K (b) and 310K (c).

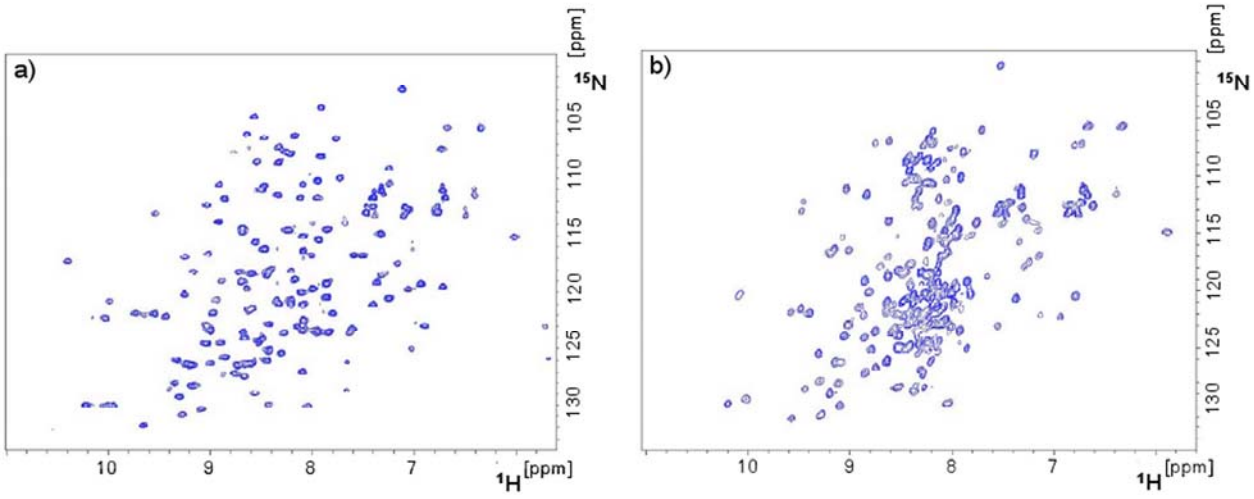

Figure 1

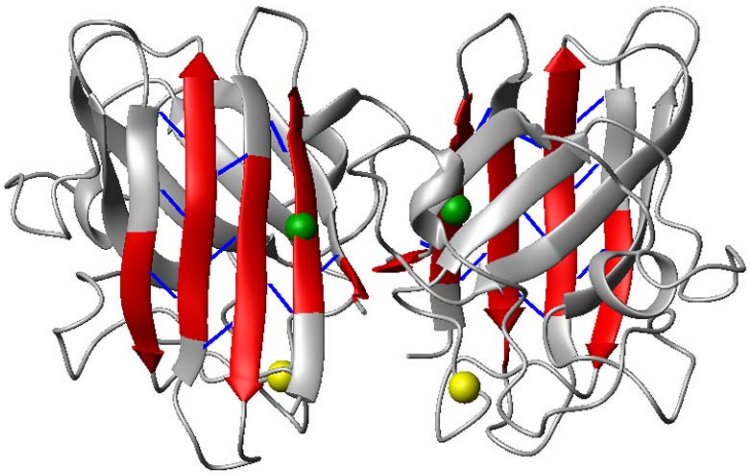

Figure 2

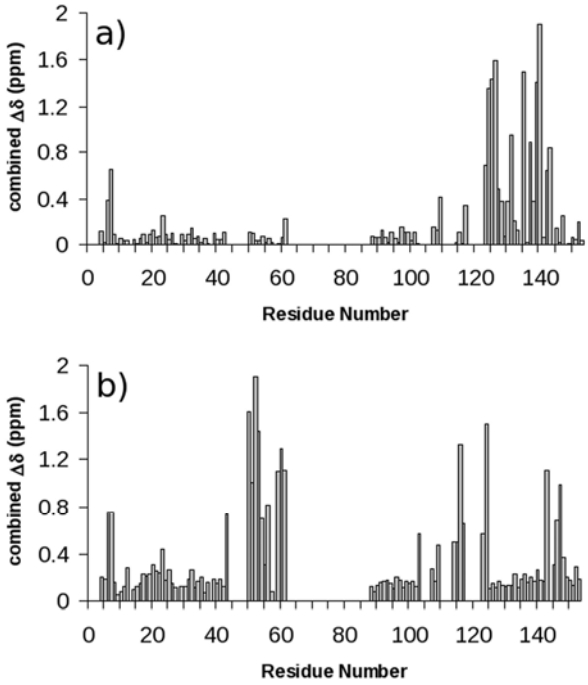
a)
combined Δδ (ppm)
2
1.6
1.2
0.8
0.4
0
0
20
40
60
80
100
120
140
Residue Number
b)
combined Δδ (ppm)
2
1.6
1.2
0.8
0.4
0
0
20
40
60
80
100
120
140
Residue Number

Figure 3

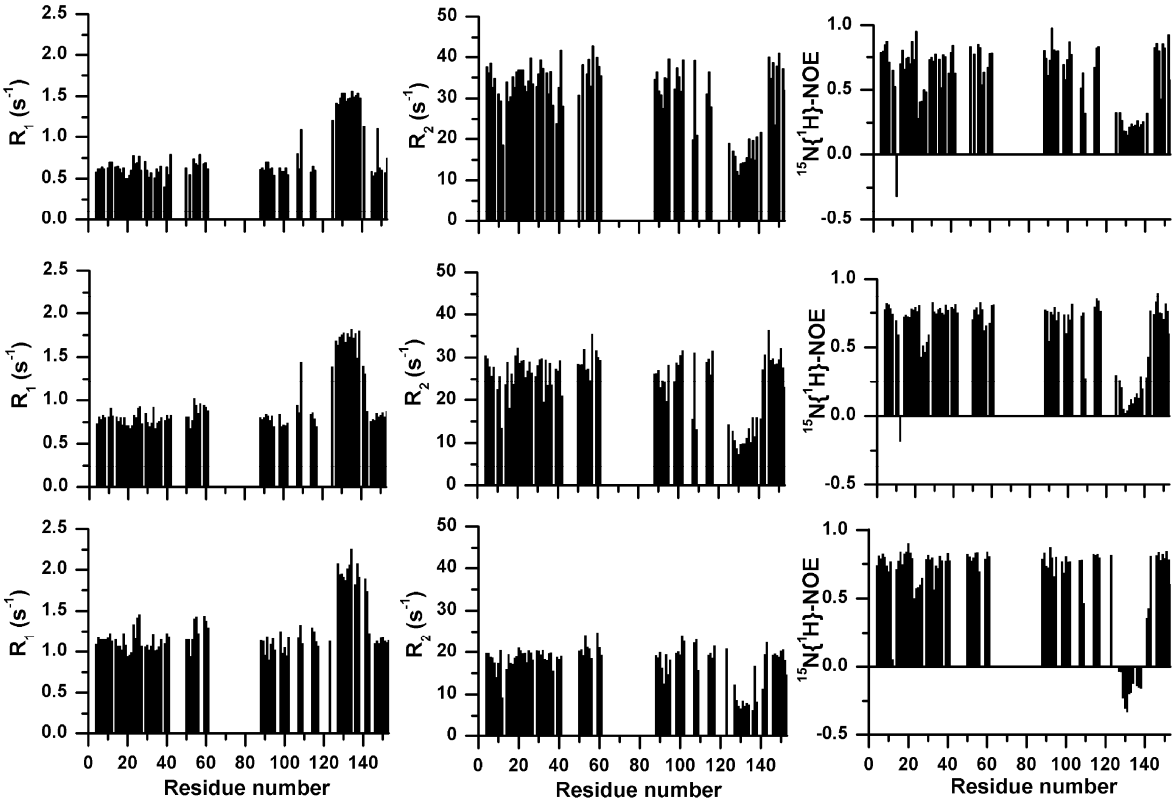

Figure 4

Supplementary Material

Table S1. NMR experiments performed on apoWTSOD1

Experiments	Dimension of acquired data points (nucleus)			Spectral width (ppm)			n[a]	Refs
	t_1	t_2	t_3	F_1	F_2	F_3		
^{1}H-^{15}N-HSQC[b]	128(^{15}N)	1024(^{1}H)		40	13		8	(1)
CBCA(CO)NH[b,c]	112(^{13}C)	40(^{15}N)	1024(^{1}H)	80	56	11	8	(2)
CBCANH[b,c]	112(^{13}C)	40(^{15}N)	1024(^{1}H)	80	56	11	16	(2)
HNCO[b,c]	80(^{13}C)	40(^{15}N)	1024(^{1}H)	17	56	11	8	(2)
HN(CA)CO[b,c]	80(^{13}C)	40(^{15}N)	1024(^{1}H)	17	56	11	16	(2)
^{15}N-edited [^{1}H-^{1}H]-NOESY[b]	264(^{1}H)	40(^{15}N)	2048(^{1}H)	11	56	11	16	(3)

[a] number of acquired scans. [b] Data acquired on a 900 MHz spectrometer, which was equipped with a riple resonance cryoprobe. The triple resonance (TXI 5-mm) probe used was equipped with Pulsed Field Gradients along the z-axis. [c] Triple resonance experiments run on a ^{2}H, ^{13}C, ^{15}N labeled protein via TROSY.
All 3D and 2D spectra were collected at 288 K, processed using the standard Bruker software (TopSpin) and analyzed through the XEASY program ((4)).

1. Bodenhausen G., Ruben D. J. (1980) Natural abundance nitrogen-15 NMR by enhanced heteronuclear spectroscopy *Chem. Phys. Lett.* **69,** 185–188.

2. Kay L. E., Ikura M., Tschudin R., Bax A. (1990) Three-dimensional triple-resonance NMR spectroscopy of isotopically enriched proteins *J. Magn. Reson.* **89,** 496–514.

3. Wider G., Neri D., Otting G., Wüthrich K. (1989) A Heteronuclear Three-Dimensional NMR Experiment for Measurements of Small Heteronuclear Coupling Constants in Biological Macromolecules *J. Magn. Reson.* **85,** 426–431.

4. Eccles C., Güntert P., Billeter M., Wüthrich K. (1991) Efficient analysis of protein 2D NMR spectra using the software package EASY *J. Biomol. NMR* **1,** 111–130.

Table S2. Data collection and refinement statistics of apo WTSOD1, apo T54R and apo I113T mutants.

	APO_WT	APO_T54R	APO_I113T
Spacegroup	C2	C2	C2
Cell dimensions (Å, °)	a= 156.51 b= 33.43 c= 114.67 β= 112.25	a= 156.94 b= 34.03 c= 114.58 β= 112.14	a= 155.90 b= 34.40 c= 115.00 β= 112.09
Resolution (Å)	30.4 – 1.9	39.2 – 2.1	106.6 – 1.9
Unique reflections	42822 (5880)	29951 (4106)	44670 (5864)
Overall completeness (%)	97.5 (92.8)	96.0 (91.2)	98.4 (90.0)
R_{sym} (%)	16.0 (43.1)	9.8 (44.3)	11.2 (36.0)
Multiplicity	6.4 (4.8)	3.3 (2.6)	5.4 (2.9)
I/(σI)	4.3 (1.8)	6.4 (1.6)	6.0 (2.1)
Wilson plot B-factor ($Å^2$)	10.63	29.83	12.24
R_{cryst} / R_{free} (%)	23.8 / 32.9	20.0 / 29.7	23.8 / 27.7
Protein atoms	4027	4028	4042
Water molecules	312	426	269
RMSD bond lengths (Å)	0.027	0.025	0.024
RMSD bond angles (º)	2.56	2.25	2.24
Mean B-factor ($Å^2$)	18.28	26.25	16.85

Table S3. Crystallographic structure analysis and comparison among apo WTSOD1, apo T54R and apo I113T mutants.

	APO_WT	APO_T54R	APO_I113T
Mean B-factor ($Å^2$)	18.28	26.25	16.85
RMSD between monomers (Å)	0.26 (A-B) 0.42 (A-C) 0.34 (A-D) 0.36 (B-C) 0.31 (B-D) 0.29 (C-D)	0.24 (A-B) 0.38 (A-C) 0.29 (A-D) 0.36 (B-C) 0.30 (B-D) 0.38 (C-D)	0.28 (A-B) 0.40 (A-C) 0.37 (A-D) 0.28 (B-C) 0.28 (B-D) 0.24 (C-D)
Close contacts (cutoff 3.5 Å)	16 (A-B) 0 (A-C) 2 (A-D) 8 (B-C) 0 (B-D) 17 (C-D)	22 (A-B) 0 (A-C) 7 (A-D) 10 (B-C) 0 (B-D) 19 (C-D)	16 (A-B) 0 (A-C) 7 (A-D) 11 (B-C) 0 (B-D) 19 (C-D)
Buried surfaces ($Å^2$)	1397 (A-B) 19 (A-C) 243 (A-D) 897 (B-C) 4 (B-D) 1926 (C-D)	1524 (A-B) 0 (A-C) 254 (A-D) 798 (B-C) 0 (B-D) 1528 (C-D)	1396 (A-B) 0 (A-C) 332 (A-D) 841 (B-C) 2 (B-D) 1403 (C-D)
Symmetry related contacts (cutoff 3.5 Å)	122	108	98
Density breaks	68-78, 125-140 (C) 67-79, 125-141 (D)	68-79, 125-141 (C) 67-78, 125-141 (D)	68-78, 125-140 (C) 68-78, 125-141 (D)

Table S4. Schematic layout of the temperature-dependence of crystallization trials for apo WTSOD1, apo T54R and apo I113T mutants, where + indicates the obtainment of single crystals and indicates their absence.

	288K	**310K**
Apo WT	+	-
(Cu_2, Zn_2) WT	+	+
Apo T54R	+	-
(Cu_2, Zn_2) T54R	+	+
Apo I113T	+	-
(Cu_2, Zn_2) I113T	+	+

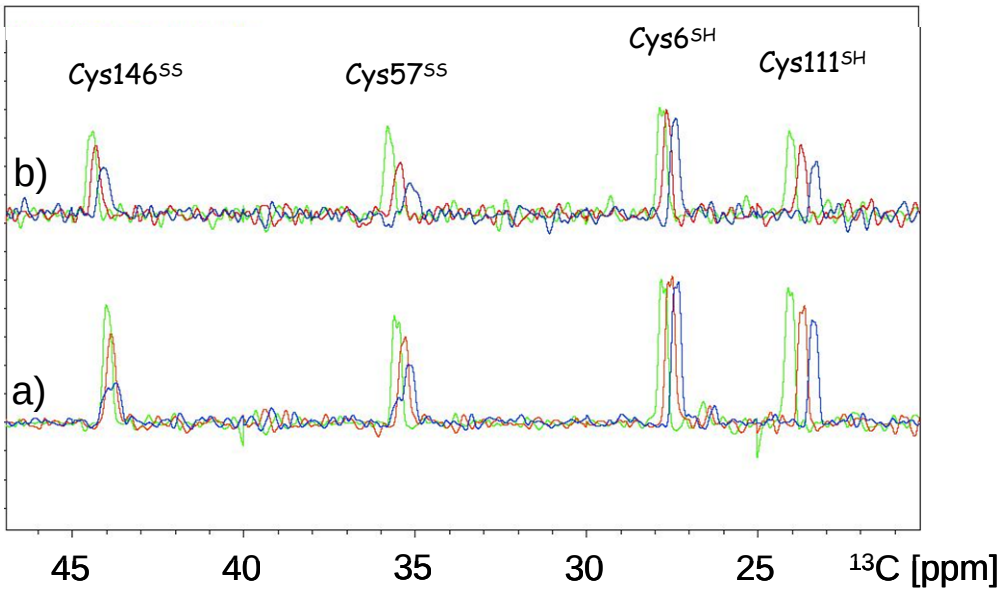

Figure S1

^{13} C ^{1}D spectra of ^{13}C, ^{15}N, ^{2}H Cys labelled SOD1 samples in the a) metallated (Zn_2, Zn_2) and b) metal free apo forms as a function of temperature: 288K (blue), 298K (red), 310K (green).

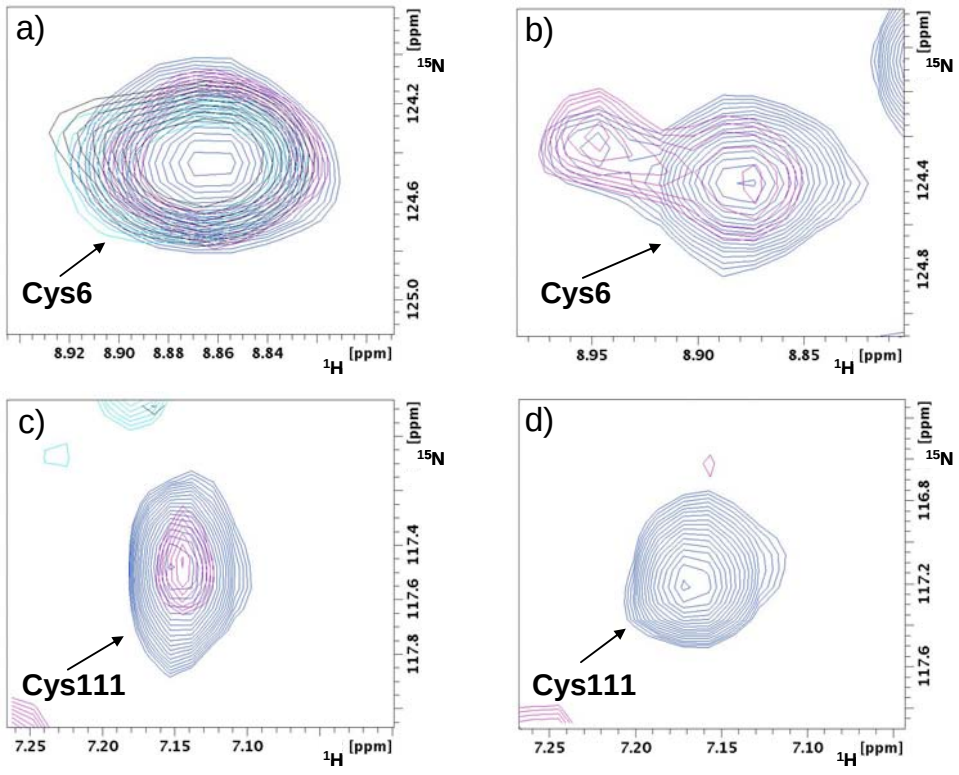

Figure S2

Comparison of the NH amide signals of Cys6 and Cys111 from ^{1}H-^{15}N HSQC spectra taken before (blue) and after twenty minutes (magenta), four hours (cyan) and twenty hours (black) the sample has been dissolved in D2O. (a, b) (Zn_2, Zn_2) WTSOD1 and (c, d) apo WTSOD1.

3.3

Preliminary data on different aspects of the oligomerization process

The research work described in the two manuscripts reported in sections 3.1 and 3.2 of this PhD thesis and the open issues risen during the described studies, led our investigations to evolve in different directions.

As part of my research activities during the PhD studies have performed further research investigations, which are presented in the following paragraphs and, which are, in part, still in progress. Even though such results have not yet been included in a formal publication, they represent an integral part of my work and a clear exemplification of how this research field, while progressing, constantly opens new and challenging issues to be faced.

In the recent years, amyotrophic lateral sclerosis (ALS) has been tightly linked, as most neurodegenerative diseases, to the presence of proteinaceous inclusions found in the tissues of FALS transgenic mice and post-mortem patients (1–3). In particular, the presence of a significant fraction of insoluble SOD1 aggregates, containing multimers cross-linked via intermolecular disulfide bonds, has been observed in spinal cords of ALS-model transgenic mice (4).

In the first article presented in this thesis (section 3.1), we have shown that WTSOD1 and its mutants, when lacking both their metal ions, form large, stable, soluble protein oligomers under physiological conditions by intermolecular disulfide bonds between the two free cysteines Cys6 and Cys111. These soluble oligomers may represent the toxic species responsible for the formation of aggregates found in *in vivo* studies. According to out findings, single point mutations in the gene codifying for the SOD1 protein induce different oligomerization rates even though all the mutated proteins give eventually rise to the same type of soluble oligomeric species when Cys6 and Cys111 are present.

The proposed mechanism has the strength of explaining how a large and diverse set of SOD1 mutant proteins all could lead to disease through the same mechanism. However, the effect of each single point mutation on the oligomerization rate has to be elucidated. The conformational properties of the apo SOD1 form with respect to the metalated one, analyzed through NMR spectroscopy (section 3.2) rationalize the propensity of the former state to oligomerize at variance with the latter, but still they do not rationalize the modulation of the oligomerization rates by the individual point mutations.

The achievements of the latter results led us to focus our research efforts into four different, but at the same time complementary, topics with the unique goal of achieving more specific and detailed information on the mechanism, which underlies the oligomerization process. The following paragraphs will present a brief description and discussion of the experiments, which have been performed on:

- biophysical characterization and oligomerization of apo D90A SOD1 mutant, the only ALS-related SOD1 mutation, reported to be recessive, at variance with the dominant nature of all the other pathogenic SOD1 mutations (paragraph 3.3.1).

- fluorescence detected guanidinium-induced protein denaturation, performed on the metal free form of WTSOD1 and a peculiar SOD1 mutant, namely T54R, characterized by the slowest oligomerization rates (paragraph 3.3.2).

- isolation of a potential intermediate in the early steps of the oligomerization process (paragraph 3.3.3).

- further preliminary structural investigations on apo dimeric SOD1 through Solid State NMR (SSNMR) spectroscopy (paragraph 3.3.4).

3.3.1 Structural and biophysical characterization of apo D90A SOD1 mutant

Among the ALS-related metal-free SOD1 mutants, which we have already shown to oligomerize at physiological conditions (section 3.1), we chose to further characterize the apo D90A protein since it is the only one mutation showing a dominant pattern of heredity among more than 100 pathogenic mutations all characterized by a dominant behavior. Uniquely, D90A SOD1 has been identified in recessive, dominant and apparently sporadic pedigrees and it mostly causes ALS as a recessive trait. The phenotype of homozygotes is stereotyped with an extended survival, whereas that of affected heterozygotes varies.

The disease, in the recessive cases, shows a slowly progressive stereotypic phenotype (5), at variance with the dominant cases, which always manifest an aggressive and variable phenotype (6). Still, D90A mutant SOD1 isolated from D90A homozygous ALS patients shows normal activity, normal Cu-binding properties, and only a minor reduction in physical stability (7).

Up to 1998 genotypic analysis of dominant and recessive D90A families indicated separate founders for recessive and dominant ALS and a disease-modifying factor linked to the recessive mutation was proposed as a possible explanation (8). Only in 2002 it has been shown that D90A homozygotes and heterozygotes are all descended from a single ancient founder. It has also been suggested that a hypothetical cis-acting regulatory polymorphism arisen close to D90A SOD1 in the recessive founder, reducing the transcription of D90A SOD1 in motor neurons, appears to influence penetrance and disease phenotype, acting as a second, disease-modifying mutation and therefore decreasing ALS susceptibility in heterozygotes and slowing disease progression (9).

Given the peculiar recessive nature of D90A, among the other dominant SOD1 mutations distributed throughout the all protein sequence, we performed a specific investigation, at molecular level, of the structural and biophysical properties of this SOD1 variant.

In the broad investigation, comprising eleven SOD1 mutants, reported in section 3.1, we have shown that also D90A, only in the demetallated form and in conditions close to physiological (37°C,100 μM protein concentration and pH=7.0), forms soluble, high molecular weight oligomers. The oligomerization rate of this mutant is comparable to the one observed for the WT protein or for mutants such as T54R, but it is significantly slower compared to other SOD1 mutants such as I113T (Figure 1).

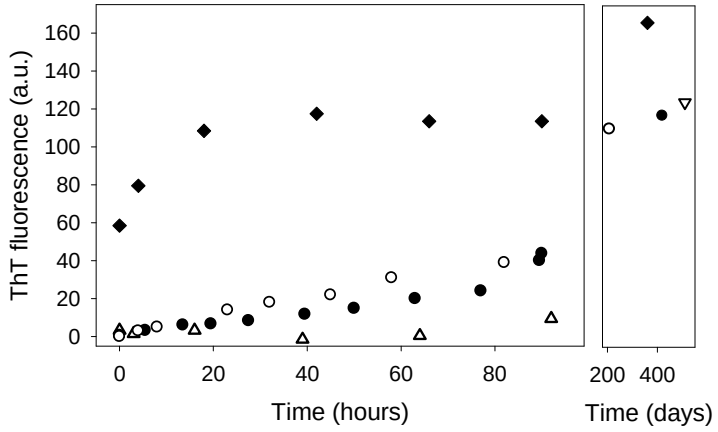

Figure 1 Formation of ThT-binding structures when apo SOD1 mutants and WT are incubated at 37 ºC. Fluorescence due to ThT binding to SOD1 mutants (presented as arbitrary units, A.U.) for apo T54R (Δ); apoD90A SOD1 (●); apoWT (O) and apo I113T SOD1 (♦) during the incubation of the samples at 37°C.

The D90A mutation is located at the protein surface on a short loop connecting β strands 5 and 6. The D90 residue is at the protein surface opposite to the dimeric interface and only one beta strand (β5) far from the zinc binding loop. The mutation implies the substitution of a residue having a solvent exposed polar acidic side chain with a non polar one.

The pattern of oligomerization of D90A, detected through ThT-binding fluorescence and already reported in (section 3.1) and Figure 1, is here investigated also through gel filtration and light scattering measurements. After about 40 hours of incubation mutant D90A, as also observed from ThT-binding measurements (Figure 1), is still essentially in the dimeric state (Figure 2A). Gel filtration data show that during the oligomerization process intermediates containing a broad distribution of high MW species can be detected. After about one year barely any dimeric species is observable, while the protein has almost completely evolved towards significantly higher molecular weights (Figure 2A).

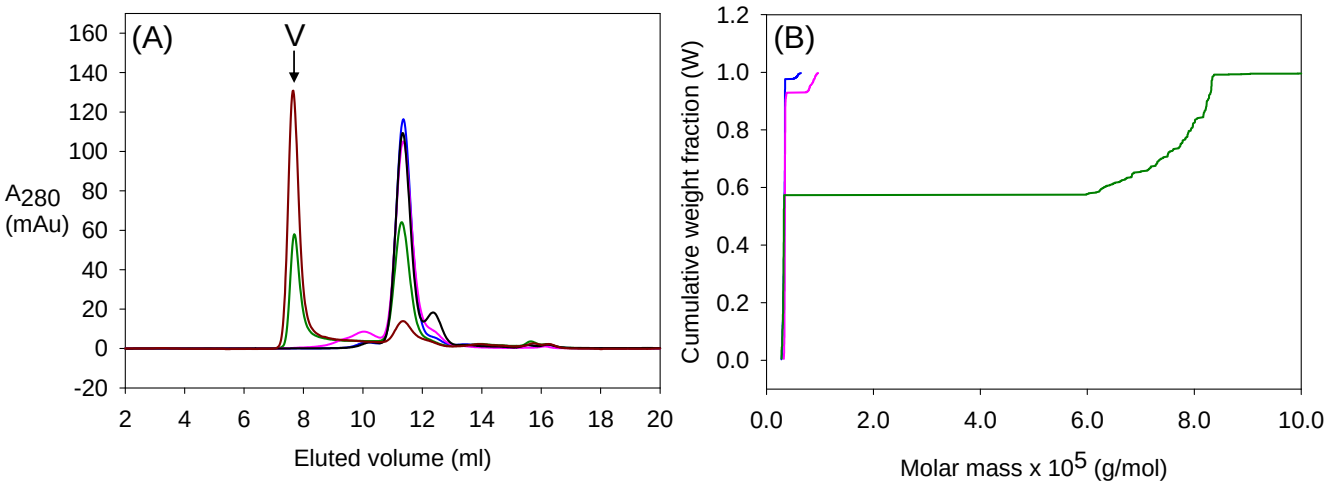

Figure 2 Formation of oligomeric structures when apo D90A SOD1 mutant is incubated at 37°C. Panel (A) shows the size exclusion chromatograms on a Superdex 75 HR 10/30 (Amersham Biosciences) column corresponding to the samples reported in panel (B), where molecular weight distribution detected by light scattering is shown. The void volume is labeled V. In all four panels the samples can be identified according to the following colors: before incubation (black), after 3 hours (blue), 10 hours (magenta), 5.5 days (green) and 1 year (brown) of incubation at 37°C.

Multi-angle light scattering analyses of specific intermediate samples along the oligomerization process also evidence that the average molecular weight is increasing as a function of time, with a decrease of the fraction of the dimeric species and the increase of that of the oligomers (Figure 2B). Multi-angle light scattering data of D90A shows that after about 5 days of incubation, even though about 50% of the sample is still in the dimeric state, a small amount of oligomeric species with molecular weight of the order of 10^6 Da has already been formed, in agreement with what already observed for the WTSOD1 protein (10), confirming that D90A and WT have similar oligomerization rates.

The oligomerization rate of apo WTSOD1 and some of its mutants, such as apoD90A, has been defined slower compared to other fast oligomerizing SOD1 mutants (section 3.1), but further explanation of such slowness has not yet been provided.

Fitting of ThT binding fluorescence data of SOD1 mutants suggests that the kinetic profile of apoD90A may be interpreted as a two-phase sigmoidal reaction profile, at variance with fast oligomerizing SOD1 mutants, such as I113T, which shows a kinetic profile better fitted with a single-phase exponential (Figure 3). The kinetic profile of the oligomerization process of apo T54R mutant can be similarly best fitted with a two-phase sigmoidal curve (data not shown).

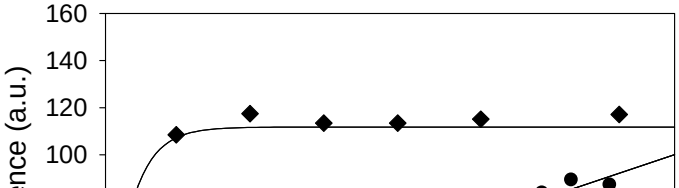

Figure 3 Formation of ThT-binding structures when apo D90A and apo I113T SOD1 mutants are incubated at 37ºC. Fluorescence due to ThT binding to SOD1 mutants (presented as arbitrary units, A.U.) for apo D90A SOD1 (●) and apo I113T SOD1 (♦) during the incubation of the samples at 37°C. Lines shown are fits to exponential and sigmoidal equations, respectively.

These results suggest that the initial slow rate of slow oligomerizing SOD1 mutants (apo D90A and apo T54R) may be determined by the existence of a rate-limiting step in which change of the dimeric structure occurs to a high-energy intermediate. In many systems such as actin, collagen, and microtubules, such high-energy intermediate is modeled as an oligomeric species that is in a highly unfavorable equilibrium with the initial structure (11–13), even though it may also be a high-energy conformation of such initial structure, as reported for polyglutamine (14). Regardless, the rate-limiting step involves such high-energy intermediate, which is defined as the species with the highest free energy and therefore lowest population (11). The initial lag phase is then followed by a period of more rapid growth. Therefore, the initial lag time may be associated to a structural rearrangement, which some mutants need to undergo, while other specific mutations facilitate/favors this initial step converting the overall process to a single step reaction. On this regard it has to be taken into account that for SOD1 it has been already reported that oligomerization most likely takes place through monomerization (15). Mutations, which facilitate protein monomerization may have faster oligomerization rates; on the contrary mutations, which favors dimer stability should show slower oligomerization rates. The crystal structure of mutant T54R in the apo state (3ECW, section 3.2) has already evidenced the existence of a mutation-related hydrogen bond, which is formed at the dimer interface, i.e. between NH2 of Arg54 of each monomer and OD1 of Asn19 of the other monomer in the same dimer (Figure 4). This interaction might lead to a partial stabilization of the dimeric state with respect to the WT protein and might correlate with the

slightly slower oligomerization rates for apo T54R compared to the WT protein (section 3.1), as oligomerization presumably occurs through monomerization (15).

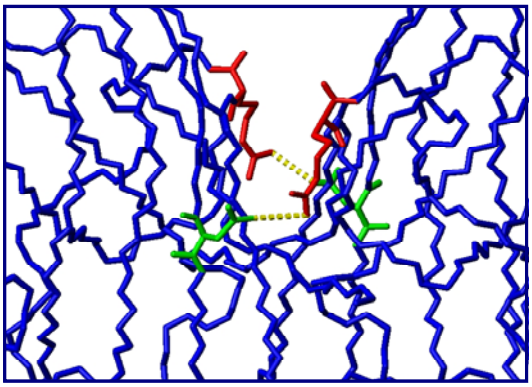

Figure 4 Mutation-related hydrogen bond formation in apo T54R. An hydrogen bond is formed at the dimer interface between NH2 of Arg54 (red) of a monomeric subunit and OD1 of Asn19 (green) belonging to the second monomeric subunit of the same dimer.

From a preliminary analysis of SOD1 crystal structure, we may predict that substitution of Asp90 with alanine, in the D90A mutant, would jeopardizes the existence of some H-bonding between the substituted residue and the backbone NHs of residues 92, 93 and 94 located on the same loop connecting β strands 5 and 6. Residue 90 is only one β strand away from the zinc-binding loop where also residue T54 is located. Destabilization of the interaction between β strands 5 and 6 may be reflected on the closeby metal binding loop affecting the stability of the dimer interface. In order to verify and support this hypothesis, crystallization trials on apo D90A are in progress.

It has already been shown that WTSOD1 hastens the ALS-like phenotype in transgenic mice overexpressing an ALS-associated human SOD1 mutant (G93A SOD1), shortening their lifespan. Formation of insoluble SOD1 dimers and multimers crosslinked through intermolecular disulfide bonds, via oxidation of SOD1 cysteine residues, was then observed in the mitochondrial fraction of the spinal cord of these transgenic mice (16).

In order to test if the mechanism proposed by us (10) for the oligomerization of both WT and mutants, could find support in these *in vivo* data, the kinetic of oligomerization of samples prepared by mixing different amount of WT and D90A mutant proteins, both in the demetalated form, was followed by monitoring the ThT-binding fluorescence increase during incubation in condition close to physiological (37°C, 100μM protein concentration and pH=7.0). Figure 5 shows that, comparing the kinetic profiles in the initial 80 hours of protein incubation, a mixture of equal amounts of WT and D90A mutant induces a 2.5-times increase

in oligomerization rate compared to the D90A mutant alone. Furthermore, as previously shown for the WT protein, the oligomerization rate of the mixture shows a linear dependence on the overall protein concentration.

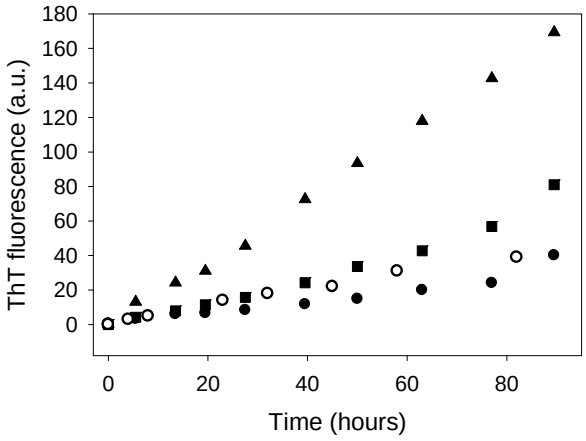

Figure 5 Formation of ThT-binding structures when apo D90A SOD1 mutant and WT are incubated at 37ºC. Fluorescence due to ThT binding to SOD1 mutants (presented as arbitrary units, A.U.) for apo D90A SOD1 (●); apo WTSOD1 (O), and a mixture apo D90A : WTSOD1 in 1:1 ratio at 100μM protein concentration (■) and 200μM protein concentration (▲) during the incubation of the samples at 37°C.

These results provide evidence for a possible relationship between the soluble oligomeric species formed during incubation of WTSOD1 and its mutants, in the demetallated form, and the aggregated multimers found in mitochondria of transgenic mice affected by ALS. As a consequence, the soluble oligomeric species, formed by the apo form of both WTSOD1 and its mutants through an oxidative process, might represent the precursor toxic species suggesting a common mechanism for ALS and fALS.

The results presented in Figure 5, in the specific case of the D90A mutation, may find support in clinical data, which evidence a slowly progressive stereotypic phenotype for D90A homozygous patients, contrasting with a more aggressive phenotype for heterozygous cases phenotype (5, 6). An alternative explanation to the cis-acting regulatory polymorphism close to D90A in the recessive cases (9), may simply be the possible co-expression of the WT SOD1 protein in heterozygous cases which would hasten the disease phenotype compared to the homozygous cases.

The structural and biophysical characterization of D90A in the demetalled form, support the hypothetical toxicity of the oligomer formed during incubation of SOD1, WT and mutants, which leads to a common mechanism for ALS and fALS and at the same time may suggest a

possible explanation for the modulation of the oligomerization rate induced by the different ALS-related SOD1 mutations.

3.3.2 Fluorescence detected guanidinium-induced protein denaturation

In order to rationalize the modulation of the oligomerization rates induced by the individual point mutations on this process, which takes place when any SOD1 protein lacks the metal ions, we investigated and compared the stability of dimeric apo WTSOD1 and one of its mutants upon addition of a denaturing agent. In particular, the effect of guanidinium hydrochloride (GdnHCl) on the metal free form of the proteins under investigation, was monitored through tryptophan fluorescence spectroscopy. The already proposed idea of a common aggregation prone monomeric intermediate for WTSOD1 and fALS-associated SOD1 mutants (15), suggests that differences in monomerization propensity of the dimeric proteins or in oligomerization propensity of the intermediate monomeric species among the SOD1 mutant proteins may be responsible for the observed modulation in their oligomerization rates.

We have selected the T54R mutant, which oligomerizes with a slightly slower rate compared to the WTSOD1 protein (section 3.1).

Investigations of the folding and thermodynamic properties though a GdnHCl analysis have been already reported for both the metallated and apo forms of the thermostable construct of WTSOD1 in which the free cysteines at positions 6 and 111 have been replaced by alanine and serine, respectively (AS form) (17, 18). In the latter article it is shown that the shape of the curve obtained for the guanidinium-induced denaturation of apo WTSOD1 is similar to the one obtained for the metalated form, but the former is shifted by >2 M to lower GdnHCl concentrations, suggesting a strong destabilization of the metal free form compared to the metalated one. Analysis of apo SOD1 concentration dependence of GdnHCl curves reveals the formation of a monomer intermediate in equilibrium with native dimer and unfolded monomer (18).

Figure 6 **s**hows a comparison of the guanidinium-induced denaturation curves, which we obtained for the apo WT protein and the selected apo mutant T54R, in which the free cysteines Cys6 and Cys111 are present.

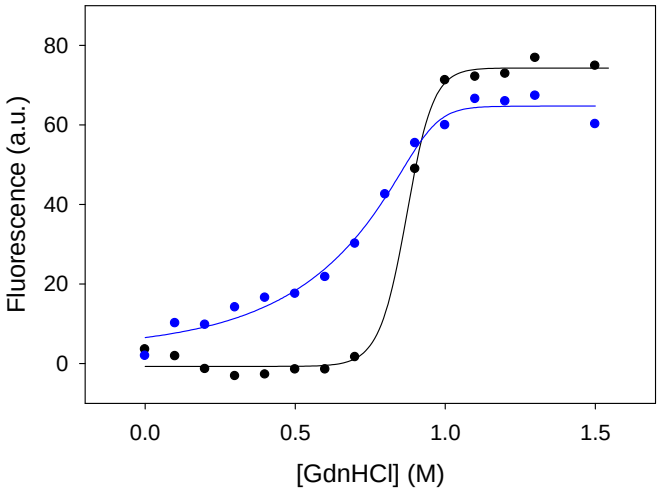

Figure 6 Equilibrium denaturation curves monitored by tryptophan fluorescence for apo WT (black) and apoT54R (blue), in 20mM phosphate buffer, pH=7.0, 25°C, 10μM protein concentration. The lines correspond to fittings to a sigmoidal model (5 parameters). Multiple datasets for each sample were collected.

A qualitative analysis of the presented data show that the shape of the apo WT unfolding profile, here reported, is similar to the one presented by Vassall et al (18) with the exception of an overall curve shift of about 0.5M to lower GdnHCl concentrations. This result evidences the net instability of WTSOD1 compared to the thermostable form (AS form), being both in their demetalated state.

It has also been suggested that according to similar studies performed on four ALS-related SOD1 mutants in their metal free form, mutations decrease protein stability, mainly by destabilizing the monomer intermediate, but also by weakening dimerization. According to these results, the effects of such mutations would propagate through the apo protein, and result in increased population of both intermediate and unfolded monomers (18).

Despite the latter results, there are no data available on the unfolding properties of mutant T54R in its metalated or demetalated state. A qualitative analyses of our preliminary results shows that the initial phase of unfolding of this mutant significantly differs from the WT. A slow progressively increasing unfolding rate of the apo T54R is observed compared to a much net steeper increase for the WT protein. This observation is in agreement with the additional mutation-related hydrogen bond observed at the dimer interface in the X-ray structure of the metal free T54R mutant (3ECW, section 3.2). At variance with what has been observed for other SOD1 mutations (18), dimer dissociation would be, in this case, positively affected by the mutation, i.e. disfavoured by the T54R mutation. An additional amount of energy may be required to overcome the extra bond cleavage during unfolding from native dimer to unfolded monomers in the apo T54R mutant compared to the apo WT protein.

This additional interaction leading to a partial stabilization of the dimeric state with respect to the WT protein, might correlate with the unusual apo T54R unfolding profile and, thereby, with the slightly slower oligomerization rate observed for apo T54R compared to the WT protein (section 3.1).

A quantitative analysis, comprising curve fitting of multiple sets of guanidinium-induced unfolding data collected at five different protein concentrations for both WT and the T54R mutant is in progress. Analysis and fitting of the obtained data will allow a better analysis and understanding of the unfolding process undergone by the apo T54R mutant compared to both the WT protein.

3.3.3 Potential intermediate in the early steps of the oligomerization process

In order to pursue and clarify the details of the oligomerization mechanism of apo WTSOD1 and its mutants, we aimed at the identification, isolation and characterization of the first building blocks of such process. According to the oligomerization process proposed by us (10), the initial dimeric oxidized apo SOD1 species should, in the early oligomerization steps, form a covalently-bound dimeric intermediate through an intermolecular disulfide bond between two apo SOD1 monomeric subunits. If the only two SOD1 free cysteines (Cys6 and Cys111) are the residues involved in the disulfide bonds formation, the incubation at 37ºC of the apo form of any of the two mutants, C6A or C111S, should induce only the formation of a covalent dimer, being their oligomerization process confined by the mutations to the initial/early steps. The identification of this apo SOD1 covalent dimer, would not only be an unprecedented peculiar SOD1 structure, but would also let us validate the suggested oligomerization process, as well as characterize the initial steps of such process.

Incubation of metal free C6A SOD1 at physiological conditions (37°C, pH=7.0, and 100μM protein concentration) for extended periods of time, showed an almost complete conversion of the initial SOD1 dimer, characterized by a hydrophobic interface, to the final covalent dimeric species, estimated to be above 90% of the initial protein content from SDS gel analysis.

The new species formed characterized by a molecular weight of about 32kDa, could be reduced to the monomeric form only in the presence of a reducing agent (DTT), as evidenced by SDS gel analysis (data not shown). The addition of trifluoroacetic acid (TFA) to the protein sample or boiling the sample in the presence or absence of TFA, which usually induce monomerization of the apo WT native hydrophobic SOD1 dimer, did not affect the dimeric nature of the apo C6A new species. The latter observations, which suggest a covalent nature of

the new apo C6A dimeric species, were also supported by fluorescence detected guanidinium-induced denaturation experiments run on the freshly purified apo C6A sample and on a second aliquot of the same sample after prolonged incubation at physiological conditions. While the guanidinium-induced denaturation curves of the freshly prepared dimeric apo C6A mutant closely resemble the sigmoidal profile presented in the previous section for the apo WTSOD1 dimeric protein, the incubated species does not show any denaturation effect up to 3M guanidinium addition.

Puzzling results were obtained from the mass spectrometry (ESI-MS and MALDI-TOF) analysis, run under non-reducing conditions, on the incubated apo C6A sample. At variance with the results obtained from the previous experiments, mass spectrometry did not evidence the presence of a predominant covalently modified species.

Further analysis, besides replicate of the experiments above described, are in progress in order to shed light on this conundrum.

In order to achieve the formation of a covalent SOD1 dimeric species alternative experiments are in progress. In analogy with the experiments performed on the apo C6A mutant, similar incubation tests are attempted on the metal free form of the C111S SOD1 mutant. Moreover, a more interesting and promising experiment will be performed incubating a mixture containing equal amounts of C6A and C111S mutants both in their demetalated forms. If the latter experiment shows the formation of a covalent dimer at variance with the incubation of each of the single mutants alone, it would suggest that the SOD1 oligomerization process takes place through the formation of covalent bonds between cysteines Cys6 and Cys111 belonging to adjacent monomers rather than between the same cysteines (namely Cys6 with Cys6 or Cys111 with Cys111) belonging to closeby monomeric subunits.

Preparation of ^{15}N labeled samples of the single cysteine mutants (C6A and C111S) is in progress in order to investigate, through NMR spectroscopy, the behavior in solution of these mutant proteins during oligomerization.

3.3.4 Further structural investigations on apo dimeric SOD1

In the second article reported in section 3.2 of this thesis, we have investigated the apo form of the dimeric oxidized WTSOD1 protein both through X-ray diffraction in crystals and NMR spectroscopy in solution. We thoroughly investigated the protein in these two physical states, observing that in solution apo WTSOD1 samples a range of conformations, highly disordered in some parts and that the solvent exposure of the reduced cysteines (Cys6 and Cys111) changes dramatically from the metallated form to the apo one. The crystal structure,

on the contrary, seems representing only one of the multiple conformations taken in solution by the protein, most likely the one, which is more similar to the one adopted by the fully metallated and more rigid form of the protein.

In order to further characterize the apo dimeric SOD1 species and to obtain additional information on its behavior towards oligomerization, we are investigating this protein form also through SSNMR spectroscopy.

A sample of ^{13}C, ^{15}N-labeled, dimeric SOD1 sample was prepared and demetallated according to the procedures described in the Material and Methods section. Microcrystals were obtained from a 0.2mM protein solution containing 0.1M MES buffer (pH=7.0), 20% PEG 6000.

Preliminary SSNMR spectra have been collected on the prepared microcrystalline samples and comparisons with the already published spectra, obtained for the fully metallated SOD1 protein by solution state NMR (19) and by SSNMR (20) spectroscopies are reported below in figures 7 and 8 respectively .

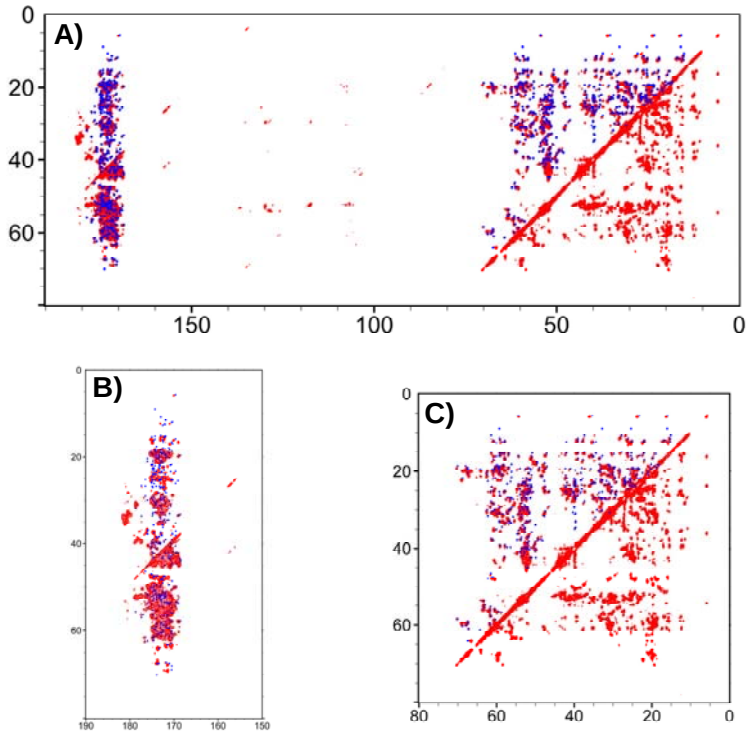

Figure 7: overlap of SSNMR spectra of microcrystalline dimeric apo WTSOD1 (13C-13C DARR; 50ms mixing; MAS frequency 14 kHz) (red), and the reconstructed picks coming from the solution assignment of dimeric fully metalated WTSOD (blue) (20). Panel B and C are partial enlargements of A.

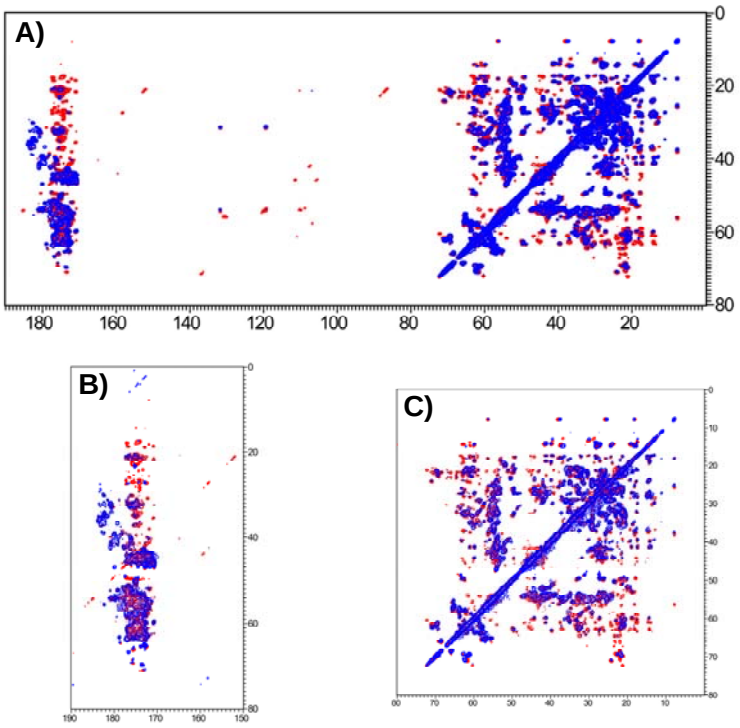

Figure 8 overlap of SSNMR spectra of microcrystalline dimeric apo WTSOD1 (13C-13C DARR; 50ms mixing; MAS frequency 14 kHz) (red), and dimeric fully metalated WTSOD1 (13C-13C PDSD 15ms (analogous to DARR)) (blue) (21). Panel B and C are partial enlargements of A.

Further spectra will be collected in order to pursue the SSNMR assignment of the apo SOD1 dimeric protein and to obtain additional and valuable information on the behaviour of the apo dimeric SOD1 form prone to oligomerize.

Materials and Methods

Sample Preparation – D90A SOD1 mutant was expressed in the *Escherichia coli* BL21(DE3) strain. Mutation was performed using a QuikChange™ site-directed mutagenesis kit (Stratagene). The protein, obtained from cells grown in LB medium, was isolated by osmotic shock in a 20mM Tris, 5mM dithiothreitol (DTT) buffer at pH=8.0. After incubation for 30 minutes at 37ºC, the protein was centrifuged at 40000 rpm for 20 minutes. Supernatant was purified following a reported procedure (21) modified by the addition of 1 mM DTT to each chromatographic buffer. The protein obtained with this procedure contained substoichiometric amounts of the metal ions. The metal ions were completely removed, at 25ºC, to prepare the demetallated (apo) form, according to previously published protocols (22), and the zinc reconstituted form was prepared, as well, as previously described (23). Metal content was checked by inductively coupled plasma mass spectrometry (ICP-MS) using a Thermo Jarrell Ash Atomscan Model 25 Sequential inductively coupled spectrometer. The

dimeric state of the apo form of the mutant at time zero of the incubation was checked through gel filtration chromatography.

The following procedure was adopted for the preparation of WTSOD1 protein and the two SOD1 mutants T54R and I113T. The *sod1* gene was cloned by PCR and inserted in Gateway pENTR/TEV/D-TOPO plasmid (Invitrogen). The plasmid was propagated and purified by MINI KIT (Invitrogen) and the sequence was verified. The LR recombination reaction was performed in order to transfer the *sod1* gene from pENTR/TEV/D-TOPO plasmid into pTH34 plasmid codifying for GB1 fusion tag. Mutations were performed using a QuikChange^{TM} site-directed mutagenesis kit (Stratagene). WTSOD1 and mutant proteins were over expressed in the *Escherichia coli* Origami pLysS strain (Novagen). The fusion proteins were obtained by growing the cells in minimal medium, in shaking flasks at 37ºC until OD_{600} = 0.7 and then induced with 0.7 mM IPTG for twelve hours at 25ºC. Proteins were isolated by sonication in a 5mM imidazol buffer at pH 8 and centrifuged at 165,000 × g for 20 minutes. Purification was performed by affinity chromatography using a nickel chelating (His-Trap) column (Armersham Bioscience) and by digestion with AcTEV protease. Protein purity was checked on a 17% polyacrilamide gel and concentration was determined by optical spectroscopy. The metal free protein was prepared according to previously published protocols (22). Zinc reconstitution was carried out as described in (23).

Spectroscopic characterization – Protein samples were 100μM in mutant SOD1 concentration (as dimer) in 20mM phosphate buffer at pH 7. The protein was incubated at 37°C to mimic physiological conditions. Optical and fluorescence spectroscopies, coupled with gel filtration chromatography, were used to monitor the formation of oligomeric species at these sample conditions. The analysis were carried out in both the zinc-bound and apo forms of the proteins.

Fluorescence was followed with Thioflavin T, (ThT) probe, which specifically binds to amyloid-like structures (24). Free ThT has excitation and emission maxima at 350 nm and 450 nm, respectively. However, upon binding to amyloid-like oligomers, the excitation and emission maxima change to 450 and 485 nm, respectively. 54μl aliquots of sample were added to 646μl of a 215μM ThT solution in a 20mM phosphate buffer at pH=7.0. The solution fluorescence emission was measured, over time of incubation, with a Cary 50 Eclipse Spectrophotometer supplied with a Single cell Peltier thermostatted cell holder regulated at 37ºC. The background fluorescence spectrum of the buffer was subtracted. The excitation wavelength was 446 nm (bandwidth 10 nm) and the emission was recorded at 480 nm (bandwidth 10 nm). Fluorescence intensity at 483 nm was plotted against time of incubation.

Monitoring SOD1 Aggregation by Gel Filtration and Light Scattering – 100µl aliquots of the incubated protein at 37ºC were periodically taken and analyzed by gel filtration on Superdex 75 HR 10/30 (Amersham Biosciences) at room temperature. The column was preequilibrated with 20mM potassium phosphate, pH=7.0, and the flow rate was 0.6 ml/min. The chromatogram, which monitors the species formed during incubation, was obtained by monitoring the absorbance at 280 nm. The Superdex 75 HR 10/30 column was also connected to a light scattering spectrometer. The online multiangle light scattering (MALS) detector (DAWN EOS, Wyatt Technology, Santa Barbara, CA) and differential refractive index (DRI) detector (Optilab DRI, Wyatt Technology) setup was used to measure the light scattered as a function of angle and absolute protein concentration of fractions eluting from the size-exclusion chromatography column. The Zimm/Debye approximations were used in the Astra software (Wyatt Technology) to estimate molar mass. Data were fit using a second-order polynomial. The analysis was performed for each one of the 20µl aliquots periodically taken from the incubation batches so as to monitor the increase in molecular weight of the soluble species formed during aggregation.

Fluorescence experiments – Steady state fluorescence measurements were made using a Cary 50 Eclipse Spectrophotometer supplied with a Single cell Peltier thermostatted cell holder regulated at 25ºC. Samples were prepared in phosphate buffer 20mM, pH=7.0 with the addition of different amount of guanidinium hydrochloride (GdnHCl) to reach a final protein concentration of 10µM. The excitation wavelength was 282 nm (bandwidth 10 nm) and the emission was recorded at 358 nm (bandwidth 10 nm). The background fluorescence spectrum of the buffer and GdnHCl was subtracted. Fluorescence intensities at 358 nm, recorded after 24 hours incubation at room temperature, were plotted against GdnHCl concentrations.

SSNMR spectroscopy – All experiments were carried out on a Bruker Avance 850 MHz Wide Bore (WB) spectrometer using a 3.2 mm triple tuned (^{1}H, ^{13}C, ^{15}N) CP-MAS probe, at various sample spinning speeds (between 10 kHz and 20 kHz), on a microcrystalline, uniformly labelled [^{15}N, ^{13}C] sample of human dimeric metal free WTSOD1. The effective sample temperature was about + 7.5°C.

Double resonance CP experiments were acquired at 14.0 kHz MAS frequency. ^{1}H 90° pulse was set to 2.65µs, and during cross-polarization ^{13}C B_1 was 78 kHz with a mixing time of 1.2 ms. A 100%/50% ramp was applied on the proton channel with a 100% power level of 101 kHz. ^{1}H decoupling power level was set to 92 kHz by using SPINAL64 (25). The DARR (26) spectrum was acquired at 14.0 kHz MAS frequency. CP conditions, pulse length, and ^{1}H decoupling conditions were analogous to those reported above. ^{13}C 90° pulse was set to 4.0 µs.

A weak ^{1}H CW radio frequency optimized at 14 kHz (Dipolar-assisted rotational resonance), was used during the 50 ms mixing time. The experiment was acquired with 64 scans for increments and t_1^{max} 11.3 ms and t_2 24.1 ms.

Reference List

1. Pasinelli P., Belford M. E., Lennon N., Bacskai B. J., Hyman B. T., Trotti D., Brown R. H. Jr. (2004) Amyotrophic lateral sclerosis-associated sod1 mutant proteins bind and aggregate with Bcl-2 in spinal cord mitochondria *Neuron* **43**, 19–30.

2. Ohi T., Nabeshima K., Kato S., Yazawa S., Takechi S. (2004) Familial amyotrophic lateral sclerosis with his46arg mutation in Cu/Zn superoxide dismutase presenting characteristic clinical features and lewy body-like hyaline inclusions *J. Neurol. Sci.* **225**, 19–25.

3. Ferri A., Cozzolino M., Crosio C., Nencini M., Casciati A., Gralla E. B., Rotilio G., Valentine J. S., Carri M. T. (2006) Familial ALS-superoxide dismutases associate with mitochondria and shift their redox potentials *Proc. Natl. Acad. Sci. U. S. A* **103**, 13860–13865.

4. Furukawa Y., Fu R., Deng H. X., Siddique T., O'Halloran T. V. (2006) Disulfide cross-linked protein represents a significant fraction of ALS-associated Cu, Zn-superoxide dismutase aggregates in spinal cords of model mice *Proc. Natl. Acad. Sci. U. S. A* **103**, 7148–7153.

5. Andersen P. M., Nilsson P., Ala-Hurula V., Keranen M. L., Tarvainen I., Haltia T., Nilsson L., Binzer M., Forsgren L., Marklund S. L. (1995) Amyotrophic lateral sclerosis associated with homozygosity for an Asp90Ala mutation in Cu, Zn-superoxide dismutase *Nat. Genet.* **10**, 61–66.

6. Mezei M., Andersen P. M., Stewart H., Weber M., Eisen A. (1999) Motor system abnormalities in heterozygous relatives of a D90A homozygous Cu, Zn-sod ALS patient of finnish extraction *J. Neurol. Sci.* **169**, 49–55.

7. Marklund S. L., Andersen P. M., Forsgren L., Nilsson P., Ohlsson P. I., Wikander G., Oberg A. (1997) Normal binding and reactivity of copper in mutant superoxide dismutase isolated from amyotrophic lateral sclerosis patients *J. Neurochem.* **69**, 675–681.

8. Al Chalabi, A., Andersen, P. M., Chioza, B., Shaw, C., Sham, P. C., Robberecht, W., Matthijs, G., Camu, W., Marklund, S. L., Forsgren, L. *et al.* (1998) Recessive amyotrophic lateral sclerosis families with the D90A sod1 mutation share a common founder: Evidence for a linked protective factor *Hum. Mol. Genet.* **7**, 2045–2050.

9. Parton M. J., Broom W., Andersen P. M., Al Chalabi A., Nigel L. P., Powell J. F., Shaw C. E. (2002) D90A-sod1 mediated amyotrophic lateral sclerosis: a single founder for all cases with evidence for a cis-acting disease modifier in the recessive haplotype *Hum. Mutat.* **20**, 473.

10. Banci L., Bertini I., Girotto S., Martinelli M., Vieru M., Whitelegge J., Durazo A., Valentine J. S. (2007) Metal-free superoxide dismutase forms amyloid-like oligomers: A possible general mechanism for familial ALS *Proc. Natl. Acad. Sci. USA* **104**, 11263–11267.

11. Ferrone F. (1999) Analysis of protein aggregation kinetics *Methods Enzymol.* **309**, 256–274.

12. Flyvbjerg H., Jobs E., Leibler S. (1996) Kinetics of self-assembling microtubules: an "inverse problem" in biochemistry *Proc. Natl. Acad. Sci. U. S. A* **93**, 5975–5979.

13. Goldstein R. F., Stryer L. (1986) Cooperative polymerization reactions. Analytical approximations, numerical examples, and experimental strategy *Biophys. J.* **50**, 583–599.

14. Chen S., Ferrone F. A., Wetzel R. (2002) Huntington's disease age-of-onset linked to polyglutamine aggregation nucleation *Proc. Natl. Acad. Sci. U. S. A* **99**, 11884–11889.

15. Rakhit R., Crow J. P., Lepock J. R., Kondejewski L. H., Cashman N. R., Chakrabartty A. (2004) Monomeric Cu, Zn-superoxide dismutase is a common misfolding intermediate in the oxidation models of sporadic and familial amyotrophic lateral sclerosis *J. Biol. Chem.* **279**, 15499–15504.

16. Deng H. X., Shi Y., Furukawa Y., Zhai H., Fu R., Liu E., Gorrie G. H., Khan M. S., Hung W. Y., Bigio E. H. *et al.* (2006) Conversion to the amyotrophic lateral sclerosis phenotype is associated with intermolecular linked insoluble aggregates of sod1 in mitochondria *Proc. Natl. Acad. Sci. U. S. A* **103**, 7142–7147.

17. Rumfeldt J. A., Stathopulos P. B., Chakrabarrty A., Lepock J. R., Meiering E. M. (2006) Mechanism and thermodynamics of guanidinium chloride-induced denaturation of als-associated mutant Cu, Zn superoxide dismutases *J. Mol. Biol.* **355**, 106–123.

18. Vassall K. A., Stathopulos P. B., Rumfeldt J. A., Lepock J. R., Meiering E. M. (2006) Equilibrium thermodynamic analysis of amyotrophic lateral sclerosis-associated mutant apo Cu, Zn superoxide dismutases *Biochemistry* **45**, 7366–7379.

19. Banci L., Bertini I., Cramaro F., Del Conte R., Viezzoli M. S. (2002) The solution structure of reduced dimeric copper zinc sod: the structural effects of dimerization *Eur. J. Biochem.* **269**, 1905–1915.

20. Pintacuda G., Giraud N., Pierattelli R., Böckmann A., Bertini I., Emsley, L. (2007) Solid-state NMR of a paramagnetic protein: assignment and study of the human dimeric oxidized Cu(II), Zn(II) superoxide dismuatse *Angew. Chem. Int. Ed.* **46**, 1079–1082.

21. Banci L., Benedetto M., Bertini I., Del Conte R., Piccioli M., Viezzoli M. S. (1998) Solution structure of reduced monomeric Q133M2 copper, zinc superoxide dismutase. why is sod a dimeric enzyme? *Biochemistry* **37**, 11780–11791.

22. McCord J. M., Fridovich, I. (1969) Superoxide dismutase. Enzymic function for erythrocuprein. *J. Biol. Chem.* **244**, 6049–6055.

23. Arnesano F., Banci L., Bertini I., Martinelli M., Furukawa Y., O'Halloran T. V. (2004) The unusually stable quaternary structure of human sod1 is controlled by both metal occupancy and disulfide status *J. Biol. Chem.* **279**, 47998–48003.

24. Krebs M. R., Bromley E. H., Donald A. M. (2005) The binding of Thioflavin-T to amyloid fibrils: localisation and implications *J. Struct. Biol.* **149**, 30–37.

25. Fung B. M., Khitrin A. K., Ermolaev K. (2000) An improved broadband decoupling sequence for liquid crystals and solids *J. Magn. Reson.* **142**, 97–101.

26. Takegoshi K., Nakamura S., Terao, T. (2001) ^{13}C ^{1}H dipolar-assisted rotational resonance in magic-angle spinning NMR *Chem. Phys. Lett.* **344**, 631–637.

4

Final conclusions and perspectives

In the recent years, the detection of protein inclusions strongly immunoreactive to SOD1 in motor neuronal cells and astrocytes of SOD1 mutant transgenic mice and ALS patients, makes aberrant SOD1 protein oligomerization one of the most accredited ALS mechanism, in agreement with similar mechanisms proposed for most neurodegenerative diseases (1–4). Furthermore, the diverse character of ALS-associated variant SOD1 proteins, shown by biophysical, biochemical and bioinorganic investigations, led to the hypothesis that SOD1 variants are likely to aggregate for different reasons or for distinct combinations of reasons (5, 6). Which are all these factors, how and in which steps of the post-translational modifications they interfere making all SOD1 mutants prone to oligomerize, eventually forcing them to give rise to the same ALS pathology, are still mysteries which need to be revealed.

Several recent publications have also presented compelling evidence that *in vivo* abnormal disulfide-crosslinking of ALS-mutant SOD1 plays a role in the oligomerization of this protein (7–9), and disulfide-linked SOD1 multimers, which are presumed to be components of higher molecular weight species or intermediates (9), have been detected mainly in mitochondria of neuronal tissues of SOD1-linked fALS patients and transgenic mice (10–12).

In chapter 3.1 we have shown that the rates of oligomerization of a set of SOD1 proteins carrying a single point mutation are different but eventually they give rise to the same type of soluble oligomeric species formed by intermolecular disulfide covalent bonds, involving Cys6 and Cys111, and by non-covalent interactions between β strands, forming amyloid-like structures capable of binding ThT (13, 14). These soluble oligomers may represent the toxic species responsible for the formation of the disulfide-linked SOD1 aggregates found in *in vivo* studies (10–12).

Our results suggest a general, unifying picture of SOD1 oligomerization that could operate when wild-type or mutant SOD1 proteins lack their metal ions. Although other mechanisms cannot be excluded for SOD1-linked fALS oligomerization, the one proposed by us has the strength of explaining how a large and diverse set of SOD1 mutant proteins all could lead to disease through the same mechanism (13, 14).

After optimizing yield of expression, protein extraction and purification of WTSOD1 and some of its mutants in the new expression plasmid codifying for the GB1 fusion tag we investigated their structural and dynamic features through NMR spectroscopy and X-ray diffraction (chapter 3.2).

We found that the metal-free state of two pathogenic mutants, T54R and I113T, is partially disordered in the crystal, at variance with what was observed in the metalated state. In

the crystal structures of the metal-free proteins, the asymmetric unit contains two biologically relevant dimers. While one of these dimers has a very well defined electron density throughout the entire sequence, the other one has clear breaks in the electron density in the regions encompassing most residues of the zinc binding (loop IV) and of the electrostatic (loop VII) loops. Cys6, involved in the formation of the intermolecular disulfide bonds during the oligomerization process, is essentially buried in the X-ray structures of all three metal-free SOD1 proteins. Even though few minor structural differences allowed us to speculate on possible explanations for the peculiar behavior towards oligomerization of some specific mutants, no general explanation was found for the broad range of oligomerization rates shown by the pathogenic SOD1 mutants.

The information obtained from the NMR spectra indicate that in solution apo WTSOD1 and the mutants samples a range of conformations, highly disordered in some parts. Higher temperatures accelerate exchange among these conformations and could populate new ones. This behaviour explains why only the disordered, partially unfolded, metal-free state has a dramatic protein flexibility which makes accessible conformations prone to oligomerize, while the rigid structure of the metalated protein is unable to do it.

Particularly striking with respect to the oligomerization process, which the apo state is undergoing at physiological conditions (13, 14), is the solvent exposure of the free cysteines (Cys6 and Cys111) observed for mutant T54R as well as for the WTSOD1 protein. While Cys111 is highly solvent exposed in both metalated and apo forms, Cys6 has a dramatically different solvent accessibility being buried and protected from the solvent in the metalated form and becoming higly solvent exposed in the apo form. Unfortunately, the I113T mutant is too unstable and oligomerizes too fast to prevent further analysis, beyond recording a simple ^{1}H-^{15}N HSQC spectrum.

Crystallization trials, performed at two different temperatures (289K and 310K) on both the apo and metalated forms of WTSOD1 and the two mutants, explained the apparent discrepancy between the different degrees of protein disorder detected for the apo proteins by X-ray and NMR investigations. While crystals of the metalated form of WTSOD1 as well as of its mutants were obtained at 288K and 310K, which is the temperature at which the oligomerization studies were carried out, the same proteins in their metal free form crystallized only at 288K. This indicates that temperature has a major influence on the crystallization of the apo state while it is almost negligible on the metalated one. This overall behaviour is consistent with the dynamic properties and conformational disorder of the apo state. As the protein is intrinsically disordered and samples a range of conformations, at higher temperatures the

interconversion among them is faster and new conformations could be sampled, thus making the lowest energy state less populated and therefore lowering the probability of crystallization. A decrease in temperature slows down the interconversion process among the various conformations and increases the population of the most stable states, which can therefore crystallize.

Overall the present extensive structural and dynamic characterization of the apo state of WTSOD1 and its mutants showed that the lack of metal ions and the subsequent protein flexibility allows the free cysteines (Cys6 and Cys111) to become exposed and therefore ready to get oxidized and to form the disulfide bonds, which give rise to the soluble, potentially toxic, oligomers.

The research projects pursued, after the above described achievements, were all conceived in order to get more insights into the mechanism of SOD1 proteins oligomerization.

The biophysical characterization and the oligomerization propensity tests performed on apo D90A SOD1 mutant, provided us valuable suggestions for an alternative interpretation of the kinetic profile of the slow oligomerizing mutants (chapter 3.3.1). Fitting of the kinetic profile of apo D90A (ThT binding fluorescence) suggests that the oligomerization of this mutant may be interpreted as a two-phase process, at variance with fast oligomerizing SOD1 mutants, such as I113T, which shows a kinetic profile better fitted with a single-phase process. Similar considerations can be done for the kinetic profile of mutant T54R, which is another slow oligomerizing SOD1 variant. These results are in agreement with structural considerations obtained from the X-ray crystal structure of the latter mutant. The presence, in the T54R protein, of an additional mutation-related hydrogen bond at the dimer interface may slow down monomerization, which has already been suggested as a required intermediate step towards protein oligomerization (15). Therefore, mutations, which facilitate protein monomerization should show faster oligomerization rates compared to mutations, which favors dimer stability. A structural analysis of apo D90A, which is in progress, may provide new insights to further support these suggestions.

D90A is the only ALS-related SOD1 mutation, reported to be recessive, at variance with the dominant nature of all the other pathogenic SOD1 mutations. Oligomerization tests performed on mixtures of D90A mutant and WTSOD1, both in their metal-free form, are in agreement with already published *in vivo* data, which show that WTSOD1 hastens the ALS-like phenotype in transgenic mice overexpressing an ALS-associated human SOD1 mutant (16). Moreover, these results may also suggest an explanation for the more aggressive

phenotype observed for D90A heterozygous cases compared to the homozygous recessive ones (16, 17).

Preliminary data collected from tryptophan-detected guanidinium unfolding experiments performed on apo WTSOD1 and the T54R mutant are in agreement with the structural information provided by X-ray crystallography (chapter 3.3.2). The different unfolding curves observed for the two apo proteins may be due to an additional amount of energy required, during the unfolding process from native dimer to unfolded monomer, by the T54R protein to overcome the cleavage of an additional mutation-related bond observed at the dimer interface of this protein compared to the WT.

Preliminary results have also been acquired on a possible intermediate of the oligomerization process, which is a SOD1 covalent dimer (chapter 3.3.3). We are in the process of isolating this intermediate using specific SOD1 mutants to stop the oligomerization process at the initial stages. The aim of this project is the structural characterization of this peculiar SOD1 covalent dimer, which may provide us with valuable information on the early steps of the oligomerization process.

Preliminary SSNMR spectra have also been collected on a microcrystalline samples of double labeled metal-free dimeric WTSOD1. Further spectra will be collected in order to pursue the SSNMR assignment of the apo WTSOD1 dimeric protein in order to obtain additional and valuable information on the behaviour of the apo dimeric SOD1 form prone to oligomerize.

SOD1 protein can be described as a “double-edged sword” to the extent that it can function as either a beneficial antioxidant or, due to a failure in metal uptake, form protein oligomers, which most likely depending upon the quality control machinery and the amount of excess apo SOD1 protein produced, may prove toxic to the cell.

Reference List

1. Shibata N., Asayama K., Hirano A., Kobayashi M. (1996) Immunohistochemical study on superoxide dismutases in spinal cords from autopsied patients with amyotrophic lateral sclerosis *Dev. Neurosci.* **18,** 492–498.

2. Cleveland D.W., Rothstein J.D. (2001) From Charcot to Lou Gehrig: deciphering selective motor neuron death in ALS *Nat. Rev. Neurosci.* **2,** 806–819.

3. Bruijn L. I., Miller T. M., Cleveland D. W. (2004) Unraveling the mechanisms involved in motor neuron degeneration in ALS *Annu. Rev. Neurosci.* **27,** 723–749.

4. Furukawa Y., O'Halloran T.V. (2006) Posttranslational modifications in Cu, Zn-superoxide dismutase and mutations associated with amyotrophic lateral sclerosis *Antioxi. Redox. Signal.* **8,** 847–867.

5. Rodriguez J.A., Shaw B.F., Durazo A., Sohn S.H., Doucette P.A., Nersissian A.M., Faull K.F., Eggers D.K., Tiwari A., Hayward L.J., Valentine J.S. (2005) Destabilization of apoprotein is insufficient to explain Cu, Zn-superoxide dismutase-linked ALS pathogenesis *Proc. Natl. Acad. Sci. USA* **102,** 10516–10521.

6. Shaw B.F., Durazo A., Nersissian A.M., Whitelegge J.P., Faull K.F., Valentine J.S. (2006) Local unfolding in a destabilized, pathogenic variant of superoxide dismutase 1 observed with H/D exchange and mass spectrometry *Journal of Biological Chemistry* **281,** 18167–18176.

7. Jonsson P.A., Graffmo K.S., Andersen P.M., Brannstrom T., Lindberg M., Oliveberg, M., Marklund S.L. (2006) Disulphide-reduced superoxide dismutase-1 in CNS of transgenic amyotrophic lateral sclerosis models *Brain* **129,** 451–464.

8. Deng H.X., Shi Y., Furukawa Y., Zhai H., Fu R., Liu E., Gorrie G.H., Khan M.S., Hung W.Y., Bigio E.H. *et al.* (2006) Conversion to the amyotrophic lateral sclerosis phenotype is associated with intermolecular linked insoluble aggregates of sod1 in mitochondria *Proc. Natl. Acad. Sci. USA* **103,** 7142–7147.

9. Furukawa Y., Fu R., Deng H.X., Siddique T., O'Halloran T.V. (2006) Disulfide cross linked protein represents a significant fraction of ALS-associated Cu, Zn-superoxide dismutase aggregates in spinal cords of model mice *Proc. Natl. Acad. Sci. USA* **103,** 7148–7153.

10. Pasinelli P., Belford M.E., Lennon N., Bacskai B.J., Hyman B.T., Trotti D., Brown R.H. Jr. (2004) Amyotrophic lateral sclerosis-associated sod1 mutant proteins bind and aggregate with Bcl-2 in spinal cord mitochondria *Neuron* **43,** 19–30.

11. Ohi T., Nabeshima K., Kato S., Yazawa S., Takechi S. (2004) Familial amyotrophic lateral sclerosis with His46Arg mutation in Cu/Zn superoxide dismutase presenting characteristic clinical features and Lewy body-like hyaline inclusions *J. Neurol. Sci.* **225,** 19–25.

12. Ferri A., Cozzolino M., Crosio C., Nencini M., Casciati A., Gralla E. B., Rotilio G., Valentine J.S., Carri M.T. (2006) Familial ALS-superoxide dismutases associate with mitochondria and shift their redox potentials *Proc. Natl. Acad. Sci. USA* **103,** 13860–13865.

13. Banci L., Bertini I., Girotto S., Martinelli M., Vieru M., Whitelegge J., Durazo A., Valentine J. S. (2007) Metal-free superoxide dismutase forms amyloid-like oligomers: A possible general mechanism for familial ALS *Proc. Natl. Acad. Sci. USA* **104,** 11263–11267.

14. Banci L., Bertini I., Boca M., Girotto S., Martinelli M., Valentine J. S., Vieru, M. (2008) SOD1 and amyotrophic lateral sclerosis: Mutations and Oligomerization *Plos ONE* **3,** e1677.

15. Lindberg M.J., Normark J., Holmgren A., Oliveberg M. (2004) Folding of human superoxide dismutase: disulfide reduction prevents dimerization and produces marginally stable monomers *Proc. Natl. Acad. Sci. USA* **101,** 15893–15898.

16. Andersen P.M., Nilsson P., Ala-Hurula V., Keranen M.L., Tarvainen I., Haltia T., Nilsson L., Binzer M., Forsgren L., Marklund S. L. (1995) Amyotrophic lateral sclerosis associated with homozygosity for an Asp90Ala mutation in Cu, Zn-superoxide dismutase *Nat. Genet.* **10,** 61–66.

17. Jonsson P.A., Backstrand A., Andersen P.M., Jacobsson J., Parton M., et al. (2002) *Neurobiol. Dis.* **10,** 327–333.